



# Aerosol–climate interactions in the Norwegian Earth System Model – NorESM1-M

A. Kirkevåg<sup>1</sup>, T. Iversen<sup>1,2</sup>, Ø. Seland<sup>1</sup>, C. Hoose<sup>2,3</sup>, J. E. Kristjánsson<sup>2</sup>, H. Struthers<sup>4,5</sup>, A. M. L. Ekman<sup>5</sup>, S. Ghan<sup>6</sup>, J. Griesfeller<sup>1</sup>, E. D. Nilsson<sup>4</sup>, and M. Schulz<sup>1</sup>

<sup>1</sup>Norwegian Meteorological Institute, Oslo, Norway

<sup>2</sup>Department of Geosciences, University of Oslo, Oslo, Norway

<sup>3</sup>Karlsruhe Institute of Technology, Institute for Meteorology and Climate Research, Karlsruhe, Germany

<sup>4</sup>Department of Applied Environmental Science, Stockholm University, Stockholm, Sweden

<sup>5</sup>Department of Meteorology, Stockholm University, Stockholm, Sweden

<sup>6</sup>Pacific Northwest National Laboratory, Richland, WA, USA

Correspondence to: A. Kirkevåg (alf.kirkevag@met.no)

Received: 10 July 2012 – Published in Geosci. Model Dev. Discuss.: 3 September 2012

Revised: 20 December 2012 – Accepted: 6 January 2013 – Published: 8 February 2013

**Abstract.** The objective of this study is to document and evaluate recent changes and updates to the module for aerosols and aerosol–cloud–radiation interactions in the atmospheric module CAM4-Oslo of the core version of the Norwegian Earth System Model (NorESM), NorESM1-M. Particular attention is paid to the role of natural organics, sea salt, and mineral dust in determining the gross aerosol properties as well as the anthropogenic contribution to these properties and the associated direct and indirect radiative forcing.

The aerosol module is extended from earlier versions that have been published, and includes life-cycling of sea salt, mineral dust, particulate sulphate, black carbon, and primary and secondary organics. The impacts of most of the numerous changes since previous versions are thoroughly explored by sensitivity experiments. The most important changes are: modified prognostic sea salt emissions; updated treatment of precipitation scavenging and gravitational settling; inclusion of biogenic primary organics and methane sulphonic acid (MSA) from oceans; almost doubled production of land-based biogenic secondary organic aerosols (SOA); and increased ratio of organic matter to organic carbon (OM/OC) for biomass burning aerosols from 1.4 to 2.6.

Compared with in situ measurements and remotely sensed data, the new treatments of sea salt and dust aerosols give smaller biases in near-surface mass concentrations and aerosol optical depth than in the earlier model version. The model biases for mass concentrations are approximately unchanged for sulphate and BC. The enhanced levels of mod-

eled OM yield improved overall statistics, even though OM is still underestimated in Europe and overestimated in North America.

The global anthropogenic aerosol direct radiative forcing (DRF) at the top of the atmosphere has changed from a small positive value to  $-0.08 \text{ W m}^{-2}$  in CAM4-Oslo. The sensitivity tests suggest that this change can be attributed to the new treatment of biomass burning aerosols and gravitational settling. Although it has not been a goal in this study, the new DRF estimate is closer both to the median model estimate from the AeroCom intercomparison and the best estimate in IPCC AR4. Estimated DRF at the ground surface has increased by ca. 60%, to  $-1.89 \text{ W m}^{-2}$ . We show that this can be explained by new emission data and omitted mixing of constituents between updrafts and downdrafts in convective clouds.

The increased abundance of natural OM and the introduction of a cloud droplet spectral dispersion formulation are the most important contributions to a considerably decreased estimate of the indirect radiative forcing (IndRF). The IndRF is also found to be sensitive to assumptions about the coating of insoluble aerosols by sulphate and OM. The IndRF of  $-1.2 \text{ W m}^{-2}$ , which is closer to the IPCC AR4 estimates than the previous estimate of  $-1.9 \text{ W m}^{-2}$ , has thus been obtained without imposing unrealistic artificial lower bounds on cloud droplet number concentrations.

## 1 Introduction

Aerosol particles scatter and absorb solar radiation and provide nuclei for condensation of water and formation of ice in air. Thus they potentially influence the natural climate as well as climate change through human activity. The efficiency of this influence depends on aerosol production, transport, and removal, and on microphysical processes such as nucleation, condensation, and coagulation that determine the composition, size, and shape of the particles. Since most of these processes are either approximately represented in global climate models or are not well known in the first place, aerosols constitute an important source of uncertainty in climate simulations and future projections. A recent overview of key challenges in understanding and modeling aerosols and their effects on climate and environment is given by Kulmala et al. (2011). Intermodel differences, and thus climate projection uncertainty, can to a large extent be attributed to aerosol–cloud interactions and cloud feedbacks (Penner et al., 2006; Forster et al., 2007; Randall et al., 2007; Hegerl et al., 2007).

This paper describes and discusses the representation of aerosols and the processes relevant for potential climate interactions in version 1 of the Norwegian Earth System Model (NorESM1). NorESM1 is a fully coupled global model that is used for simulations under the CMIP5 protocol for the upcoming fifth assessment report from IPCC (Bentsen et al., 2012; Iversen et al., 2012). Model-representation of processes leading to anthropogenic aerosol radiative forcing is described here, whilst estimates of climate response are discussed by Bentsen et al. (2012), Iversen et al. (2012), and Tjiputra et al. (2012). Sand et al. (2013) present a model study on Arctic climate response to remote and local forcing of black carbon, also using NorESM1.

The scheme for calculating the life cycle of aerosol particles along with their optical and physical properties is developed from the version thoroughly described by Seland et al. (2008) and Kirkevåg et al. (2008). NorESM1 further incorporates extensions for cloud microphysics with prognostic cloud droplet number concentration (Storelvmo et al., 2006; Hoose et al., 2009) and for wind-driven sea salt emissions (Struthers et al., 2011). Changes in the NorESM1 aerosol module are discussed relative to these papers, in particular Seland et al. (2008). The role of natural aerosols in the earth system in general, and for modulating climate impacts of anthropogenic aerosols in particular, is emphasized.

The core version of NorESM, NorESM1-M, which is used in this study, is based on version 4 of the Community Climate System Model (CCSM4) developed at the US National Center for Atmospheric Research (NCAR) (Gent et al., 2011). This system's atmospheric component, the Community Atmosphere Model version 4 (CAM4; Neale et al., 2010) is changed to include the aerosol module developed for NorESM1 and is referred to as CAM4-Oslo.

Potential climate impacts of aerosols are partly direct effects linked to increased scattering and absorption of solar

radiation (e.g. Charlson et al., 1992), and partly indirect effects via induced changes in cloud microphysics. The radiative forcing of the direct effects at the top of the atmosphere can be negative or positive depending on the relative importance of the changes in absorption and scattering. This relative importance depends on the anthropogenic aerosols but also on the natural aerosols and the albedo of the underlying surface. The indirect effect of pure water clouds, however, exerts a negative radiative forcing through increased cloud droplet number and decreased cloud droplet size (the first indirect effect; Twomey, 1977). Much more uncertainty is associated with the second indirect effect (Albrecht, 1989), associated with changes in cloud water content and cloudiness (Stevens and Feingold, 2009).

The semi-direct effect is potentially positive due to decreased low level cloudiness when increased aerosol absorption reduces relative humidity (Hansen et al., 1997) or due to reduced boundary-layer turbulent fluxes and cumulus clouds (Ackerman et al., 2000). We have not specifically studied the semi-direct effect in the present paper, although it is included in the model experiments which couple the aerosols and their radiative forcing online with the atmospheric thermodynamics (see Sect. 4.4). The potential magnitude of the semi-direct effect on the net radiative budget at the top of the atmosphere is characterized as small in the IPCC AR4, and the level of scientific understanding is furthermore characterized as very low (Denman et al., 2007).

There is a range of potential indirect effects associated with ice- and mixed-phase clouds (e.g. Denman et al., 2007). These are neither discussed in this paper nor currently included in NorESM, although research development is ongoing for later inclusion (Hoose et al., 2010; Storelvmo et al., 2011; see also Gettelman et al., 2010). Preliminary results indicate a partial compensation of the indirect effects of pure water clouds, but the uncertainties are still large, e.g. concerning the ice-nucleating ability of soot.

Climate effects of anthropogenic aerosols depend on the amount, size and physical properties of natural particles that to a large extent constitute a background for the physical properties attained by anthropogenic particulate matter. Through their number density, size, and shape, primary particles provide surface area for condensation of particulate matter produced in the gas phase. Similarly, particles that are sufficiently small to be subject to Brownian diffusion may stick to larger, pre-existing particles through coagulation. If condensation or coagulation takes place, the pre-existing particles will strongly influence the physical properties of the thus produced secondary particulate matter. New small particles are swiftly nucleated with initial growth by self-condensation in air with little pre-existing particulate surface area available for immediate condensation (Kulmala et al., 2005).

Pre-existing primary particles may also act as cloud condensation nuclei (CCN) and thus influence the occurrence of cloud droplets in which further secondary particulate matter may be produced by heterogeneous reactions. When the

cloud droplets evaporate, a residual aerosol with new properties is left behind.

Information about the properties of aerosols that would exist without the presence of man-made components is not directly available, and data for processes that constrain their physical properties are uncertain (e.g. Dentener et al., 2006). Such processes take place in clear air, in cloud droplets, and involve biogeochemical interactions with the oceans and the land surface (e.g. Barth et al., 2005). Primary natural particles include sea salt produced from evaporating sea spray and mineral dust from dry land under windy conditions. The sea spray consists of a mixture of sea salt and organic compounds, mostly water-insoluble (Facchini et al., 2008). Natural forest fires produce submicron primary particles as smoke (an internal mixture of soot and organic carbon). Natural biogenic and biological particles constitute at present very uncertain components of the natural background of primary particles (e.g. Jaenicke, 2005; O'Dowd et al., 2004; Leck and Bigg, 2005). Secondary particles that occur naturally include sulphate oxidized from volcanic SO<sub>2</sub> or originating from oceanic DMS or terrestrial sulphides. Particulate nitrate is oxidized from NO<sub>x</sub> produced in air by lightning or from nitrification/denitrification processes in soils. Secondary organic aerosols (SOA) stem from terpenes and isoprene emitted from living forest under favourable conditions (Dentener et al., 2006; Hoyle et al., 2007).

Primary biological aerosol particles (PBAP) include plant fragments, pollen, bacteria, plankton, fungal spores, viruses, and protein crystals (Jaenicke, 2005). Measurements have shown that PBAP is potentially an important part of atmospheric aerosols, varying from 10 % (marine) and 22 % (urban/rural) to 28 % (remote continental) of the total aerosol volume for particles above 0.2 µm equivalent radius (Matthias-Maser and Jaenicke, 1995). O'Dowd et al. (2004) found that the measured organic material constituted 65 % of the submicron marine aerosol mass at Mace Head (Ireland) during periods of high biological activity in the North Atlantic Ocean, and as much as 83 % of the fine mode (radii from 0.03–0.0625 µm). The organic fraction was observed to increase dramatically as particle size decreased, from 3 to 83 %, over the size range investigated by Cavalli et al. (2004). Bigg et al. (2004) reported large bacterial concentrations in the surface microlayer of open water in the central Arctic Ocean in summer, with bacteria length ranging from 0.6 to 3 µm. However, the number of bacteria above biologically active oceans is dwarfed by the large number of particles consisting of biogenic organic aggregates and colloids (Després et al., 2012). Lohmann and Leck (2005) failed to explain the observed CCN population only by DMS oxidation products and sea salt particles. Observations suggest that bursting of air bubbles during whitecap formation is responsible for injecting bioparticles into the atmosphere (O'Dowd et al., 2004; Leck and Bigg, 2005; Fahlgren et al., 2010).

Inclusion of primary natural aerosols which were missing in earlier model calculations will affect the direct and

indirect effects of anthropogenic aerosols in otherwise pristine conditions. In climate models where cloud-droplet number concentrations (CDNC) are calculated explicitly, the values are frequently constrained by prescribing a lower bound. Lohmann et al. (2000) showed that a reduction of the minimum cloud droplet number concentration (CDNC) from 40 to 10 cm<sup>-3</sup> led to a 70 % increase in the joint first and second indirect effect. In the previous version of CAM-Oslo, an increase in CDNC by 15 cm<sup>-3</sup> everywhere gave a 42 % decrease in the indirect radiative forcing (Kirkevåg et al., 2008). As demonstrated by Hoose et al. (2009) the assumed lower bound is in many cases unrealistically high. The new aerosol treatment in CAM4-Oslo has been developed with special attention to natural aerosols, and applies a lower CDNC bound of only 1 cm<sup>-3</sup>.

Some emission scenarios for aerosols and precursor gases (Penner et al., 2001) indicate a gradual change to a more absorbing aerosol globally as emission reduction measures for acidifying compounds become effective. However, nitrate aerosols have similar radiative and water-activity properties as sulphate, but are neglected in most climate models at present. In Europe, particulate nitrate accounts for about 10–20 % of the dry aerosol mass (Putaud et al., 2004). Both measurements and model results indicate that nitrate has remained at the same level since around 1990 (Fagerli et al., 2008). Adams et al. (2001) suggest that the radiative forcing due to nitrate will gradually exceed that of sulphate towards the end of this century. Nitrate and its effect on climate are not yet included in CAM4-Oslo, but are presently being studied in a research version.

After a very brief overview of NorESM1 and CAM4-Oslo, Sect. 2 describes the representation of aerosol life-cycling and the optical and physical properties of particles in CAM4-Oslo. Changes with respect to earlier published versions are emphasized. Section 3 describes the specific configuration of the model and the experiments carried out for this paper, and Sect. 4 presents results for the main experiments including comparison with observational data. In Sect. 5 a range of sensitivity tests is presented and discussed. Most of the model amendments presented in Sect. 2 are discussed in Sect. 5. Finally, main conclusions are drawn in Sect. 6.

## 2 Model description: NorESM1 and CAM4-Oslo

NorESM1 (Version 1 of the Norwegian Earth System Model) is an Earth System Model that to a large extent is based on NCAR CCSM4.0 (Gent et al., 2011; Versteinsten et al., 2010) when run without interactive carbon-cycling, and NCAR CESM1.0, although with CCSM4 model setup, when run with online ocean carbon cycle. The former version, used in this work, is the core version of NorESM (Bentsen et al., 2012; Iversen et al., 2012), named NorESM1-M. The latter version (Tjiputra et al., 2012) is named NorESM1-ME. Both NorESM1 versions use CAM4-Oslo for the atmospheric part

**Table 1.** Initial modal size parameters, mass densities and accommodation coefficients for primary emitted log-normal aerosol size modes. The aerosol compounds are explained in Fig. 1. BC(ac) is an externally mixed fractal agglomerate with particle radius dependent density, giving  $507 \text{ kg m}^{-3}$  averaged over all sizes.

Mode	Median radius ( $\mu\text{m}$ )	Standard deviation	Mass density ( $\text{kg m}^{-3}$ )	Accommodation coefficient for $\text{SO}_4$ condensation
SO4(n)	0.0118	1.8	1841	1
BC(n)	0.0118	1.8	2000	0.3
OM(a)/BC(a)	0.04	1.8	1500/2000	0.5
SO4(ac)	0.075	1.59	1841	1
BC(ac)	0.1	1.60	507	0.3
SS(a)	0.022	1.59	2200	1
SS(ac)	0.13	1.59	2200	1
DU(ac)	0.22	1.59	2600	0.3
SS(c)	0.74	2.0	2200	1
DU(c)	0.63	2.0	2600	0.3

of the model, and an updated version of the isopycnic ocean model MICOM (Assmann et al., 2010; Otterå et al., 2010). CAM4-Oslo is a version of CAM4 (Neale et al., 2010) with separate representation of aerosols, aerosol–radiation and aerosol–cloud interactions. The model uses the finite volume dynamical core for transport calculations, with horizontal resolution  $1.9^\circ$  (latitude) times  $2.5^\circ$  (longitude) and 26 levels in the vertical, as in the original CAM4.

The sea ice and land models in the two NorESM1 versions are basically the same as in CCSM4 and CESM1, respectively. However, the tuning of the snow grain size for fresh snow on sea ice is adjusted in the fully coupled NorESM1, and the albedo effects of soot and mineral dust aerosols deposited on snow and sea ice are based on the aerosol calculations in CAM4-Oslo.

Since this paper focuses on pure atmospheric processes associated with aerosols, experiments are made using the data ocean and sea ice model of NCAR's CCSM4 coupled to CAM4-Oslo, instead of the fully coupled NorESM1-M. For a broader description of NorESM1-M and associated CMIP5 experiments, the reader is referred to Bentsen et al. (2012) and Iversen et al. (2012).

## 2.1 Aerosols and their interactions with radiation and clouds in CAM4-Oslo

The modeling of aerosol processes in CAM4-Oslo is extended from CAM-Oslo versions described and studied by Seland et al. (2008), Kirkevåg et al. (2008), Storelvmo et al. (2006), Hoose et al. (2009), and Struthers et al. (2011). Apart from a few modifications of the parameter tuning for cloud micro- and macrophysics that were necessary when run as a part of NorESM1-M, the changes we have introduced in the development of CAM4-Oslo are all related to aerosols and their interactions with radiation and warm cloud microphysics. The description in this paper emphasizes changes

relative to the versions described in the above mentioned works, in particular Seland et al. (2008).

To estimate how aerosol particles influence solar radiation and cloud microphysics, their number concentrations, chemical composition, and physical shape need to be estimated as a function of equivalent particle radius over a range from a few nanometers to a few micrometers. This is partly because the interaction with radiation varies strongly with the ratio between radius and radiative wavelength and the dielectric properties of the particles; and partly because the ability for particles to act as cloud condensation and ice nuclei depends on hygroscopicity, size, and molecular structure of the particles. In global climate models these aerosol properties will have to rely on approximations and parameterizations.

Our approach differs from the often applied modal method such as e.g. M7 (Stier et al., 2005) and MAM3 (Liu et al., 2012). The details of the approach are described by Seland et al. (2008), although the principles probably are more easily understood from the description of the simpler aerosol life cycle scheme in Iversen and Seland (2002, 2003) and the corresponding scheme for size-resolved aerosol physics in Kirkevåg and Iversen (2002). As in Seland et al. (2008), the aerosol life cycle scheme calculates mass concentrations of aerosol species. These mass concentrations are tagged according to production mechanisms in clear and cloudy air. There are up to four size modes for each of these tagged mass concentrations (nucleation, Aitken, accumulation, and coarse mode). The processes are gas phase and aqueous phase chemical production, gas to particle nucleation, condensation on pre-existing aerosol surfaces, and coagulation of smaller particles onto pre-existing Aitken, accumulation and coarse mode particles. The chemical components are sulphate ( $\text{SO}_4$ ), black carbon (BC), organic matter (OM), sea salt (SS), and mineral dust (DU). In addition comes water, which is mixed into the particles based on their hygroscopicity and the ambient relative humidity.

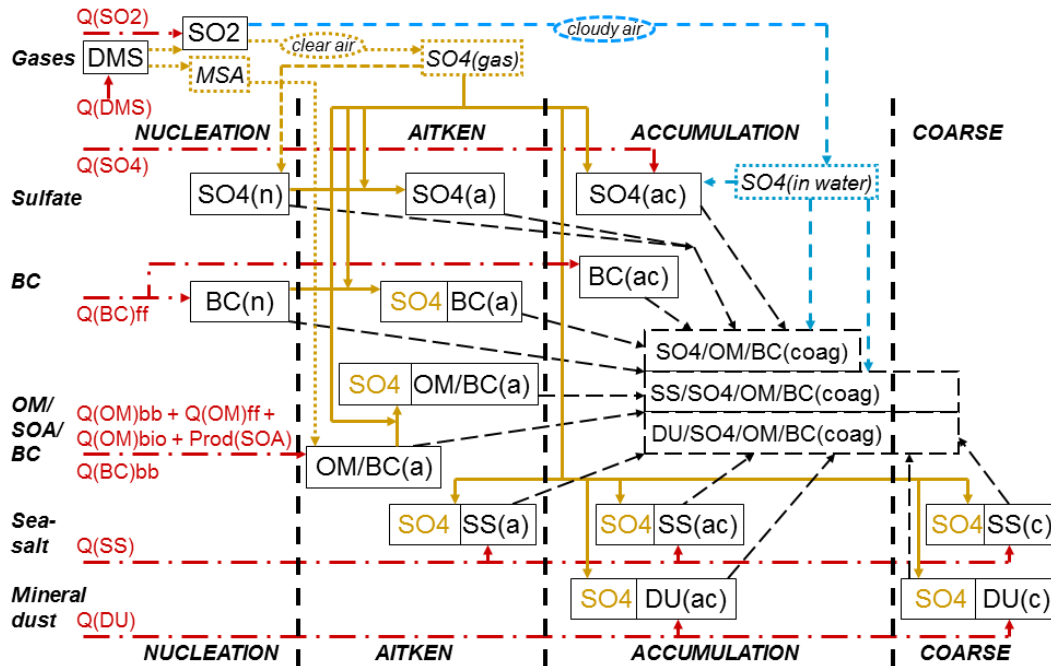


**Fig. 1.** Schematic for aerosol particle processing in CAM4-Oslo. The source terms on the left side, labeled  $Q(X)_y$ , where  $X$  is the constituent name and  $y$  is the source type, may come from primary emission or secondary production. The source labels bb, ff and bio respectively indicate biomass burning, fossil fuel combustion, and biogenic sources. Primary particles are emitted (dashed-dotted arrows) as accumulation-mode sulphate ( $SO_4(ac)$ ), nucleation and accumulation mode black carbon ( $BC(n)$ ,  $BC(ac)$ ), Aitken mode BC ( $BC(a)$ ), internally mixed Aitken mode organic matter and BC ( $OM/BC(a)$ ), Aitken, accumulation, and coarse mode sea salt ( $SS(a)$ ,  $SS(ac)$ ,  $SS(c)$ ), accumulation and coarse mode mineral dust ( $DU(ac)$ ,  $DU(c)$ ). Model calculated gas-phase components are DMS and  $SO_2$ . Gaseous sulphate ( $SO_4(gas)$ ) produced in air is assumed to be transformed to nucleation-mode sulphate ( $SO_4(n)$ , dotted arrow) if insufficient particle surface area is available for condensation (solid arrows). Sulphate produced by in cloud water droplets ( $SO_4(in\ water)$ , short-dashed arrow) is partly added to  $SO_4(ac)$  but mainly to a broad internal mixture of accumulation and coarse mode particles (of which there are two types with respect to complexity). Long-dashed arrows represent coagulation which contributes to the latter particle types.

The aerosol mass concentrations calculated in the life cycle scheme (and transported in the model) are 11 components for externally mixed particles emitted or produced in air. These are the 10 modes listed in Table 1, where one of the modes,  $OM(a)/BC(a)$ , contains two components. In addition there are 9 components which are tagged to production mechanisms in air or cloud droplets, so that the size-resolved transformations into internal mixtures by interactions with the above 11 compounds can be estimated a posteriori by use of look-up tables (see below). These 9 components are:  $SO_4(cond)$ , the part of the sulphate mass produced in gas phase by oxidation of  $SO_2$  by OH ( $SO_4(gas)$  in Fig. 1), which is estimated to condense on existing particles (note that the remaining part is assumed to produce nucleation mode sulphate,  $SO_4(n)$ );  $SO_4(a)$  is the part of the nucleation-mode sulphate [ $SO_4(n)$ ] mass which is subject to condensation of gaseous sulphate produced in clear air and thus produces externally mixed sulphate in the Aitken mode;  $SO_4(coag)$  is the mass of sulphate originating from  $SO_4(n)$ ,  $SO_4(a)$  and  $SO_4(cond)$  which coagulates with Aitken, accumulation and coarse mode particles in clear air (assuming

the same transfer rate for  $SO_4(cond)$  as for  $SO_4(a)$ );  $SO_4(in\ water)$  is the mass of sulphate oxidized from  $SO_2$  in cloud droplets and the part of  $SO_4(n)$  and  $SO_4(a)$  that is collected by cloud droplets and ends up in accumulation and coarse mode particles after evaporation;  $BC(cond, n)$  is the mass of Aitken mode BC originating from  $BC(n)$  after condensation of  $SO_4(cond)$ ;  $BC(cond, a)$  is the mass of accumulation mode BC originating from  $OM/BC(a)$  after condensation of  $SO_4(cond)$ ;  $BC(coag)$  is the mass of BC originating from  $BC(n)$ ,  $BC(a)$ ,  $OM/BC(a)$  and  $BC(ac)$  that coagulates in clear air or in cloud droplets that subsequently evaporate and end up as accumulation and coarse mode particles;  $OM(cond, a)$  is the mass of OM originating from  $OM/BC(a)$  after condensation of  $SO_4(cond)$ ;  $OM(coag)$  is the mass of OM originating from  $OM/BC(a)$  that coagulate in clear air or in cloud droplets, which subsequently evaporate and end up as accumulation and coarse mode particles. This adds up to 20 aerosol components in addition to two gaseous precursors ( $SO_2$  and dimethyl sulphide, DMS).

Figure 1 gives an updated schematic representation of the aerosol processes in CAM4-Oslo, which facilitates

comparison with the corresponding schematic for CAM-Oslo in Fig. 1 of Seland et al. (2008). It should be noted that the externally mixed OM mode from fossil fuel combustion, labeled OM(a) in Seland et al. (2008), is removed in this work. The rationale for this is that the recommended size distribution for organic matter from fossil fuel is the same as for biomass burning particles (Dentener et al., 2006), and that the relative fraction of fossil fuel OM is small compared to OM emitted from biomass burning. This was in an early version of CAM4-Oslo shown to give very small changes in concentrations and lifetime of OM, and small changes in the estimated aerosol properties in general.

As in Seland et al. (2008), the internally mixed mass from the processes described above is only added to and distributed onto the primary particles when calculating aerosol size distributions and optical properties for use in the cloud droplet activation code and in the radiative transfer code (cf. Kirkevåg and Iversen, 2002). The particle numbers and sizes are estimated here based on assumptions about the primary particles that are emitted or produced in air, of which there are 10 modes with log-normal size distributions as detailed in Table 1. In the separate scheme for size-resolved aerosol physics these modes are changed in accordance with the processes to which the aerosol mass concentrations are tagged in the life cycle scheme, and are described without assuming log-normality. As described in detail by Kirkevåg and Iversen (2002), the size distributions of number and mass concentrations used in the look-up tables (see below) are estimated by solving the discrete form of the respective continuity equations, using 44 size-bins with radii ( $r$ ) ranging from 0.001 to 20  $\mu\text{m}$ . The size bins are equally wide (width = 0.1) along a  $\log_{10}(r)$  axis, so that the resolution, in terms of linear radius  $r$ , is finest for the smallest particle sizes. Hygroscopic swelling is treated as described by Seland et al. (2008), i.e. by use of the Köhler equation on the form of Eq. 13 in Kirkevåg and Iversen (2002). Optical properties are finally estimated from Mie-theory whilst CCN activation is estimated based on supersaturations calculated from Köhler theory (Abdul-Razzak and Ghan, 2000).

This chain of processes is, however, not calculated directly during integration of NorESM1 or CAM4-Oslo. The optical and physical properties of the aerosols are instead estimated by interpolating between pre-calculated values in look-up tables. The process-tagged aerosol mass concentrations and relative humidity (RH) (grid box mean values) are given as input to the tables. When apportioning condensate and coagulated material between the primary particle modes, condensed  $\text{SO}_4$  is lumped together with coagulated  $\text{SO}_4$  as input to the look-up tables for sea salt, mineral dust and  $\text{SO}_4(\text{ac})$  particles. As in Seland et al. (2008), this is done in order to keep the number of dimensions (for interpolation) of the look-up tables for each internally mixed mode down to five (cf. Kirkevåg et al., 2005). Output from one set of tables are dry aerosol modal radii and standard deviations based on log-normal fits to the size distributions, which are used as input

to the CCN activation calculations (Hoose et al., 2009; see also Abdul-Razzak and Ghan, 2000). From a second set of look-up tables, spectrally resolved mass-specific extinction, single scattering albedo, and asymmetry factor are used to estimate the influence of aerosols on shortwave radiation. The maximum RH value in the look-up tables for these optical parameters is 99.5%. The tables are thoroughly described in Sect. 2.8 in Seland et al. (2008), see also Kirkevåg and Iversen (2002).

The main advantage of this approach, described above, is that the degree of internal vs. external mixing can be estimated based on physicochemical processes instead of explicit assumptions, and that the CPU costs are low compared to the full sectional approach. A disadvantage is that there is no explicit information about the size and mixing state of the aerosol masses (after growth) in the life cycle scheme. A further disadvantage of this method is its rigidity. The need for complex and huge look-up tables makes it cumbersome to introduce changes to the basic physical properties of the aerosol, such as the assumed size parameters at time of emission of primary particles.

Apart from some exceptions described in Sect. 2.1.6, the sulphur chemistry is as described by Seland et al. (2008). Prescribed oxidant fields are still used, but now with an updated replenishment rate of  $\text{H}_2\text{O}_2$  in clouds (see Sect. 2.1.6). The DMS fraction converted into MSA is calculated explicitly by use of reaction rates given by Seinfeld and Pandis (1998).  $\text{SO}_2$  is oxidized to sulphuric acid gas [ $\text{SO}_4(\text{gas})$ ] in clear air by OH, and to particulate sulphate in aqueous-phase cloud droplets [ $\text{SO}_4(\text{in water})$ ] with an efficiency which is determined by the availability of  $\text{H}_2\text{O}_2$ , ozone, liquid water, and the rate of dynamic replenishment of cloudy air.

Gaseous sulphate is not kept as a tracked variable, but is assumed to immediately either condense on pre-existing particles or, if available particle surface area is insufficient, to produce new nucleation mode particles. This means that available  $\text{H}_2\text{SO}_4$  gas which is not depleted by condensation within a time step is simply assumed to nucleate to form  $\text{SO}_4(\text{n})$  mode particles, with size parameters as given in Table 1. All particles are subject to condensation deposition of gaseous sulphate with an assumed accommodation coefficient given in Table 1. Particles that are inefficient cloud condensation nuclei (such as pure BC and dust) may be transformed to become hydrophilic as they become internally mixed or coated by sulphate. Neither MSA (methane sulphonic acid), biogenic OM, nor natural secondary organic aerosols (SOA) are separate variables, but are approximated to have the same properties as other OM compounds.

Aerosol components dissolved in cloud water are not kept as separate tracked variables but are either scavenged or added to the general concentrations in air. The sulphate produced by oxidation in cloud water droplets is thus distributed on accumulation mode sulphate and on accumulation and coarse mode particles in internal mixtures resulting from coagulation in clear and cloudy air. This coagulation depletes

the number of nucleation and Aitken mode particles by increasing the mass, but not the number, of accumulation and coarse mode particles. Details concerning gaseous and aqueous sulphur chemistry, the processes of nucleation, condensation, and coagulation, and calculations of wet scavenging and dry deposition are given in Sect. 2.3 and Table 1 in Iversen and Seland (2002, 2003), with extensions in Sects. 2.3 through 2.8 in Seland et al. (2008). Some parameter values are changed in the present paper and also fitted to the new components not included in Seland et al. (2008). These are described in the next subsections.

### 2.1.1 Emissions of aerosols and aerosol precursors

Aerosol and aerosol precursor emissions have been updated. As indicated in Fig. 1, emissions of 11 components are required (DMS, SO<sub>2</sub>, SO<sub>4</sub>, fossil fuel and biomass burning BC and OM, biogenic OM and SOA production, sea salt, and mineral dust). Several of these components can stem from both natural and anthropogenic sources and represent preindustrial and present-day stages in societal development.

Assumed preindustrial (PI) and present-day (PD) emissions used in Seland et al. (2008) were for the years 1750 and 2000 from Phase I of the AeroCom intercomparison exercise (e.g. Schulz et al., 2006, see also the official AeroCom web pages at <http://aerocom.met.no>) with emission data from Dentener et al. (2006). The new PI and PD emission years are taken as year 1850 and 2000 for CMIP5 simulations, and year 1850 and 2006 for use in the Phase II extension of AeroCom (Schulz et al., 2009; Koffi et al., 2012b; Myhre et al., 2012; Samset et al., 2012). The emission years 1850 for PI and 2006 for PD are used as the standard in this paper, but test simulations with 1750 and 2000 emissions are also performed.

All simulations for years 1850 and 2000 employ emissions of SO<sub>2</sub>, primary OM (POM) and BC from fossil-fuel and bio-fuel combustion and biomass burning, taken from the IPCC AR5 data sets (Lamarque et al., 2010; Smith et al., 2011; Van der Werf et al., 2006; Schultz et al., 2008; Mieville et al., 2010; Buhaug et al., 2009; Eyring et al., 2009; Lee et al., 2009). When finalizing this paper, it was discovered that BC emissions from aviation had been inadvertently neglected for the IPCC AR5 dataset. A sensitivity test revealed that the impact on radiative forcing is negligible ( $< 0.001 \text{ W m}^{-2}$ ).

In the 2006 simulations the emissions for year 2000 are replaced by the AeroCom Phase II emissions dataset. This dataset also includes emissions estimates of BC, SO<sub>2</sub> and POM from aviation. Since the IPCC AR5 year 2000 emissions of biomass burning aerosols are 2D fields, we have assumed that these emissions have the same vertical profile as in the former Phase I of AeroCom, which was used in Seland et al. (2008).

An important part of the updated aerosol treatment in CAM4-Oslo is the treatment of natural background aerosols. These are particularly important for assessing the magni-

tude of the indirect effect of aerosols (see e.g. Kirkevåg et al., 2008; Hoose et al., 2009; Iversen et al., 2010), as well as for estimates of the total aerosol optical depth and absorption. Emissions of biogenic DMS, SO<sub>2</sub> from tropospheric volcanos, and mineral dust are unchanged from Seland et al. (2008). The following two subsections present more details about new treatments of natural emissions of SOA from vegetation, biogenic organic particles from oceans (Spracklen et al., 2008), and the temperature and wind-driven production of sea salt (Struthers et al., 2011).

### 2.1.2 Production of natural biogenic OM, SOA and MSA

Production of natural SOA from biogenic processes in land vegetation is taken into account as yield rates from terpene emissions and treated as emissions of POM. This is the same treatment as in Seland et al. (2008), but the total global emissions have been increased from  $19.1 \text{ Tg yr}^{-1}$  to  $37.5 \text{ Tg yr}^{-1}$ . This is the production rate of natural SOA minus a natural isoprene contribution estimated by Hoyle et al. (2007) in a model experiment where semi-volatile species were not allowed to partition to ammonium sulphate aerosol. Even larger production rates were found when this partitioning was allowed. Tsigaridis and Kanakidou (2003) suggested that the biogenic SOA production from volatile organic compounds (VOC) may range from 2.5 to as much as  $44.5 \text{ Tg yr}^{-1}$ .

Due to insufficient quantitative information about the sources, biogenic oceanic OM is usually neglected in global climate models, even though it potentially contributes significantly to total OM (Matthias-Maser and Jaenicke, 1995; Bigg et al., 2004; Cavalli et al., 2004; O'Dowd et al., 2004; Jaenicke, 2005; Meskhidze et al., 2011; Després et al., 2012). Sources of this aerosol are thought to be primary emissions (POM) of organic-enriched sea spray aerosol from bubble bursting, and SOA formation from gas phase VOC emitted from the ocean surface (Facchini et al., 2008; Spracklen et al., 2008). In CAM4-Oslo we have included such a bio-aerosol in a simplified way and treated it as POM. Since data for the spatial and temporal distribution of the organic content in seawater are not available on global scale, these biogenic OM emissions have, as a first approximation, been given the same spatial distribution as the prescribed AeroCom fine mode sea salt emissions. The global total of  $8 \text{ Tg yr}^{-1}$  is based on Spracklen et al. (2008). For comparison, the fossil fuel OM emission sources for 2006 amount to  $6.3 \text{ Tg yr}^{-1}$ .

MSA, an oxidation product from DMS, was in Seland et al. (2008) assumed to be swiftly deposited without influencing the calculated aerosol properties. In CAM4-Oslo, however, MSA is treated as an additional contribution to the primary ocean-biogenic OM with an OM to S (Sulphur) mass ratio that is assumed to be the same as that of MSA to S (3:1).



**Table 2.** Polynomial coefficients for the least square fitted modal sea salt number emission fluxes in Eq. (1).

Mode	$A_n$	$B_n$	$C_n$
SS(a), $n = 1$	0.0	$-3.36 \times 10^6$	$1.05 \times 10^9$
SS(ac), $n = 2$	0.0	$1.18 \times 10^5$	$-1.14 \times 10^7$
SS(c), $n = 3$	$3.06 \times 10^3$	$-1.67 \times 10^6$	$2.29 \times 10^8$

Like the other OM emissions, both the two new contributions to oceanic OM described above are assumed to be emitted in the hydrophilic OM/BC Aitken mode; see Fig. 1.

### 2.1.3 Sea salt emissions

A major upgrade in the natural aerosol treatment from the model version of Seland et al. (2008) is the replacement of the prescribed sea salt emissions with prognostic sea salt emissions based on Struthers et al. (2011). These emissions depend on 10-m wind speed ( $U_{10}$ ) and sea surface temperature (SST) (Mårtensson et al., 2003), and are regulated by the sea ice cover as in Nilsson et al. (2001). The number flux ( $\text{flux}_n$ ) of each of the three log-normal sea salt modes (Seland et al., 2008) at the point of emission, before hygroscopic growth and aerosol processing, have been fitted to the Mårtensson et al. (2003) parameterization by using a quadratic function of SST:

$$\text{flux}_n = W \cdot (A_n \cdot \text{SST}^2 + B_n \cdot \text{SST} + C_n), \quad (1)$$

where  $W$  is the white cap fraction

$$W = 0.000384 \cdot U_{10}^{3.41}. \quad (2)$$

This gives a simplified modal sea spray emission parameterization, compared to the detailed size distribution by Mårtensson et al. (2003), that still preserves most of the wind and temperature dependency found in the original parameterization. The wind dependence is unchanged from Struthers et al. (2011). However, due to a simplified fitting of the coarse sea salt mode to the Mårtensson et al. (2003) parameterization, tropical sea salt burdens were somewhat exaggerated in Struthers et al. (2011). The SST dependence in the accumulation (SS(ac)) and coarse (SS(c)) modes in Table 1 of Struthers et al. (2011) has therefore been updated to improve the fit for particles with diameters greater than  $2.5 \mu\text{m}$ , where the source parameterization of Monahan et al. (1986) is recommended. The revised coefficients are listed in Table 2.

### 2.1.4 Mass ratio OM/OC for biomass burning organic matter

We have increased the assumed mass ratio of particulate organic matter (OM) to organic carbon (OC) for biomass burning emissions from 1.4 to 2.6. This number is taken from Formenti et al. (2003) and is also used by Myhre et al. (2009).

It leads to significantly improved aerosol optical depths and absorption optical depths compared to observations and sun photometry retrievals in biomass burning dominated areas (see Sect. 5). The OM to OC mass ratio for SOA and for emissions from fossil fuel combustion is kept at 1.4, as in Seland et al. (2008).

### 2.1.5 Transport and removal in convective clouds

In the original CAM4 from NCAR, the convective cloud-cover is calculated explicitly. Hence, the volume available for convective scavenging is available directly. This is also the same formulation as in the chemistry transport model Mozart (Barth et al., 2000). Comparing CAM4 with CAM3, which was the host model of CAM-Oslo (used by Seland et al., 2008), changes have been made to the deep convection scheme by including the effects of deep convection in the momentum equation and using a dilute approximation in the plume calculation, which permits detrainment at all levels as opposed to only at the cloud top. These changes gave an improved representation of deep convection that occurs considerably less frequently but with higher intensity in CAM4 than in CAM3 (Gent et al., 2011). Based on the improved formulation of clouds with the dilute plume approximation (DPA) in CAM4, and on the resulting sulphate vertical distributions near the ITCZ, which are comparable to Seland et al. (2008), the special adjustment for aerosol processes in convective clouds (described in detail in Sect. 2.7 in Seland et al., 2008, see also Iversen and Seland, 2004), has been removed in CAM4-Oslo. We have also removed the somewhat ad hoc assumption of full mixing of aerosols between convective cloud updrafts and downdrafts. A more realistic description should reflect the mixing generated by the horizontal shear between updrafts and downdrafts and the vigorous turbulence inside deep convective clouds. Assuming full mixing is a radical assumption resulting in a minimum vertical transport of boundary-layer aerosols. Combined with the increased efficiency of scavenging by convective precipitation, systematically underestimated aerosol burdens are likely to result. On the other hand, the choice we have made for CAM4-Oslo is prone to contribute to overestimates. This is more thoroughly discussed in Sects. 4 and 5.

### 2.1.6 Oxidant fields

As in CAM-Oslo, tropospheric oxidant fields ( $\text{OH}$ ,  $\text{O}_3$ ,  $\text{H}_2\text{O}_2$ ) for use in the sulphate chemistry and the aerosol life cycle model are taken from simulations with a Chemical Transport Model (CTM). We have replaced the oxidant fields in Seland et al. (2008) with data from the most recent version of the oxidant chemistry in Oslo-CTM2 (Berntsen et al., 1997).  $\text{H}_2\text{O}_2$  is thus generally more abundant in lower tropospheric layers in CAM4-Oslo than in the version of Seland et al. (2008). Zonally and annually averaged, the new  $\text{H}_2\text{O}_2$  values are smaller in the upper troposphere (above



**Table 3.** Calculated global annual mass budget numbers for the individual modelled species in CAM4-Oslo (this work) and in Seland et al. (2008) (Se08). Simulation period: year 3–7. The upper values in a table cell are for present-day emissions, PD, and the lower for preindustrial emissions, PI. Emission years are 1850 (PI) and 2006 (PD) for CAM4-Oslo, and 1750 (PI) and 2000 (PD) for S2008. For DMS, SS, and DU, emissions are the same for PI and PD. For gaseous precursors, the fractions of chemical loss are also included. Numbers in parenthesis give the percentage of this loss, which respectively concerns gaseous oxidation of DMS to MSA, and aqueous-phase oxidation of SO<sub>2</sub> to sulphate. Sources and burdens of sulphur species are given as Tg S.

Spec.	Total Emissions [Tg yr <sup>-1</sup> ]		Total Sources [Tg yr <sup>-1</sup> ]		Burden [Tg]		Lifetime [days]		Wet Dep. [%]		Chemical Loss [%]	
	This work	Se08	This work	Se08	This work	Se08	This work	Se08	This work	Se08	This work	Se08
DMS	18.0	18.2	18.0	18.1	0.12	0.10	2.40	2.09			100 (27.1)	100 (25.3)
SO <sub>2</sub>	84.4	68.6	97.6	82.2	0.28	0.29	1.05	1.27	7.2	9.0	63.6 (85.0)	71.4 (85.2)
PI	16.4	14.9	29.6	28.4	0.086	0.084	1.06	1.08	11.2	10.0	78.4 (87.3)	81.0 (86.9)
PD	2.2	1.8	64.4	60.4	0.68	0.66	3.84	3.96	91.9	92.3		
SO <sub>4</sub>	0.4	0.38	23.6	23.4	0.21	0.24	3.19	3.80	94.1	93.4	n.a.	n.a.
PI	10.6	7.7	10.7	7.7	0.24	0.14	8.10	6.74	74.8	75.0		
PD	3.1	1.4	3.1	1.4	0.059	0.027	7.03	7.08	72.9	80.8	n.a.	n.a.
BC	166.7	65.6	182.9	65.6	3.82	1.30	7.63	7.22	80.3	80.2		
PI	97.3	33.3	112.8	33.2	2.24	0.64	7.23	7.05	77.6	80.6	n.a.	n.a.
PD	6411	7925	6459	7711	4.91	5.76	0.28	0.27	45.6	26.2	n.a.	n.a.
SS	1668	1678	1676	1671	11.72	10.40	2.55	2.27	25.2	35.9	n.a.	n.a.
DU												

about 500 hPa), much smaller in the stratosphere, but larger in most of the lower troposphere, amounting to an increase by a factor larger than 2 in parts of the tropics.

Furthermore, the H<sub>2</sub>O<sub>2</sub> replenishment time in cloudy air has been changed from a fixed 1 h value (Seland et al., 2008) to a 1–12 h range, depending on the cloud fraction. Within this 1–12 h range the replenishment time is assumed proportional to  $(1.1 - c_{\max})^{-2}$ , where  $c_{\max}$  is the maximum cloud fraction in the atmospheric column. This is to account for the increase in time required for mixing larger volumes of air. The effect of this increased replenishment time would be opposite to the increased levels of H<sub>2</sub>O<sub>2</sub> in the lower troposphere.

### 2.1.7 Scavenging of mineral dust and gravitational settling

Modeled near-surface mineral concentrations were underestimated approximately by a factor of 2 in Seland et al. (2008). This negative bias may to some extent have been caused by missing mineral dust emissions, since the only source included in the emission data set is major desert areas. On the other hand, the in-cloud scavenging coefficient for mineral dust was probably on the high side, since the assumed value of 1.0 implies that all mineral particles regardless of size or composition can be activated to form cloud droplets. In Hoose et al. (2009) the in-cloud scavenging coefficient for mineral dust was reduced to 0.1, leading to considerably extended residence times for mineral dust. In CAM4-Oslo, where the same mineral dust emissions are applied as in the

two previous studies, we use an intermediate in-cloud mineral scavenging coefficient value of 0.25, in agreement with the dominance of insoluble material. This yields about 25 % wet deposition globally averaged (Table 3), close to the median value of 28 % for 15 AeroCom Phase I models in a study by Huneus et al. (2011). The individual model averages in that work range from 16 % to 66 %.

Gravitational settling, which predominantly influences the largest particles, is now extended to all atmospheric levels in CAM4-Oslo, rather than in the lowermost level only (Seland et al., 2008). This is calculated at all heights, starting from the top of the model and calculating the contribution from each level to the model levels below. As a result the simulated aerosol removal is more efficient in general, particularly for coarse mode aerosols.

### 2.2 Cloud droplet spectral dispersion

In Seland et al. (2008) a diagnostic relation between the aerosols and the liquid cloud droplet number (CDNC) was used for stratiform clouds, while liquid water content (LWC) was a prognostic variable (Rasch and Kristjánsson, 1998).

A preliminary sensitivity test involving prognostic calculation of both CDNC and LWC, with activation of CCN following Abdul-Razzak and Ghan (2000), indicated a reduction of the first indirect forcing (the radius effect) by 36 % due to compensating effects not accounted for in the diagnostic scheme. One such compensating effect is the competition for available water vapour, which leads to smaller realized supersaturations for polluted present-day conditions than the

more pristine preindustrial conditions. Another effect is the loss of cloud droplets due to collision-coalescence processes, evaporation and freezing, which were not considered in the diagnostic scheme of e.g. Seland et al. (2008), therefore giving larger CDNC in general in that study. The corresponding reduction in the joint first and second indirect forcing was estimated to 38 % in Kirkevåg et al. (2008), using the same model version. The prognostic double moment cloud microphysics scheme has later become standard for stratiform clouds in the model (Storelvmo et al., 2006, 2008; Hoose et al., 2009).

As described by Hoose et al. (2009), calculation of realized supersaturation uses the subgrid updraft velocity following Morrison and Gettelman (2008) and employs look-up tables for aerosol particle modal radii and standard deviations in the calculation of activated CCN concentrations, used in subsequent calculations of CDNC and effective (with respect to scattering of light) cloud droplet radii ( $r_{\text{eff}}$ ). For convective clouds these quantities are estimated by simply assuming a supersaturation of twice the value for stratiform clouds.

A novelty compared to Hoose et al. (2009) is the introduction of a parameterization of cloud droplet spectral dispersion, allowing the shape of the cloud droplet spectrum to vary with changing aerosol loading.

The new formulation for cloud droplet spectral dispersion in CAM4-Oslo is taken from Eq. (2) in Rotstajn and Liu (2009), where the spectral shape factor  $\beta$  ( $\beta \equiv r_{\text{eff}}/r_v$ ;  $r_v$  being the mean volume radius) is expressed as a monotonically increasing function of CDNC:

$$\beta = \frac{(1 + 2\varepsilon^2)^{2/3}}{(1 + \varepsilon^2)^{1/3}}, \quad (3)$$

where the relative dispersion  $\varepsilon$  is given by

$$\varepsilon = 1 - 0.7 \exp(-0.003 \cdot \text{CDNC} \cdot \text{cm}^3). \quad (4)$$

In both CAM4 (Neale et al., 2010) and CAM-Oslo (Kirkevåg et al., 2008; Seland et al., 2008; Hoose et al., 2009; Struthers et al., 2011),  $\beta$  was prescribed to values of 1.08 over oceans and 1.14 over land, independent of CDNC, following Martin et al. (1994). With the new treatment of Rotstajn and Liu (2009), we obtain larger  $\beta$  values for higher levels of particle pollution. The new  $\beta$  is always larger than about 1.085. Thus  $\beta$  is now larger over the oceans, and also over land whenever CDNC exceeds about 45–50  $\text{cm}^{-3}$ .

The first indirect effect is determined by the relative change in  $r_{\text{eff}}$  (Twomey, 1991), and since  $r_{\text{eff}} = r_v \times \beta$ , the end result of the new  $\beta$  formulation is expected to be a smaller IndRF. Using an empirical scheme for CDNC as a function of aerosol mass concentrations, Rotstajn and Liu (2009) showed that this  $\beta$  formulation gave a 34 % reduction in the magnitude of the indirect radiative forcing. In this work we find a significantly smaller sensitivity to the  $\beta$  formulation; see Sect. 5. A recent survey of cloud microphysical data from

five field experiments by Brenguier et al. (2011) casts a new light on the issue of cloud droplet dispersion, but we have not attempted to include the results of that study here.

### 2.3 Parameter tuning

CAM4-Oslo applies the standard configuration of NCAR CAM4 with respect to model physics, i.e. the Rasch and Kristjánsson (1998) scheme for stratiform cloud microphysics and the CAM-RT radiation scheme (Collins et al., 2006), which were also used by both Seland et al. (2008) and Hoose et al. (2009). In order to obtain a realistic NorESM1-M model climate while maintaining a net radiative balance at top of the atmosphere (TOA), some of the cloud micro- and macrophysical parameters have been adjusted (Bentsen et al., 2012; Iversen et al., 2012) compared to the values used in CAM4. The minimum threshold for relative humidity in a model grid cell for formation of low clouds,  $\text{rhminl}$ , has been reduced from 91 to 90 %. The critical mean droplet volume radius for onset of auto-conversion, denoted  $r_{3lc}$  in Rasch and Kristjánsson (1998), has been increased from 10  $\mu\text{m}$  (Kristjánsson, 2002) to 14  $\mu\text{m}$ . The value 15  $\mu\text{m}$  was used in Collins et al. (2006) and Seland et al. (2008). Furthermore, following Kristjánsson (2002), the precipitation rate threshold for suppression of auto-conversion of cloud water to rain has been increased from 0.5 to 5.0  $\text{mm d}^{-1}$ . This is the same value as used by e.g. Seland et al. (2008) and Hoose et al. (2009). Impacts of these changes on modelled aerosol properties, direct radiative forcing (DRF), cloud droplet number concentrations (CDNC), effective droplet radii ( $r_{\text{eff}}$ ), liquid water path (LWP), and the indirect radiative forcing of aerosols (IndRF) are discussed in Sect. 5.

## 3 Model configuration and experiment setup

For this study, CAM4-Oslo/NorESM1-M has been set up to use the data ocean and sea ice models from CCSM4, running a series of 7-yr offline simulations with IPCC AR5 or AeroCom aerosol and precursor emissions, see Sect. 2.1.1. The *Ctrl* simulations (standard model version with all processes updated) are labelled PI and PD in Tables 3 through 7, where PI corresponds to aerosol emissions for year 1850 (“preindustrial”) and PD corresponds to aerosol emissions for the year 2006 (“present-day”). All simulations use “present-day” (year 2006) concentrations of greenhouse gases (GHG). Running the model in an offline mode means, in this case, that the meteorology is driven by prescribed aerosol and cloud droplet properties of the standard CAM4 (but with CAM4-Oslo stratiform cloud tuning) in all the experiments. Hence, the meteorology is the same in all simulations, except for a single sensitivity experiment where some of the tuning parameters for stratiform clouds have been changed. Calculation of the second indirect effect as a radiative forcing is as described by Kristjánsson (2002), i.e. by use of parallel calls

**Table 4.** Aerosol optical depth (AOD) and absorptive optical depth (ABS) at 550 nm, top of the atmosphere direct radiative forcing (DRF), cloud droplet number concentrations (CDNC) and effective cloud droplet radii ( $r_{\text{eff}}$ ) at 870 hPa, liquid water path (LWP), and indirect radiative forcing (IndRF) for a range of experiments. The generic notation PDpreXX denotes an experimental setup as for the reference *Ctrl*, with present-day (PD) emissions for year 2006, except for aerosol component XX where preindustrial (PI) emissions for year 1850 are applied. The difference PD-PDpreXX thus estimates the contribution of aerosol component XX to the changes from year 1850 to 2006. XX is SO<sub>4</sub> for sulphate, BCff for fossil fuel BC, OMff for fossil fuel organic matter, and BCOMbb for internally mixed BC and OM from biomass burning. The ZERO experiment is used to estimate the DRF of preindustrial aerosols relative to a clean atmosphere, by assuming AOD = 0. The data in the last row are not from the forcing experiments, but from the *Online* experiment (see Table 5).

Experiment (with statistics from year 3–7)	AOD (550 nm)	ABS (550 nm)	DRF at TOA (W m <sup>-2</sup> )	DRF at Surface (W m <sup>-2</sup> )	CDNC (870 hPa) (cm <sup>-3</sup> )	$r_{\text{eff}}$ (870 hPa) ( $\mu\text{m}$ )	LWP (g m <sup>-2</sup> )	IndRF at TOA (W m <sup>-2</sup> )
<i>Ctrl</i> PD (2006)	0.153	0.00618			53.3	9.40	130.9	
PD-PI	0.0527	0.00357	-0.0765	-1.83	16.9	-0.358	3.94	-1.20
PDpreSO <sub>4</sub>	0.119	0.00605			42.2	9.69	128.1	
PD-PDpreSO <sub>4</sub>	0.0342	0.00013	-0.481	-0.528	11.1	-0.286	2.80	-0.761
PDpreBCff	0.151	0.00452			53.8	9.38	131.2	
PD-PDpreBCff	0.00173	0.00166	0.374	-0.404	-0.500	0.0218	-0.264	0.0684
PDpreOMff	0.151	0.00615			52.6	9.42	130.7	
PD-PDpreOMff	0.00166	0.000027	-0.0334	-0.049	0.719	-0.0183	0.223	-0.0812
PDpreBCOMbb	0.137	0.00435			48.5	9.46	130.1	
PD-PDpreBCOMbb	0.0159	0.00183	0.0710	-0.867	4.85	-0.0581	0.837	-0.315
ZERO	0	0			53.3	9.40	130.9	
PRE (1850)	0.100	0.00261			36.4	9.76	127.0	
PRE-ZERO	0.100	0.00261	-1.64	-2.98	0	0	0	-
PD (2006) <i>Online</i>	0.152	0.00731			49.2	9.50	130.3	
PD-PI <i>Online</i>	0.0586	0.00476	-	-	14.0	-0.332	4.70	-

to the condensation scheme as well as the scheme for radiative transport in the model.

The anthropogenic direct (DRF) and indirect forcing (IndRF) by aerosols since 1850 are found from the difference in net radiation energy fluxes between PD and PI. Our results are based on the last 5 simulated years, except for the separate sensitivity test runs defined in Sect. 5 (Tables 5–7): here we instead show results from year 7 after a restart of the model from February year 6. All results are for short-wave fluxes only, except for the online simulations discussed in Sect. 4.4, where the CAM4-Oslo aerosols are allowed to affect the meteorology through their direct, semi-direct, and indirect effects on the radiation budget.

Each of the sensitivity experiments discussed in Sect. 5 is constructed by reverting each (or parts of each) of the model updates described in Sect. 2, back to the original treatment in Seland et al. (2008), Hoose et al. (2009), or Struthers et al. (2011). In this way we are able to assess how much each of the updates has improved or changed the model results, and to better understand differences in model behavior between CAM4-Oslo and other global models.

The additional simulations listed in Table 4 are forcing experiments originally set up for estimating DRF for separate aerosol species (Myhre et al., 2012; Samset et al., 2012). However, in this paper also IndRF and relevant diagnostics for cloud droplet properties and cloud liquid water paths are examined. The only exception is the ZERO experiment. Here

the aerosol extinction is set to 0 in the radiative transfer calculations, with no other changes. This means that the aerosol life cycle and the cloud droplet properties are as in the *Ctrl* (PD) experiment, so that only optics and DRF are affected.

## 4 Results

In order to validate the aerosol calculations in CAM4-Oslo and verify the results from the simulations labeled *Ctrl*, we here discuss the aerosol concentrations, burdens, lifetimes, optical properties, and effects on clouds and radiation in the model. We compare calculated results with earlier model versions and with available observations or retrievals from remotely detected signals. Results of the sensitivity tests are discussed in Sect. 5.

Although not formally a part of the present study, more results from CAM4-Oslo as well as several other models, can be found at the AeroCom web-site: <http://aerocom.met.no/data.html>, where results labeled as CAM4-Oslo-Vcmip5 are from *Ctrl*, CAM4-Oslo-Vcmip5online are from runs with online interactions with meteorological fields, and CAM4-Oslo-Vcmip5semi2000 are from runs with year 2000 as PD. The CAM-Oslo model version of Seland et al. (2008) is labeled UIO\_GCM\_V2.

**Table 5.** Definition of sensitivity tests discussed in Sect. 5. Se08 refers to Seland et al. (2008). Note: Due to different cloud tuning, the *cldtunorig* experiments do not have the same meteorology as the other offline experiments (but PD and PI for *cldtunorig* have the same meteorology).

Identification	Short description
<i>Ctrl</i>	Standard Reference. All processes updated. Emissions years: PD = 2006; PI = 1850.
<i>natOM</i>	As <i>Ctrl</i> , but with natural OM as in Se08.
<i>natOMocn</i>	As <i>Ctrl</i> , but no biogenic OM from oceans and MSA, as in Se08.
<i>bbPOM</i>	As <i>Ctrl</i> , but OM/OC = 1.4, as in Se08.
<i>Struthers11</i>	As <i>Ctrl</i> , but tuning of sea salt emissions as in Struthers et al. (2011).
<i>dustscavin</i>	As <i>Ctrl</i> , but in-cloud scavenging efficiency for dust = 1, as in Se08.
<i>cldtunorig</i>	As <i>Ctrl</i> , but tuning of cloud microphysics as in NCAR CAM4 (Neale et al., 2010).
<i>gravdep2d</i>	As <i>Ctrl</i> , but gravitational settling only in the lowest model layer, as in Se08.
<i>convmix</i>	As <i>Ctrl</i> , but convective mixing of aerosols and precursors as in Se08.
<i>noBCac</i>	As <i>Ctrl</i> , but no primary emissions of BC(ac), i.e. all BC is emitted as BC(n).
<i>replH2O2</i>	As <i>Ctrl</i> , but replenishment time of H <sub>2</sub> O <sub>2</sub> = 1 h, as in Se08.
<i>no coating</i>	As <i>Ctrl</i> , but without coating of dust and BC in CCN activation.
<i>prescrβ</i>	As <i>Ctrl</i> , but effective cloud droplet radii parameterized as in Se08, Hoose et al. (2009), and Neale et al. (2010).
<i>EmPD2000</i>	As <i>Ctrl</i> (all processes updated). Emissions years: PD = 2000; PI = 1850.
<i>EmPI1750</i>	As <i>Ctrl</i> (all processes updated). Emissions years: PD = 2006; PI = 1750.
<i>Online</i>	As <i>Ctrl</i> , but with online interactions between aerosol forcing and atmospheric dynamics.

#### 4.1 Global aerosol budgets and atmospheric residence times

Table 3 compares the budgets and atmospheric residence times of CAM4-Oslo with the model version presented by Seland et al. (2008). Total source numbers are here simply assumed to equal the total deposition, since production of secondary aerosols is not standard output in the model. Due to numerical inaccuracies and finite simulation lengths, this assumption is seen (from primary sea salt and mineral dust in Table 3) to be accurate to within about 1 %. Figures 2 and 3 show maps of annual aerosol burdens and how the respective mass mixing ratios varies with height, zonally averaged.

For mineral dust, wet scavenging efficiency is reduced in CAM4-Oslo compared to Seland et al. (2008), taking into account that mineral dust is not hygroscopic. This leads to a considerably reduced fraction of wet deposition of dust. Despite a more effective gravitational deposition due to the updated treatment of gravitational settling (see Table 6), we therefore find an increase in the global atmospheric burden and residence time (12 %).

The sea salt burden is about 15 % lower than in Seland et al. (2008), in agreement with the smaller emissions (19 %). In spite of the enhanced importance of gravitational settling, the fraction deposited by precipitation scavenging is considerably higher in this work. This is probably a consequence of the wind- and SST-driven emissions in CAM4-Oslo. Strong winds over oceans are often co-located with precipitation. The prescribed emissions in Seland et al. (2008) would more often, and erroneously, not be associated with the actual storms predicted in the atmospheric model, leaving a higher preference for dry rather than wet deposition.

Other major changes result from differences in emission inventories when changing from 2000 to 2006 for present-day (PD) conditions and from 1750 to 1850 for preindustrial conditions (PI).

Some of the changes in burdens since Seland et al. (2008) can be directly related to changes in atmospheric residence times. The residence times given in Table 3 are close to values from many other models of the same type as CAM4-Oslo; see e.g. Textor et al. (2006). For sulphate there is a considerable decrease for preindustrial conditions, while for present-day conditions there is a much smaller decrease. For OM and BC changes are relatively minor for preindustrial conditions, while there is an increase in residence time for the present-day. The increase is particularly large for BC. For the difference (PD-PI), an increase in atmospheric residence times is thus evident for all the three aerosol components, but it is considerably larger for BC than for OM and sulphate. Since removal of these components to a large extent is determined by precipitation scavenging, and their residence times are much too short for the components to reach a well-mixed state, changes in the geographical distribution of major emission sources influence the residence time. This is in addition to changes in the efficiency of dry and wet removal processes.

If cloud volume and liquid water abundance were approximately the same as in Seland et al. (2008), the increased levels of lower tropospheric H<sub>2</sub>O<sub>2</sub> would tend to reduce the lifetime of both SO<sub>2</sub> and sulphate, by increasing the low-level oxidation and producing sulphate in layers exposed to wet scavenging. Even though slightly reduced lifetimes are indeed calculated (Table 3), the reduction is counteracted by the slower replenishment of H<sub>2</sub>O<sub>2</sub> in cloudy air and the more

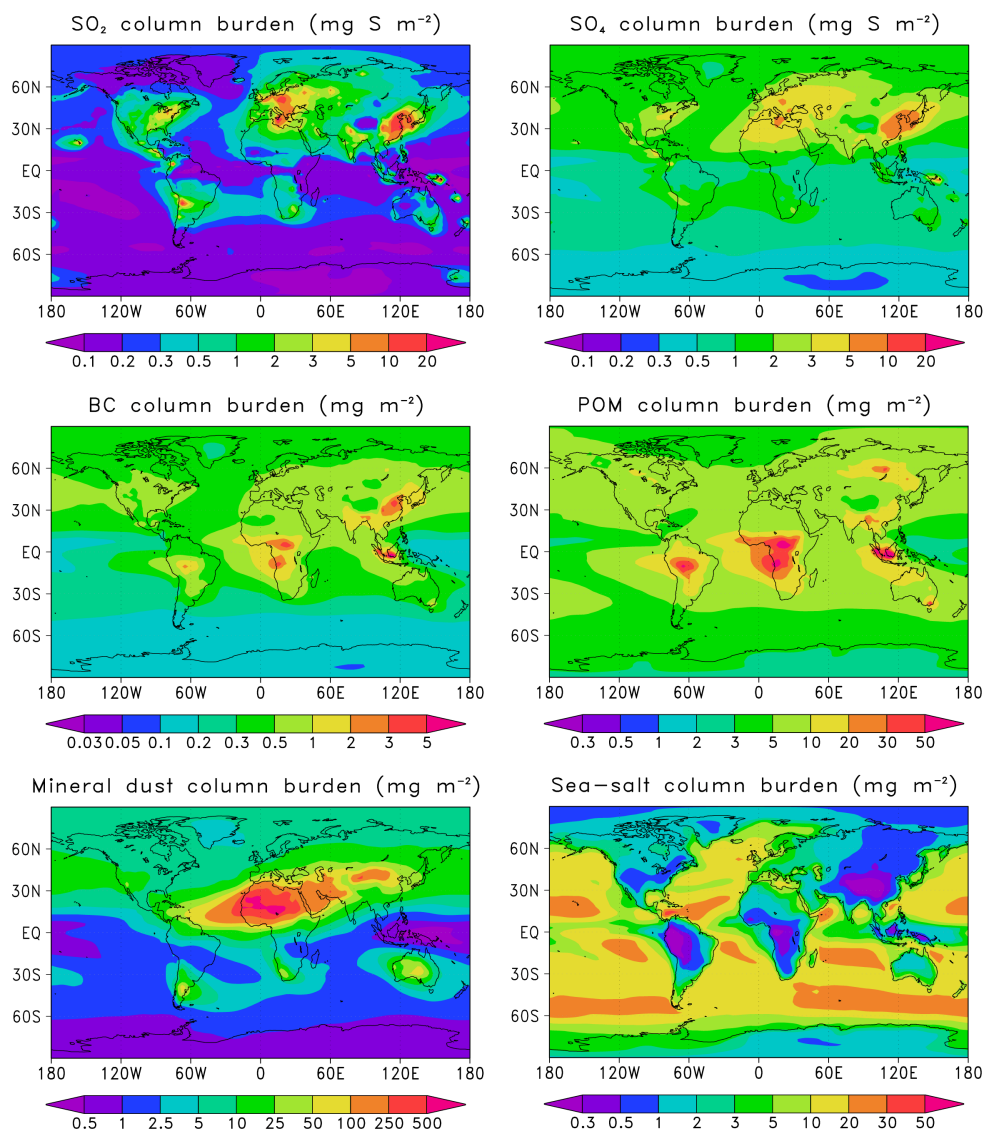


**Fig. 2.** Annually averaged vertically integrated mass columns of SO<sub>2</sub> and aerosol constituents in the *Ctrl* simulation. Globally averaged columns are 0.554 mg S m<sup>-2</sup> for SO<sub>2</sub>, 1.34 mg S m<sup>-2</sup> for sulphate, 0.466 mg m<sup>-2</sup> for BC, 7.49 mg m<sup>-2</sup> for POM, 23.0 mg m<sup>-2</sup> for mineral dust, and 9.62 mg m<sup>-2</sup> for sea salt.

efficient vertical transport in deep convective clouds which brings low level air up to the middle and upper troposphere when mixing between downdrafts and updrafts is neglected. Furthermore, low-level liquid water content and clouds are generally less abundant (a factor 60–80 % of the cloud cover in Seland et al., 2008) in CAM4-Oslo (not shown). It can also be noted from Table 3 that the changes in wet scavenging and the overall fraction of SO<sub>2</sub> oxidized in clouds are negligible.

## 4.2 Comparison with measurements

### 4.2.1 Surface mass concentrations

Figure 4 compares modeled and measured near-surface mass concentrations for each aerosol constituent. As described in more detail by Seland et al. (2008), the measurements span the years 1996–2002 and have been made available through the AeroCom project (<http://aerocom.met.no>) from the AEROCCE, AIRMON, EMEP, GAW, and IMPROVE measurement networks. The EMEP data are from year 2002. Since results from a climate model are not designed to replicate single short-term observations but at best their overall statistics, monthly averaged data over the entire measurement period

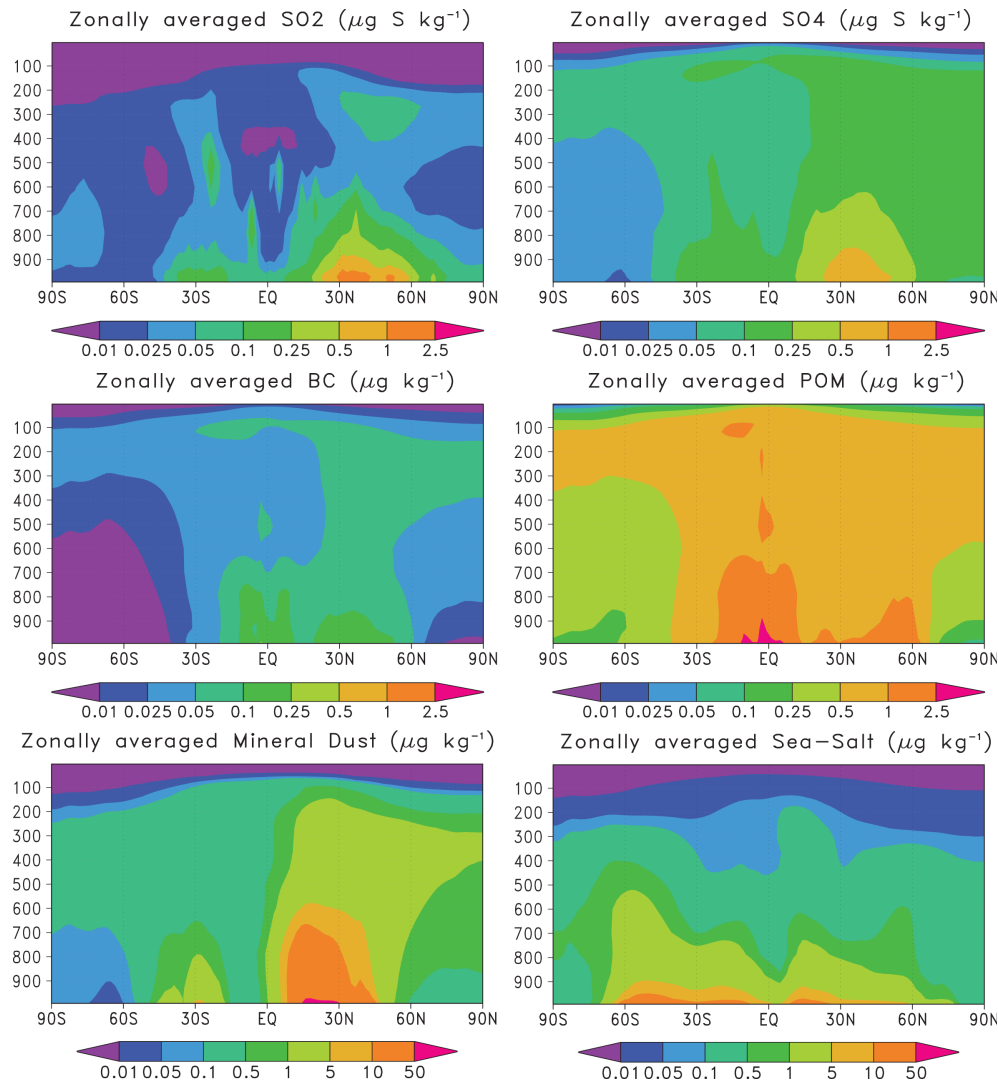


**Fig. 3.** Annually and zonally averaged mass mixing ratios of  $\text{SO}_2$  and aerosol constituents in the *Ctrl* simulation.

are compared. The correlation coefficients and the fractions of modeled values lying within a factor 2 and 10 of the measured values are listed in the figure legends.

With the relatively small scavenging coefficient compared to Seland et al. (2008), we now get a 7% positive bias in the average mineral dust concentration compared to the observed values in Fig. 4. This is a considerable improvement from the 55% underestimate in Seland et al. (2008). Only 15% of the modelled values were within a factor of 2 of the measurements in Seland et al. (2008) whilst the corresponding percentage in this work is 44%. The correlation coefficient is increased from 0.34 to 0.48. Ignoring the outliers for the highest concentrations in the upper right corner of the figure (sites close to the Sahara), there is still a negative bias in remote regions far from deserts. This may be an indication of missing sources, e.g. from semi-deserts or smaller deserts which are not included in the model, agricultural re-

gions, process industry, and road transport. Even though the treatment of deposition has been updated since Seland et al. (2008) and Hoose et al. (2009), the possibility that the deposition of mineral dust is still overestimated cannot be ruled out, e.g. close to sources where many dust-compounds are hydrophobic.

Although the sea salt emissions are parameterized in a more physically based manner (temperature and wind dependency) than in Seland et al. (2008), where the emissions were simply prescribed, modeled near-surface sea salt mass concentrations in CAM4-Oslo are in poorer agreement with the available observations. We estimate a 27% positive bias, with 42% of the data within a factor of 2 of the measurements and a correlation coefficient of 0.58, compared to 3%, 41% and 0.73, correspondingly, in Seland et al. (2008). Overestimates are smaller for high concentrations than for lower concentrations. The prescribed emissions used in that

**Table 6.** Calculated global annual burdens and residence times ( $\tau$ ) for the individual modelled species for the sensitivity tests defined in Table 5. Data from the *Ctrl* and the *Online* experiments are from the simulation year 7. The sensitivity tests are restarted from the *Ctrl* PD and PI experiments 11 months before the beginning of year 7, taking the first 11 months as spin-up. Results of the sensitivity tests are shown when their changes relative to *Ctrl* are larger than 1 % (normal types) and 5 % (bold types). The upper values in a table cell are for present-day emissions (PD) and the lower for preindustrial emissions (PI). For the *no coating* and *prescr $\beta$*  experiments, burdens and residence times are identical to *Ctrl*.

Experiment	SO <sub>2</sub>		SO <sub>4</sub>		BC		OM		SS		DU		
	Burden [Tg]	$\tau$ [days]	Burden [Tg]	$\tau$ [days]	Burden [Tg]	$\tau$ [days]	Burden [Tg]	$\tau$ [days]	Burden [Tg]	$\tau$ [days]	Burden [Tg]	$\tau$ [days]	
<i>Ctrl</i>	PD	0.287	1.068	0.690	3.901	0.243	8.300	3.933	7.849	4.931	0.277	11.700	2.548
	PI	0.0868	1.072	0.209	3.214	0.0600	7.124	2.264	7.322				
<i>natOM</i>	PD							<b>3.158</b>	8.112				
	PI							<b>1.484</b>	7.513				
<i>natOMocn</i>	PD							<b>3.529</b>	8.032				
	PI							<b>1.859</b>	7.511				
<i>bbPOM</i>	PD							<b>2.855</b>					
	PI							<b>1.838</b>					
<i>Struthers11</i>	PD									<b>6.935</b>	<b>0.293</b>		
	PI												
<i>dustscavin</i>	PD							7.860				<b>8.628</b>	<b>1.880</b>
	PI												
<i>cldtunorig</i>	PD			<b>0.644</b>	<b>3.682</b>	0.234	7.971	3.764	7.513				
	PI	0.0857	1.058	<b>0.199</b>	<b>3.088</b>	0.0578	6.872	2.181	7.062	4.790	0.270	11.55	2.515
<i>gravdep2d</i>	PD			0.710	4.019	0.251	8.560	4.044	8.075				
	PI			0.214	3.295	0.0608	7.130	2.303	7.452	<b>7.284</b>	<b>0.409</b>	<b>16.77</b>	<b>3.654</b>
<i>convmix</i>	PD	<b>0.266</b>	<b>0.990</b>	<b>0.554</b>	<b>3.154</b>	<b>0.196</b>	<b>6.682</b>	<b>3.104</b>	<b>6.217</b>	<b>4.50</b>	<b>0.25</b>	<b>10.95</b>	<b>2.39</b>
	PI	<b>0.0823</b>	<b>1.010</b>	<b>0.184</b>	<b>2.821</b>	<b>0.0511</b>	<b>6.072</b>	<b>1.825</b>	<b>5.939</b>				
<i>noBCac</i>	PD					<b>0.194</b>	<b>6.618</b>						
	PI					<b>0.0528</b>	<b>6.268</b>						
<i>repH2O2</i>	PD	<b>0.265</b>	<b>0.986</b>	0.676	3.742								
	PI	<b>0.0819</b>	<b>1.011</b>	0.202	3.214								
<i>EmPD2000</i>	PD	<b>0.241</b>	1.106	<b>0.592</b>	3.800	<b>0.172</b>	8.115	<b>2.859</b>	7.576				
	–												
<i>EmPI1750</i>	–												
	PI	<b>0.0817</b>		<b>0.197</b>		<b>0.0267</b>	6.935	<b>1.918</b>	7.219				
<i>Online</i>	PD	0.280	1.045	<b>0.640</b>	<b>3.619</b>	<b>0.280</b>	<b>9.518</b>	<b>4.786</b>	<b>9.515</b>	<b>4.458</b>	<b>0.254</b>	11.54	2.510
	PI			<b>0.190</b>	<b>2.950</b>	<b>0.0559</b>	<b>6.648</b>	<b>2.106</b>	<b>6.816</b>	<b>4.602</b>	<b>0.254</b>	11.30	2.461

work were pre-calculated values (Dentener et al., 2006) with winds from a reanalysis of the meteorology for year 2000. Due to identical meteorology in all offline configurations of the present model setup, the modeled sea salt emissions are the same whether the anthropogenic emission year is assumed to be 2000 or 2006. However, we do find considerable improvement in the sea salt concentrations compared to the earlier version of the emission parameterization used in Struthers et al. (2011); see Sect. 5.2.

Modeled SO<sub>4</sub> concentrations are somewhat overestimated (23 %) and slightly more so than in Seland et al. (2008), but with approximately the same correlation coefficient (0.64) and percentage of modeled values within a factor of 2 of the measurements (77 %).

BC is underestimated with the same amount (18 %) as in Seland et al. (2008), but with a slightly lower correla-

tion coefficient (0.43). One might suspect that this is a result of using 2006 instead of 2000 BC emissions in the *Ctrl* simulation. When we instead use the 2000 emissions (the *EmPD2000* simulation, see Sect. 5.1), the correlation coefficient indeed improves (0.49), but the overall underestimate gets more severe (36 %). Also when comparing modeled AOD with ground and satellite based remote retrievals in Fig. 6, we get larger underestimates for most latitudes with the 2000 emissions. This is not caused by the differences in BC emissions only.

OM concentrations are compared with measured OC concentrations in Fig. 4. The model does not keep track of the OM/OC ratio, resulting from the mixing of OM from different sources. Thus OC in the present model version is not known. The comparison with measured OC therefore requires an estimate of the (unknown) OM/OC mass ratio



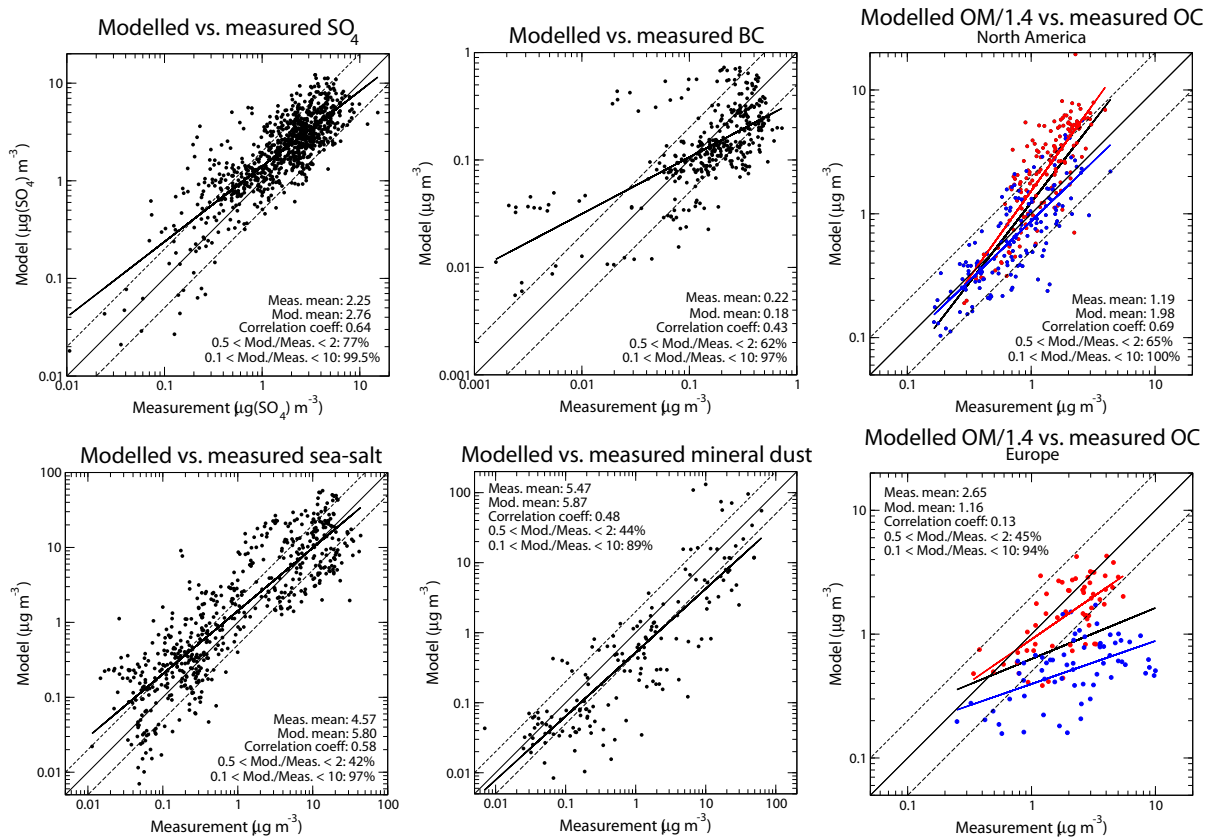


**Fig. 4.** Modeled versus measured monthly mean ground-level mass concentrations of selected aerosols. The measurements, all from 1996–2002, are made available through the AeroCom project from the AEROCE, AIRMON, EMEP, GAW and IMPROVE measurements networks. The European (EMEP) data are from year 2002, however, and OC data are here given as  $\text{PM}_{10}$ , while the North American OC data are given as  $\text{PM}_{2.5}$ . The European OC measurements have therefore here been scaled by a factor 0.72, to account for the difference between  $\text{PM}_{2.5}$  and  $\text{PM}_{10}$ . The OM data have been split into summer (April–September, red) and winter (October–March, blue). The straight diagonal solid and dashed lines define identical results and a factor 2 difference between the modeled and measured data, respectively. The bold solid lines are regression lines for summer (red), winter (blue) and the full year (black).

in the model. We should also keep in mind other potential sources of disagreement, such as uncertain emission magnitudes, missing emission categories, and vertical mixing conditions.

The modeled OM partly originates from fossil fuel combustion with an assumed OM/OC ratio of 1.4, and biomass burning with an assumed ratio of 2.6. See Sect. 2.1.4. Emissions of natural biogenic OM, SOA (treated as primary OM) and MSA are given directly as OM. Therefore the OM/OC ratios for these compounds are not required in the model itself. OM/OC ratios are typically somewhat larger than 1.4 for natural biogenic OM and SOA (e.g. Bergström et al., 2012), and for MSA ( $\text{CH}_4\text{O}_3\text{S}$ ) it is as large as 8.0. However, since MSA is not abundant over continents, its impact on surface mass concentrations to be compared with observations are assumed small, except at coastal measurement sites. In Fig. 4 we have chosen to compare modeled OM/1.4 with measured OC, assuming that OM/1.4 is an upper estimate of the modeled OC concentration. These model values are thus

representative for OC which mainly originates from fossil fuel combustion sources, but are otherwise overestimates.

For the North American stations the modeled OM/1.4 is 66 % larger than the measured OC, while it was 9 % smaller in Seland et al. (2008). Here, 65 % of the data are within a factor of 2 of the measurements, and the correlation coefficient is 0.69. Hypothetically, assuming that all OM were from biomass burning, we should have compared OM/2.6 with the measured OC values, yielding a 10 % negative bias. Splitting the data in NH summer (April–September) and winter (October–March), marked in red and blue in Fig. 4, reveals that the correlation coefficient is about the same for both seasons, 0.69 and 0.68 respectively, but that the overestimates are mostly confined to the summer ( $\sim 100\%$ ) and that the modeled values of OM/1.4 are very close to the observed OC in winter ( $\sim 1\%$ ). This may suggest that sources with OM/OC ratios which are higher than 1.4 dominate in summer, or that OC concentrations are overestimated in summer.

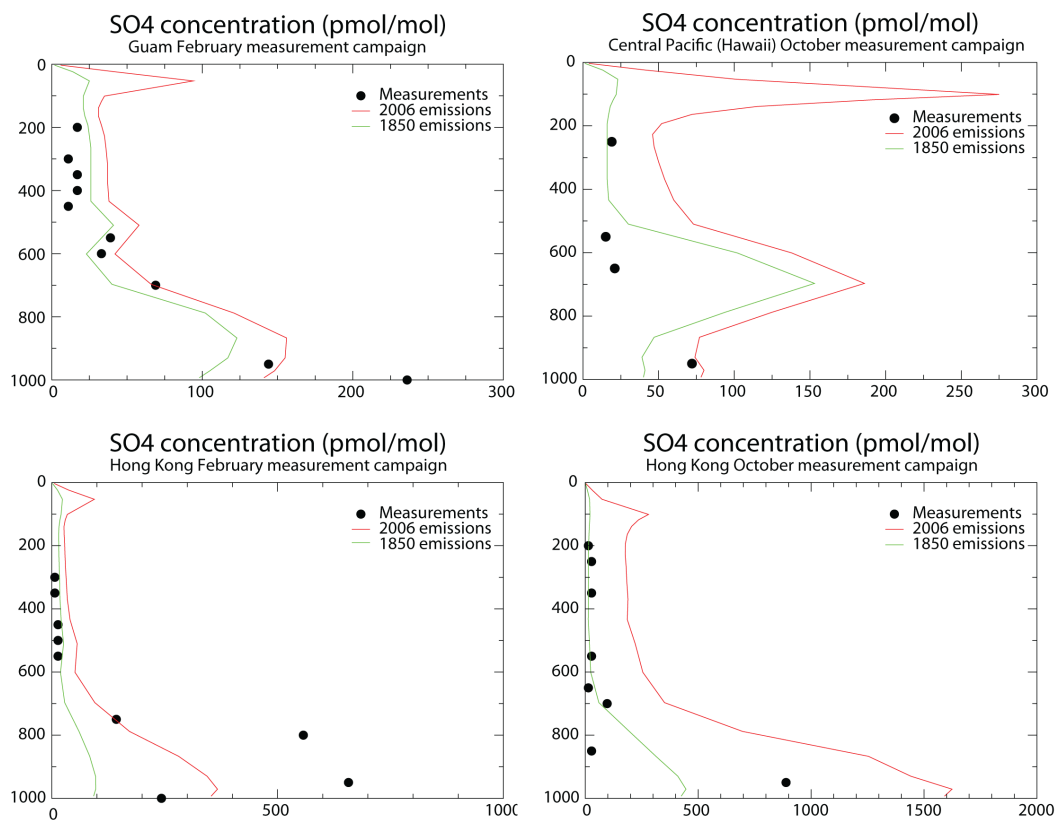


**Fig. 5.** Vertical profiles of SO<sub>4</sub> mixing ratios compared to flight measurements from the Pacific Exploratory Mission (PEM) over the period 1996–1999 presented in Barth et al. (2000). The circles denote measurements, and continuous red and green lines represent the *Ctrl* PD and PI simulations, respectively.

However, the validation results for the European stations, using the OM/OC ratio of 1.4, suggest that modeled OM is still considerably underestimated in large regions. The difference in model bias between European and North American stations is to some extent caused by different measurement statistics. While the recommendation for the North American OC measurements (IMPROVE, rural background stations) is to use PM<sub>2.5</sub> aerosol fraction, the European OC data (EMEP, including also some urban background stations) represent the PM<sub>10</sub> fraction and may therefore contain additional coarse particulate OM. Only a tiny mass fraction of OM with particle diameters exceeding 2.5 μm is produced in our model, however, and coarse mode primary biogenic OM is not included in the emissions. In the scatter plot for Europe we have roughly estimated the PM<sub>2.5</sub> fraction of measured OC by multiplying the measured PM<sub>10</sub> OC concentrations with 0.72. This number is based on three individual European stations which have both PM<sub>2.5</sub> and PM<sub>10</sub> data (Yttri et al., 2011), Birkenes in Norway, Melpitz in Germany and Montseny in Spain, where the PM<sub>2.5</sub>/PM<sub>10</sub> ratios for OM are estimated at 0.76, 0.74 and 0.67, respectively.

Taking the correction factor of 0.72 into account, modeled OM/1.4 for all stations and all the months is on average 46 %

smaller than measured OC, compared to a 65 % underestimate in Seland et al. (2008). These underestimates may be partly due to underestimated emissions for Europe. Seland et al. (2008) used 2000 emissions, without some of the extreme forest fire episodes that we find in the 2006 emissions. Using 2000 emissions also in CAM4-Oslo, we also get a larger underestimate of about 53 %. If we remove two observations of large forest fires, the August data from Braganca in Spain and the April data from Virolahti in Finland, our modeled OM/1.4 average with the 2006 emissions is 60 % lower than the measured OC concentrations.

Here it should be noted that anthropogenic SOA is not modeled in CAM4-Oslo, a source which could contribute significantly to OM mass, especially close to polluted urban areas. Since a larger fraction of the North American stations are located in rural areas than the European stations, this missing source may explain why OM is underestimated in particular in Europe. Removing three European stations with urban conditions (Bologna, Edinburgh, and Gent), modeled OM/1.4 is still on average 56 % smaller than measured OC. For this final selection of observations and stations used in Fig. 4, i.e. all except for the three urban stations and two monthly observations influenced by forest fires, 45 % and

**Table 7.** Aerosol optical depth (AOD) and absorptive optical depth (ABS) at 550 nm, top of the atmosphere direct radiative forcing (DRF), cloud droplet number concentrations (CDNC) and effective cloud droplet radii ( $r_{\text{eff}}$ ) at 870 hPa, liquid water path (LWP), and indirect radiative forcing (IndRF) for *Ctrl* and the sensitivity experiments defined in Table 5. See the main text or Table 6 for the definition of simulation periods. DRF and IndRF are not estimated for the *Online* experiment.

Experiment		AOD (550 nm)	ABS (550 nm)	DRF at TOA ( $\text{W m}^{-2}$ )	DRF at Surface ( $\text{W m}^{-2}$ )	CDNC (870 hPa) ( $\text{cm}^{-3}$ )	$r_{\text{eff}}$ (870 hPa) ( $\mu\text{m}$ )	LWP ( $\text{g m}^{-2}$ )	IndRF at TOA ( $\text{W m}^{-2}$ )
<i>Ctrl</i>	PD 2006	0.154	0.00632			52.4	9.41	130.5	
	PI 1850	0.101	0.00264			36.0	9.77	126.6	
	PD-PI	0.0535	0.00369	-0.0724	-1.89	16.4	-0.359	3.93	-1.20
<i>natOM</i>	PD 2006	0.143	0.00615			46.0	9.96	124.9	
	PI 1850	0.090	0.00245			28.3	10.48	119.0	
	PD-PI	0.0529	0.00370	-0.0673	-1.89	17.7	-0.528	5.94	-1.90
<i>natOMocn</i>	PD 2006	0.148	0.00623			48.5	9.85	126.1	
	PI 1850	0.094	0.00254			31.4	10.33	120.8	
	PD-PI	0.0532	0.00369	-0.0706	-1.89	17.0	-0.479	5.25	-1.66
<i>bbPOM</i>	PD 2006	0.142	0.00608			47.8	9.50	129.5	
	PI 1850	0.096	0.00254			32.0	9.87	125.6	
	PD-PI	0.0461	0.00354	+0.0722	-1.68	15.7	-0.370	3.96	-1.20
<i>Struthers11</i>	PD 2006	0.159	0.00632			52.1	9.43	130.5	
	PI 1850	0.106	0.00264			35.7	9.79	126.5	
	PD-PI	0.0535	0.00369	-0.0694	-1.88	16.4	-0.362	3.94	-1.21
<i>dustscavin</i>	PD 2006	0.143	0.00597			52.5	9.41	130.6	
	PI 1850	0.089	0.00235			35.7	9.78	126.5	
	PD-PI	0.0536	0.00362	-0.103	-1.89	16.8	-0.372	4.06	-1.23
<i>cldtunorig</i>	PD 2006	0.147	0.00603			51.1	8.92	100.0	
	PI 1850	0.096	0.00255			35.2	9.25	97.9	
	PD-PI	0.0500	0.00351	-0.0855	-1.81	15.9	-0.330	3.09	-1.28
<i>gravdep2d</i>	PD 2006	0.168	0.00683			52.0	9.44	130.2	
	PI 1850	0.113	0.00298			35.6	9.80	126.3	
	PD-PI	0.0544	0.00385	-0.0263	-1.93	16.4	-0.364	3.96	-1.21
<i>convmix</i>	PD 2006	0.132	0.00518			53.4	9.40	129.1	
	PI 1850	0.089	0.00229			37.0	9.74	125.4	
	PD-PI	0.0429	0.00289	-0.0972	-1.48	16.5	-0.340	3.67	-1.15
<i>noBCac</i>	PD 2006	0.153	0.00585			52.4	9.41	130.4	
	PI 1850	0.101	0.00257			36.0	9.77	126.6	
	PD-PI	0.0529	0.00329	-0.164	-1.78	16.4	-0.358	3.91	-1.20
<i>replH2O2</i>	PD 2006	0.154	0.00632			52.3	9.41	130.4	
	PI 1850	0.100	0.00264			35.9	9.77	126.6	
	PD-PI	0.0534	0.00368	-0.0703	-1.88	16.4	-0.356	3.87	-1.19
<i>no coating</i>	PD 2006	0.154	0.00632			48.4	9.44	130.1	
	PI 1850	0.101	0.00264			31.2	9.87	125.5	
	PD-PI	0.0535	0.00369	-0.0724	-1.89	17.3	-0.426	4.52	-1.31
<i>prescr<math>\beta</math></i>	PD 2006	0.154	0.00632			52.4	9.14	130.5	
	PI 1850	0.101	0.00264			36.0	9.57	126.6	
	PD-PI	0.0535	0.00369	-0.0724	-1.89	16.4	-0.425	3.93	-1.34
<i>EmPD2000</i>	PD 2000	0.135	0.00460			48.3	9.47	129.7	
	PI 1850	0.101	0.00264			36.0	9.77	126.6	
	PD-PI	0.0346	0.00197	-0.0997	-1.04	12.3	-0.296	3.10	-0.908
<i>EmPI1750</i>	PD 2006	0.154	0.00632			52.4	9.41	130.5	
	PI 1750	0.095	0.00193			32.1	9.90	125.3	
	PD-PI	0.0589	0.00438	-0.0416	-2.20	20.3	-0.488	5.20	-1.53
<i>EmPD2000 &amp; EmPI1750</i>	PD 2000	0.135	0.00460			48.3	9.47	129.7	
	PI 1750	0.095	0.00193			32.1	9.90	125.3	
	PD-PI	0.0399	0.00267	-0.0689	-1.36	16.1	-0.425	4.37	-1.23
<i>Online</i>	PD 2006	0.151	0.00725			49.0	9.50	130.3	
	PI 1850	0.092	0.00247			34.6	9.86	124.4	
	PD-PI	0.0588	0.00478	-	-	13.4	-0.342	5.89	-

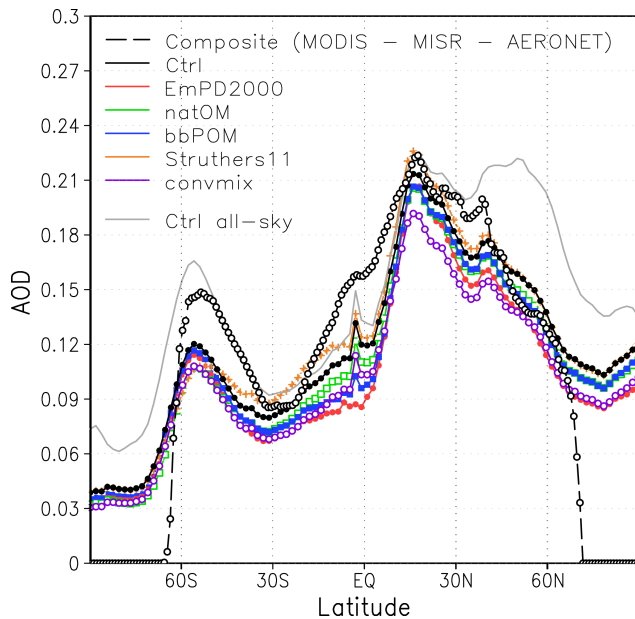


**Fig. 6.** Zonally and annually averaged clear-sky aerosol optical depth (AOD) at 550 nm from ground- and satellite-based retrievals (S. Kinne, personal communication, 2007), and calculated with CAM4-Oslo for year 7 of the *Ctrl* experiment and a selection of sensitivity tests. For comparison with the clear-sky AOD, also all-sky AOD at 550 nm is shown for the *Ctrl* simulation (gray solid line).

94 % of the data are within a factor of 2 and 10 of the measurements, respectively. We believe that the European OM model bias might be even larger because SOA usually has a higher OM/OC ratio than fossil fuel POM. When chemical aging of POM and SOA is taken into account, model estimates by Bergström et al. (2012) yield OM/OC ratios above 1.9 for most of Europe, exceeding 2.0 in parts of Southern Europe. In summary, if assuming that all OM was in the form of SOA with an OM/OC ratio of 2.0, the bias would be 16 % instead of 66 % for North America, and –69 % instead of –56 % for Europe.

When the OM data are split into two seasons in the figure, we find that the modeled OM/1.4 for Europe in summer is much closer to the observed OC concentrations than in winter. Bias and correlation coefficients for the summer are –24 % and 0.58, compared to –80 % and 0.24 for winter. This result indicates that the missing anthropogenic SOA, which would be formed mainly when levels of photo-oxidants are high in summer, cannot explain all of the discrepancies. The winter bias for OM is more plausibly explained by underestimated emissions of biogenic OM from bio-fuels (e.g., wood-burning). Furthermore, strong inversions in the winter will lead to very high surface concentrations close to ground surface emission sources, while elevated emissions from stacks will not contribute to surface concentrations. Since such inversions are shallow and lo-

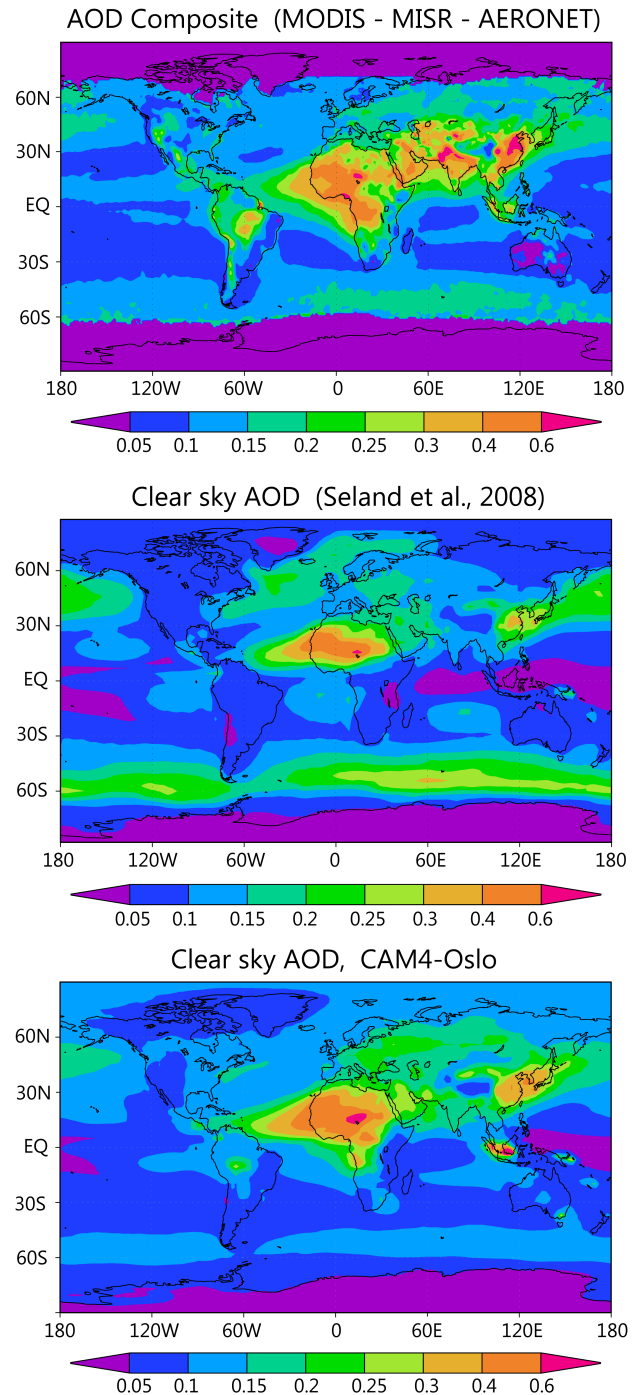


**Fig. 7.** Annually averaged clear-sky aerosol optical depth (AOD) at 550 nm from ground- and satellite-based retrievals in the upper panel (S. Kinne, personal communication, 2007), as calculated in Seland et al. (2008) in the middle panel, and calculated with CAM4-Oslo (*Ctrl*) in the lower panel.

cal in nature, they are poorly represented in climate models. Hence, this continental winter phenomenon may intermittently give rise to large underestimates of aerosol mass concentrations near the surface. This is possibly less of a problem for the North American stations because their location further south makes them less prone to inversions, and because the more pristine location of the stations makes them less exposed to anthropogenic organic aerosols than the European stations.

#### 4.2.2 Vertical concentration profiles

Figure 5 shows modeled vertical profiles of sulphate volume mixing ratios compared with flight campaign measurements from the Pacific Exploratory Mission (Barth et al., 2000). As in Seland et al. (2008), the model compares reasonably well with observations at low altitudes, while overestimating the mixing ratios in the upper troposphere, where the modeled preindustrial sulphate levels are closer to the observations than the present-day levels. Although the ad hoc assumption of full mixing of aerosols between convective cloud updrafts and downdrafts in Seland et al. (2008) has been removed in CAM4-Oslo (see Sect. 2.1.5), the sulphate profiles are quite similar to Fig. 8 in that work. We get slightly improved results for Guam at all heights and for Hawaii up to about 400 hPa, where the positive biases are smaller in CAM4-Oslo. For Hong Kong the overestimates are larger at all heights for the October data. For the February data we find only small changes in the middle and upper troposphere and a reduction of the overestimate for the near ground level, while the underestimate of the lower troposphere maximum is more pronounced than in Seland et al. (2008).

#### 4.2.3 Column-integrated optical properties

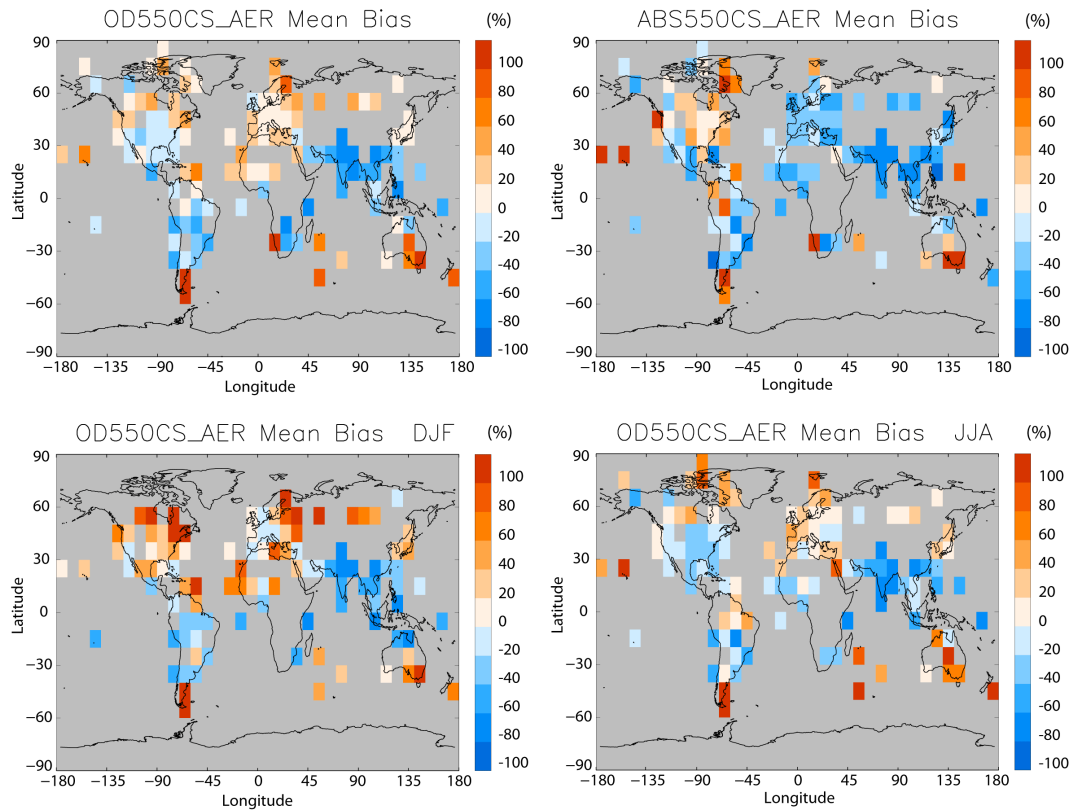
Figures 6 and 7 compare modelled aerosol optical depth with a composite of ground- and satellite-based remote retrievals. The results in Fig. 6 also corroborate the new OM treatment: both of the tests using an older version (bbPOM and natOM, see Sects. 5.3 and 5.4) give too low a clear-sky aerosol optical depth (AOD) at most latitudes. The clear-sky aerosol optical depth is estimated as all-sky optical depth weighted with the clear-sky fraction, based on total cloud cover in the model. This clear-sky definition gives larger weight to conditions when sun photometer observations can be made.

Figure 8 shows biases in modelled optical properties compared with ground-based sun photometry retrievals (AERONET, years 2000–2009). As seen from Figs. 6, 7 and 8, annually averaged AOD is underestimated in most regions. In large parts of the tropics and subtropics the model underestimates both AOD and absorption AOD (ABS), see Fig. 8. The strongest and most persistent negative biases throughout the year are found in South Asia. As in the previous model version by Seland et al. (2008), too much and too frequent precipitation over the Indian Ocean and parts of the continent

of southern Asia (not shown) lead to exaggerated wet deposition estimates, which probably explains some of the negative biases for that region. In the densely populated South Asian region we also anticipate that we missed important contributions from secondary aerosol formation of organics, and possibly also mineral dust from dry soils.

On the other hand, AOD is overestimated in some (mostly remote) regions at high latitudes, but more so compared to AERONET than the composite product in Fig. 7. In some regions the respective AOD biases even have opposite signs, e.g. in parts of North America. CAM4-Oslo probably produces excessive tropospheric aerosol concentrations at high latitudes, where most other models are biased on the low side. This may in particular be the case in the Arctic and the Antarctica, where observations are still too sparse to facilitate verification for a good range of conditions. In these regions CAM4-Oslo does indeed yield larger aerosol burdens, AOD, and ABS than most other AeroCom models (Myhre et al., 2012; Samset et al., 2012).

As also seen from Fig. 7, annually averaged AOD is better represented in CAM4-Oslo than in Seland et al. (2008). The improved results in the present work may be due to several of the model updates. In addition to the updated PD emissions, the new natural OM treatment and updated assumptions about OM/OC ratio for biomass burning OM are important contributors. The modified convective transport also reduces the bias in the areas influenced by biomass burning, although as discussed in Sect. 5.1.1, it probably exaggerates the amount of aerosols in the upper troposphere. We also find an improvement related to mineral dust when comparing modelled and retrieved seasonal AOD for specific dust dominated AERONET stations (not shown). This is a combined result of several changes implemented after the version by Seland et al. (2008) as detailed in Sect. 5. The new treatment of gravitational settling, for instance, tends to reduce the dust concentrations, whilst the increased vertical transport in convective clouds tends to increase the concentrations at middle and upper levels, and the reduced in-cloud scavenging for mineral dust increases the general abundance of dust, in particular far from the major source regions. In North Africa and the few AERONET stations of the northern tropical Atlantic and the Caribbean Sea, there is a positive AOD bias averaged over the year, see Fig. 8. The AOD bias in western North Africa is mainly positive, but small in spring (MAM, not shown) and negative in summer (JJA). Here ABS remains negatively biased throughout the year (seasonality not shown). This may be due to seasonal and possibly spatial biases in the mineral dust emissions or in the transport of mineral dust from North Africa. The lack of coupling between model wind fields and the (prescribed) mineral dust emissions, given from meteorological conditions for one year only, may also lead to systematic biases in the transport and deposition. In addition the results may be influenced by model biases in biomass burning in the Sahel region and further south (see e.g. Ridley et al., 2012).



**Fig. 8.** Biases compared to AERONET (in %) in estimated clear-sky aerosol optical depth (AOD at 550 nm, upper left and lower panels) and aerosol absorption optical depth (ABS at 550 nm, upper right panel) with CAM4-Oslo. AOD and ABS biases in the upper row are yearly averaged, and AOD biases in the lower row are for NH winter (DJF) and summer (JJA). The AERONET retrievals are from the period 2000–2009, and are made available through the AeroCom project.

The scatter plots and frequency histograms in Fig. 9 are for monthly AOD, ABS and ANG (Ångström parameter) from CAM4-Oslo vs. AERONET stations worldwide, excluding the stations situated above 1000 m altitude. Modelled clear-sky AOD and ABS are underestimated by approximately 8 % and 32 %, respectively. The frequency histograms reveal that CAM4-Oslo produces too few of the lowest and highest AOD and ABS values, whilst intermediate values are overrepresented. Since the surface concentrations in Fig. 4 do not show the same behavior, the positive bias for low to intermediate values of AOD and ABS may indicate that the model produces too high aerosol concentrations at middle and upper levels in the model atmosphere. Representation of aerosol processes that are known to be associated with large uncertainties in GCMs in general may contribute to these biases, such as the treatment of vertical transport and mixing of aerosols or the assumed size of BC particles from rapid fossil fuel combustion near the point of emission. The negative bias for high values could possibly be an indication of missing coarse mode OM or other aerosol components (e.g. nitrate, anthropogenic SOA, non-desert dust). We cannot rule out the possibility that some of the skewness in the frequency histograms could be the result of a more general

misrepresentation of aerosol dispersion and aerosol particle size in the model, affecting aerosol microphysics and subsequent lifetimes, column burdens and optical depths.

The Ångström parameter (e.g. Seinfeld and Pandis, 1998), here defined as

$$\text{ANG} = -\ln\left(\frac{\text{AOD}_{870}}{\text{AOD}_{440}}\right) / \ln\left(\frac{870}{440}\right), \quad (5)$$

provides an indirect measure of the modelled particle sizes for the bulk aerosol, and can be compared with AERONET retrievals. For the wavelengths 440 and 870 nm, unfortunately only all-sky AOD data are available in the model output. This leads to overrepresentation of the larger particle sizes, since the relative humidity and hygroscopic growth of soluble aerosols is larger in cloudy than clear-sky conditions, and it can probably explain some of the bias toward low ANG values in the frequency histogram in Fig. 9. In the PD *Ctrl* simulation, globally averaged clear-sky AOD divided by all-sky AOD at 550 nm is 0.84 (see also Fig. 6), but since we do not know the wavelength dependency of this ratio, it is difficult to tell how much of the ANG bias we can attribute to this effect.



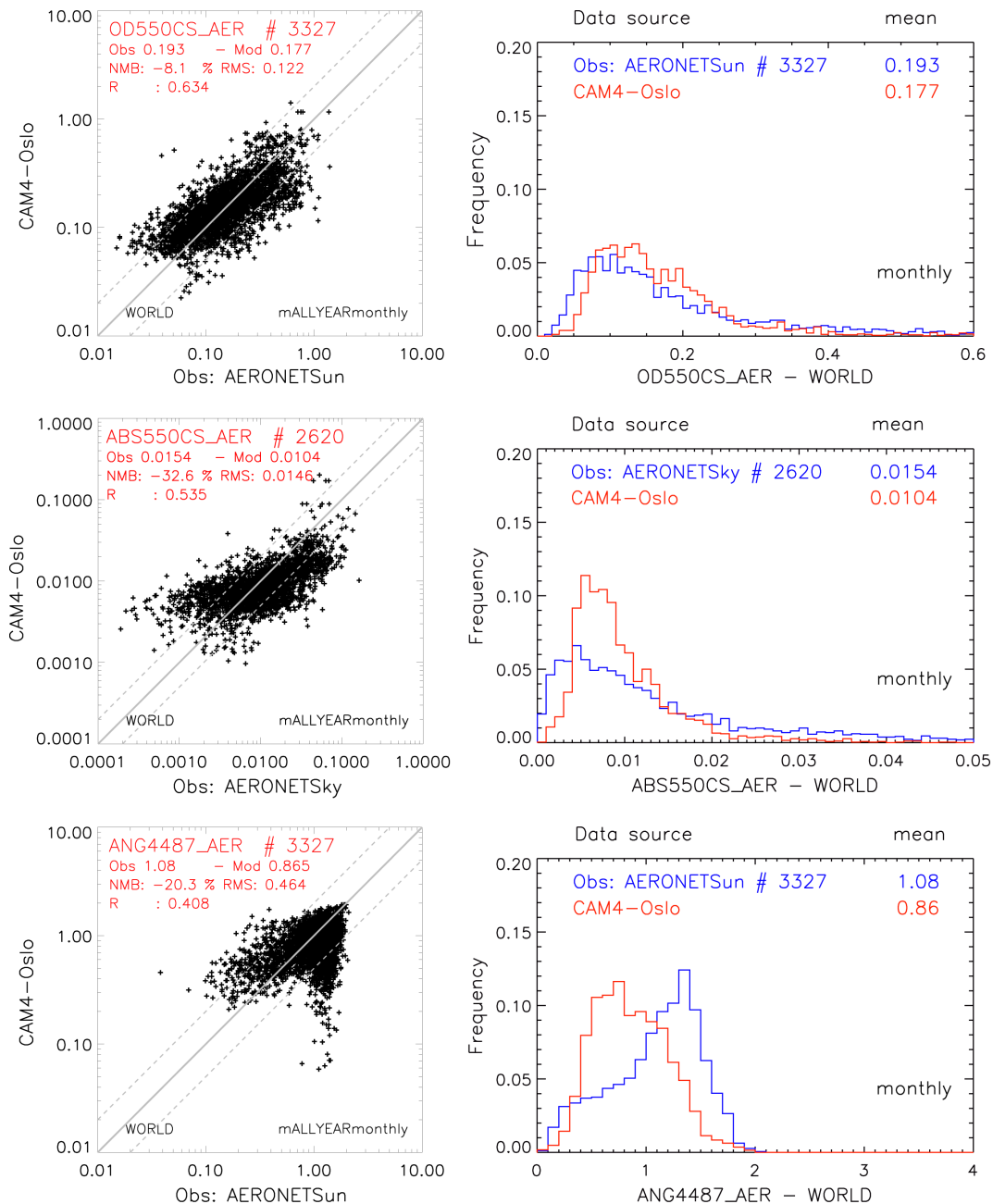


**Fig. 9.** Model-calculated vs. retrieved aerosol optics data from AERONET, shown as scatterplots (left) and frequency histograms (right). Upper row: modeled clear-sky AOD at wavelength 550 nm vs. AERONET. Middle row: modeled clear-sky ABS (absorption AOD) at wavelength 550 nm vs. AERONET ABS. Lower row: ANG (Ångström parameter) calculated from all-sky AOD at 440 and 870 nm. The AERONET retrievals are from the period 2000–2009, and are made available through the AeroCom project.

Averaged over all stations and all months, ANG is underestimated by about 20%. The largest bias of -31% is found in the NH winter (DJF), constituting much of the right side branch in the ANG scatter plot, and the smallest bias, only -11%, is during NH summer (JJA). The lowest and highest correlation coefficients are found for the same two seasons, -0.02 and 0.66 respectively, compared to 0.41 averaged over the whole year. As in Seland et al. (2008), ANG

values exceeding 1.5 (fine particles) are mainly confined to tropical and subtropical land areas, especially in the biomass burning season, and values below 0.5 (coarse particles) are found mainly over or directly downstream of oceans or large deserts, with maxima over oceans in winter. In the corresponding PD *Online* simulation (see Table 6), which is the most relevant simulation for climate response studies, ANG is somewhat improved for all seasons compared to the offline



simulation (*Ctrl*). The global bias is here  $-16\%$ , annually averaged.

#### 4.2.4 Vertical extinction profiles

Figure 10 shows annually averaged extinction coefficient profiles over ocean and land, globally, and for winter (DJF) and summer (JJA) over land in Europe and North America, all for the *Ctrl PD* simulation compared with nighttime CALIOP (Cloud-Aerosol Lidar with Orthogonal Polarization) data for year 2007 (B. Koffi, personal communication, 2012), the first full year where the CALIOP instruments were in operative mode. CALIOP data preparation has been described by Koffi et al. (2012a). As in several other AeroCom models studied by Koffi et al. (2012a) and Koffi et al. (2012b), the aerosol extinction in CAM4-Oslo seems to be overestimated in the upper troposphere. It is probable that this is an effect of a too efficient vertical transport in deep convective clouds in the model (Sects. 2.1.5 and 5.11).

However, an underestimate of the aerosol extinction in the upper troposphere by the CALIOP retrieval algorithm would also contribute to such biases. Such underestimates in the CALIOP data are possibly due to a relatively high detection limit for significant aerosol layers, identified by the retrieval algorithm. According to Koffi et al. (2012a) the detection limit at night for the 5 km CALIOP layer product is estimated to be between  $0.010$  and  $0.015 \text{ km}^{-1}$ , and atmosphere layers with no detected aerosols are assumed to have zero aerosol extinction in that work as well as in Fig. 10. Globally and annually averaged extinction in *Ctrl* is smaller than the detection limit at all heights above roughly 2–3 km altitude, which clearly makes the model vs. CALIOP validation of the aerosol profile in the upper troposphere very uncertain. Assuming a background aerosol extinction of  $0.005 \text{ km}^{-1}$  (instead of zero), which is on the high end of a range of background values from satellite retrievals (Kent et al., 1998) and actually close to the globally averaged extinction at 10 km height in CAM4-Oslo ( $0.006 \text{ km}^{-1}$ ), Koffi et al. (2012a) found that this was enough to reverse the conclusion about the AeroCom model performance in the upper atmosphere, with the exception for one model which still overestimated the extinction at high altitudes.

There are also clear biases in the profiles in the boundary layer and up to about 2 km height, where models with coarse vertical resolution are not capable of capturing the observed maximum at about 0.5 km height (Koffi et al., 2012a). Averaged over all land grid points globally, our model seems to capture both the vertical slope and the maximum extinction reasonably well in the lower troposphere, although the maximum is overestimated by about 30 % compared to CALIOP. Over oceans the modeled maximum is located too close to the sea surface, and the extinction values are underestimated by up to about 50 % in the lower 1.5 km a.s.l. The aerosol extinction is overestimated by up to about 100 % between 1.5 and 3 km height a.s.l.

For continental Europe, here defined as approximately the area spanned by the EMEP stations in Fig. 4 (land between  $35\text{--}70^\circ \text{ N}$  and  $10^\circ \text{ W--}40^\circ \text{ E}$ ), the annually averaged extinction profile (not shown) is very similar to the global land profile, but with somewhat larger biases above 2 km. For continental North America, here defined as approximately the same area as spanned by the IMPROVE stations in Fig. 4, minus Hawaii, Bermuda and Denali (land between  $25\text{--}50^\circ \text{ N}$  and  $65\text{--}125^\circ \text{ W}$ ), the respective extinction values (not shown) instead have a negative bias below 4 km height, but only very small biases below 0.5 km. These regional features are consistent with the annually averaged AOD biases in Fig. 8. However, this should be interpreted with caution, since the AERONET stations do not cover as wide areas as the CALIOP retrievals, and unlike the AERONET data, CALIOP also include results for nighttime and overcast conditions.

The mid- and bottom panels in Fig. 10 show the winter (DJF) and summer (JJA) extinction profiles for continental Europe and North America, revealing a very distinct seasonal behavior. In summer the biases are large and positive above about 4–5 km, although still mostly within the CALIOP detection limit, and negative (up to about 60 %) in the lower 4–5 km. This is consistent with exaggerated convective transport in the model, see Sect. 5.11.

In winter the positive biases in the upper troposphere are smaller for both the regions, and over North America it is small all the way down to sea level (for coastal sites).

Over Europe, the near-surface extinction bias is much larger in winter, and we have not been able to reach a clear conclusion as to why it is so large. The major contributions to all-sky AOD over the European continent during winter are from sulphate (42 %) and organic matter (30 %), followed by sea salt (15 %), mineral dust (12 %), and BC (1 %). Using the same dataset as in Fig. 4, but limited to the 37 European stations, we find a positive bias of only 2 % in the modeled near-surface sulphate mass concentrations ( $2.93 \mu\text{g m}^{-3}$ ) in winter. As already shown in Sect. 4.2 there is a significant negative bias in the modeled OM in Europe in the winter season. It is difficult to reconcile this and the relatively modest (positive and negative) biases in AOD for DJF in Fig. 8 (AERONET) with the large positive biases in extinction (CALIOP) in both the boundary layer and in the upper troposphere. Excessive hygroscopic swelling under very humid conditions, consistent with overcast conditions (included in CALIOP but not in AERONET), could possibly lead to such overestimates in the all-sky aerosol extinction. The clear-sky AOD estimates, however, which are representative for low to intermediate relative humidities, do not seem to support this. In Fig. 8 we find areas with both under- and overestimates for Europe in winter. Uncertainties and systematic biases in the different remote retrievals may also be a possible explanation, although there is only reliable AERONET data from daytime and clear-sky conditions available for performing such inter-comparisons (see e.g. Schuster et al., 2012). The choice of

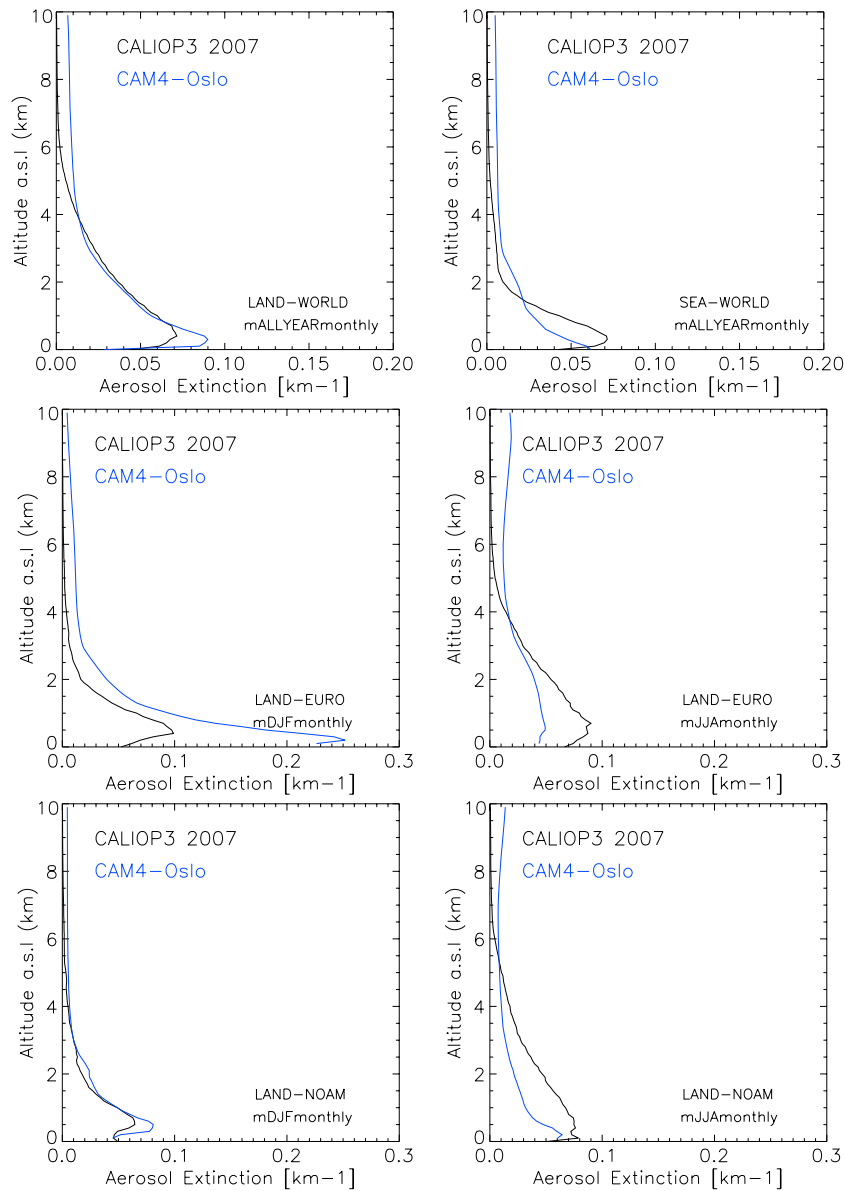


**Fig. 10.** CAM4-Oslo and CALIOP annually or seasonally averaged extinction coefficient profiles ( $\text{km}^{-1}$ ), continents and oceans globally, and for continental Europe ( $35\text{--}70^\circ\text{ N}$  and  $10^\circ\text{ W}\text{--}40^\circ\text{ E}$ ) and North America ( $25\text{--}50^\circ\text{ N}$  and  $65\text{--}125^\circ\text{ W}$ ) for the winter (DJF) and summer (JJA) seasons. The model data are all-sky estimates at  $550\text{ nm}$ , while the CALIOP data are for  $532\text{ nm}$  wavelength and for year 2007.

screening and averaging procedure for near-surface extinction data from CALIOP is potentially also a source of large uncertainty (Winker et al., 2012). Disregarding obvious sampling issues (e.g. day vs. night, clear-sky vs. all-sky, horizontal and temporal coverage), the AOD from AERONET and the AOD calculated as vertically integrated extinctions from CALIOP indeed differ significantly (not shown).

For North America, the biases in AOD from AERONET and in the vertical extinction profiles from CALIOP agree, both indicating overestimated light extinction by aerosols in winter. For comparison to the European values above, the all-sky AOD contributions are here mainly from organic matter

(44 %) and sulphate (34 %), followed by mineral dust (12 %), sea salt (7 %), and BC (3 %).

### 4.3 Aerosol effects on radiation and clouds

Table 4 lists annual globally averaged estimates of optical and cloud microphysical properties associated with the aerosols in *Ctrl*, as well as the direct (DRF) and indirect radiative forcing (IndRF) due to changes from preindustrial (PI, year 1850) to present-day (PD, year 2006) conditions. Figure 11 shows the respective maps of DRF and IndRF at TOA. DRF and IndRF are diagnosed in the way described

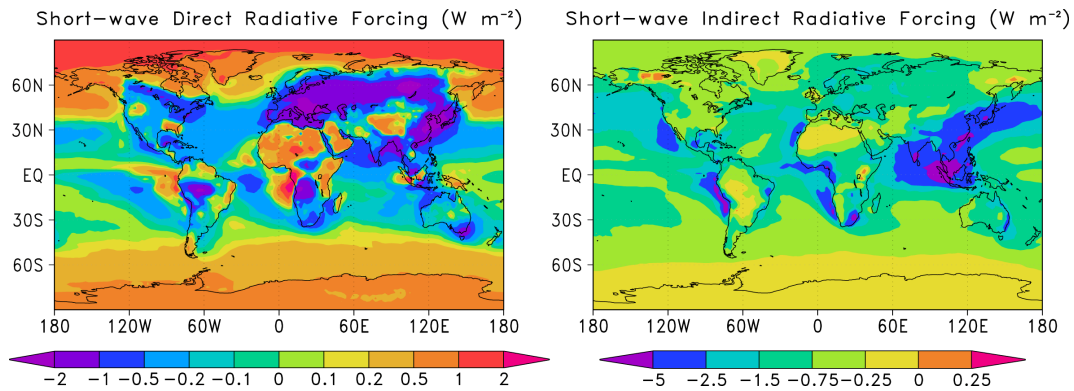


**Fig. 11.** Modeled annual direct (left,  $-0.08 \text{ W m}^{-2}$ ) and indirect (right,  $-1.20 \text{ W m}^{-2}$ ) top of the atmosphere short-wave radiative forcing in the control simulations (*Ctrl*, years 3–7).

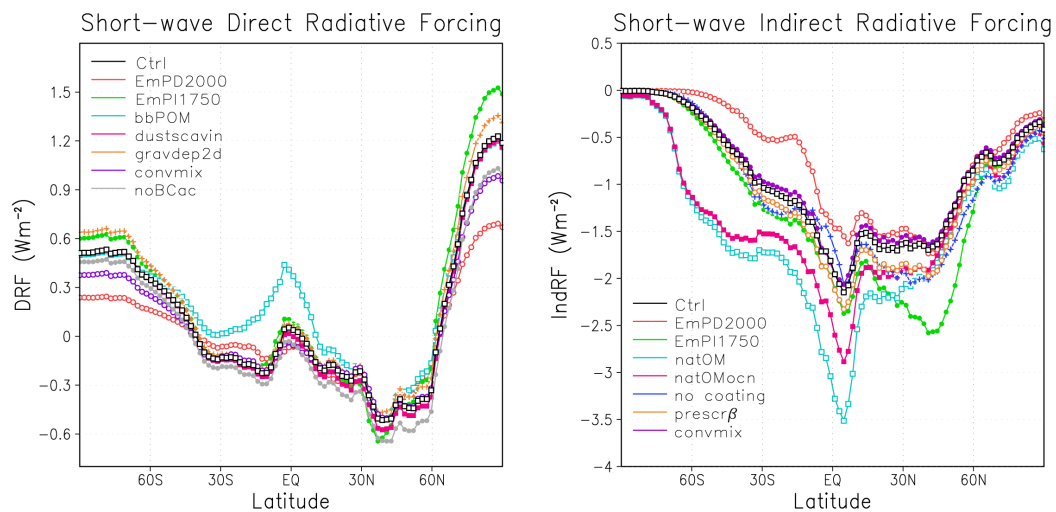


**Fig. 12.** Modeled annual, zonally averaged direct (left) and indirect (right) top of the atmosphere short-wave radiative forcing ( $\text{W m}^{-2}$ ) for the *Ctrl* experiment (year 7) and the sensitivity tests with largest impacts on aerosol forcing.

by Seland et al. (2008), i.e. as differences in all-sky radiative forcing between PD and PI conditions. Although there are differences in forcing values, the regional distributions are quite similar to those estimated by Seland et al. (2008). Negative DRF values due to sulphate and OM below  $-2 \text{ W m}^{-2}$  are estimated over parts of South America, Africa, Europe and East Asia, with two local minima of about  $-3 \text{ W m}^{-2}$  over East Asia. Positive DRF values are found in areas with large BC and OM concentrations (PD-PI) combined with high surface albedos or extensive low clouds, with values exceeding  $1.2 \text{ W m}^{-2}$  over the Arctic sea ice and reaching  $3 \text{ W m}^{-2}$  near the biomass burning areas in southern parts of the tropical African west coast. Globally averaged DRF is  $-0.08 \text{ W m}^{-2}$ , compared to  $+0.03 \text{ W m}^{-2}$  in Seland et al. (2008).

For IndRF, a combination of high concentrations of sulphate and OM and the presence of clouds with high susceptibility produce minimum values of about  $-7.5 \text{ W m}^{-2}$  over

southeastern Asia and the stratocumulus region just off the west coast of South America. Also a few areas with slightly positive IndRF ( $< 0.2 \text{ W m}^{-2}$ ) are found, namely in the Arctic and over eastern Africa. These positive values can be traced back to OM emissions and mass concentrations in the lower troposphere that are lower under PD than PI conditions. Globally averaged IndRF is  $-1.20 \text{ W m}^{-2}$ , compared to  $-1.88 \text{ W m}^{-2}$  in Hoose et al. (2009). The changes in DRF and IndRF from earlier model versions to CAM4-Oslo are due to changes in emissions as well as parameterizations of aerosols and cloud microphysics, and are discussed in more detail in Sect. 5.

Table 4 also lists component-specific contributions to each of the key properties. The main contributors to the increment in AOD from PI to PD are sulphate (65 %) and internally mixed OM/BC from biomass burning (bb, 30 %), while fossil fuel (ff) BC and OM each contribute with approximately 3 %. Due to non-linear effects, probably related to

small differences in size and mixing state of the internally mixed aerosol in these experiments, the sum of each contribution is (only) about 1.5 % larger than the total AOD increment for PD-PI of 0.0527. The corresponding contributions to ABS (absorption AOD) are 4 % for sulphate, 51 % for bb BC and OM, 46 % for ff BC, and only 1 % for ff OM. For ABS the non-linear effect thus gives rise to a 2 % larger sum than the total PD-PI increment of 0.00357. Note that non-absorptive components such as sulphate may also contribute to ABS, if internally mixed with absorptive aerosols.

The TOA DRF contributions from each of these aerosol species (PD-PI) are estimated to about  $-0.48 \text{ W m}^{-2}$  for sulphate,  $+0.37 \text{ W m}^{-2}$  for fossil fuel BC,  $-0.03 \text{ W m}^{-2}$  for fossil fuel POM, and  $+0.07 \text{ W m}^{-2}$  for biomass burning BC and OM. Since there are contributions of both signs and the total forcing is close to zero, the sum is here as much as 10 % weaker than the total. The absolute difference between the two is very small, however, and much smaller than the estimate by Ghan et al. (2012). The sum of each of the negative contributions to DRF at the ground surface is  $-1.85 \text{ W m}^{-2}$ , which is much closer to the total of  $-1.83 \text{ W m}^{-2}$  in relative terms (1 %). For a further discussion of the direct aerosol effect aspect of these experiments, see Myhre et al. (2012) and Samset et al. (2012).

Similarly, the main contributors to the PD-PI increments in cloud droplet number concentration and effective cloud droplet radius at 870 hPa (CDNC and  $r_{\text{eff}}$  respectively) are sulphate (66 % and 80 %) and internally mixed bb OM/BC (29 % and 16 %), while ff BC (−3 % and −6 %) and ff OM (4 % and 5 %) contribute much less. The corresponding contributions to the liquid water path (LWP) increments are 71 % for sulphate, 21 % for bb OM/BC, −7 % for ff BC, and 6 % for ff OM. The sum of each contribution is approximately 3 % smaller than the total change (PD-PI) for CDNC, 5 % smaller for  $r_{\text{eff}}$ , and 9 % smaller for LWP. As for the aerosol optics, these non-linear effects can probably be attributed to effects of internal mixing of aerosols, e.g. larger changes in effective particle size when all condensate and coagulated aerosol components are added at once rather than one at a time, and to subsequent changes in the competition for water vapour for activation of aerosol particles to cloud droplets.

The individual contributions to the indirect forcing (IndRF) due to the joint radius and lifetime effects are estimated to  $-0.76 \text{ W m}^{-2}$  for sulphate,  $+0.07 \text{ W m}^{-2}$  for fossil fuel BC,  $-0.08 \text{ W m}^{-2}$  for fossil fuel POM, and  $-0.32 \text{ W m}^{-2}$  for BC and POM from biomass burning. Thus the sum of each of the contributions is here only  $-1.09 \text{ W m}^{-2}$ , 9 % lower than the total indirect forcing of  $-1.20 \text{ W m}^{-2}$ . As expected from the non-additive changes in  $r_{\text{eff}}$  and LWP discussed above, as well as the non-linear nature of cloud susceptibility and the indirect effect of aerosols in general, radiative forcing estimated as a sum of its individual contributions is less accurate for the indirect effect than for the direct effect.

The DRF of all natural and anthropogenic aerosols up to year 1850 is found from *Ctrl* PI-ZERO in Table 4, and is estimated at  $-1.6 \text{ W m}^{-2}$  at TOA, globally averaged. Regionally this DRF at TOA ranges between  $-13 \text{ W m}^{-2}$  just off the west coast of West Africa, due to large mineral dust burdens, to about  $+0.7 \text{ W m}^{-2}$  over parts of the Arctic north of  $80^\circ \text{ N}$ , where the positive contributions are mainly from BC. Global DRF at the ground surface is about  $-3.0 \text{ W m}^{-2}$ , with regional maximum (in strength) just off the west coast of Africa in the tropics, and as weak as  $-0.15 \text{ W m}^{-2}$  in parts of the Arctic and the Antarctica. Similarly, *Ctrl* PD-ZERO gives a DRF by all PD aerosols of  $-1.7 \text{ W m}^{-2}$  at TOA and  $-4.8 \text{ W m}^{-2}$  at the ground surface.

#### 4.4 Online atmospheric calculations

The last rows in Tables 4, 6 and 7 show results from online versions of the *Ctrl* PD and PI simulations, *PD Online* and *PI Online*, where the aerosols are allowed to affect the meteorology. In these simulations the net SW flux difference at TOA (not a forcing as such) is estimated at  $-1.23 \text{ W m}^{-2}$ , quite close to the combined SW DRF and IndRF of  $-1.28 \text{ W m}^{-2}$  in the offline (*Ctrl*) simulations. While the LW IndRF (a lifetime effect) is very small in the offline simulations, only  $-0.01 \text{ W m}^{-2}$ , the net LW flux difference from PD-PI *Online* is  $+0.67 \text{ W m}^{-2}$ . Including cloud and aerosol feedbacks, the total estimated net radiative effect (SW-LW) of aerosols is  $-1.89 \text{ W m}^{-2}$ , compared to a forcing of  $-1.29 \text{ W m}^{-2}$  in the offline version of the model.

This positive feedback is probably due to the considerable increase in POM burdens in the online vs. the offline simulations, giving as much as 61 % larger anthropogenic POM burdens globally averaged, see Table 6. For BC the increase is 22 %. This again can at least partly be explained by changes in the precipitation patterns from the offline to online model setup (not shown): the online precipitation rates are smaller over and downstream major POM and BC emissions, in particular biomass burning areas in South America and in central Africa, where the largest increases in burdens are found. Globally averaged, the precipitation rates do not differ very much, however: in the *Online* simulations they are  $2.84 \text{ mm d}^{-1}$  for PD and  $2.88 \text{ mm d}^{-1}$  for PI, compared to  $2.83 \text{ mm d}^{-1}$  in the offline simulations, *Ctrl* PD and PI.

For  $\text{SO}_4$  a larger fraction of the sources for PD are located outside the tropics, aqueous chemistry is an additional and complicating factor, and the link between regional changes in sulphate aerosol and precipitation is not as obvious as for POM and BC.  $\text{SO}_4$  burdens are actually smaller both for PD and PI, giving about 7 % smaller anthropogenic burdens in the *Online* simulations. As for BC and POM, the largest changes are found over areas with high burdens, i.e. large parts of East and South Asia, southern Europe and North Africa, as well as eastern parts of North America.

## 5 Effects of model changes and sensitivity tests

One of the recurring questions during the CAM4-Oslo development period has been “what are the reasons for the difference in modeled direct and indirect radiative forcing compared to previous CAM-Oslo versions?” In this section we study more closely the effects of various changes in emissions and aerosol-related parameterizations in CAM4-Oslo compared to Seland et al. (2008), Hoose et al. (2009) and Struthers et al. (2011), which represent three versions of the predecessor to CAM4-Oslo. In one of the subsections we study the effects of changes due to tuning of cloud parameters compared to CAM4 (Gent et al., 2011). The nature of the changes is described in Sect. 2 and each of the respective subsections below.

All the sensitivity experiments are defined in Table 5. The globally and annually averaged results for burdens and residence times are given in Table 6, and the effects on aerosol optics and DRF and cloud properties and IndRF are listed in Table 7. Figures 6 and 12 show zonally averaged clear-sky AOD, DRF and IndRF results from *Ctrl* and each sensitivity experiment. For clarity, results from sensitivity experiments with only very small changes have been omitted in these figures.

In each sensitivity experiment either an alternative aerosol and precursor emission inventory has been used, or an alternative version of the treatment of aerosols or stratiform cloud macro- and microphysics. Since the alternative versions are almost exclusively older versions (except for the *noBCac* test in Sect. 5.12), here we discuss the effects of the sensitivity tests as the difference *Ctrl* minus *Test*.

### 5.1 Changes caused by new basic emission years

Note that DMS, sea salt and mineral dust emissions are not affected by the changes in emission years in these offline simulations.

Switching from year 1750 (the *EmPII1750* experiment) to 1850 for PI (*Ctrl*) in CAM4-Oslo increases the estimated preindustrial burdens considerably for both sulphate, BC and OM, see Table 6. The increase is more than a factor 2 for BC. Using 2006 (*Ctrl*) instead of 2000 for PD emissions (the *EmPD2000* experiment) also gives increased present-day aerosol burdens of these three major components, but considerably more for BC and OM than for sulphate. Notice that the difference between the PD and the PI burdens include both natural and anthropogenic contributions (except for DMS, sea salt and dust), and that the difference between 2000 and 2006 emissions indeed include the effects of forest fires in 2006.

In total, the impacts on the difference PD-PI when using 1850 and 2006 rather than 1750 and 2000 as emission base years are 22 % increased burden increments for sulphate, 26 % for BC, and 77 % for OM. The increase for OM is considerably influenced by the forest fires in 2006.

When comparing burdens in CAM4-Oslo with the data from Seland et al. (2008) in Table 3, we notice that the increase in OM burdens for PI (250 %) and PD (194 %) are only slightly larger than expected from the increase in total sources (240 % and 179 %, respectively), but much larger than what we would expect from the shift in base year for the emissions, i.e. from *EmPII1750* to *Ctrl PI* (18 %) and from *EmPD2000* to *Ctrl PD* (38 %). This is mainly (but not only) because biogenic ocean emissions and MSA are now included in OM, as well as increased levels of secondary organics (SOA) from forests, see Sect. 2.1.2.

However, the PD-PI increment of OM burden is 139 % larger than in Seland et al. (2008), which is also much larger than the 77 % expected from the shift in basic emission years from Table 6. Similarly, the PD-PI increment of BC is 64 % larger than in Seland et al. (2008), compared to the expected 26 % from the shift in basic emission years. One important contribution to this increase is the changed treatment of convective mixing between convective downdraft and updraft plumes, which is particularly important for POM and BC since the changes in emissions are large in areas with high convective activity. The change in convective mixing concerns all aerosol components, however, leading to increased mass mixing ratios at high altitudes in CAM4-Oslo, see Fig. 3 cf. Fig. 4 in Seland et al. (2008). The new treatment of convective mixing is discussed separately in Sect. 5.11.

The consequence of this increase in BC (in Table 3) is to enhance the absorption of solar radiation, which alone should lead to a more positive DRF at top of the atmosphere (TOA) than in Seland et al. (2008). The total difference (PD-PI) for sulphate burden is only about 12 %, which is smaller than expected from the changes in emission years (22 %). This is probably associated with the reduced atmospheric residence time of both SO<sub>2</sub> and sulphate in CAM4-Oslo. From Table 3 it can be inferred that a larger fraction of SO<sub>2</sub> is dry deposited, leaving a smaller fraction for sulphate production. This further enhances the relative importance of the aerosol light absorption properties over scattering, but the large increase in the difference (PD-PI) for OM burdens (139 %) works in the opposite direction. The net change in DRF at TOA is negative.

To separate changes in radiative forcing introduced by new emissions from the effect of all other changes since Seland et al. (2008), we compare our forcing estimates from *Ctrl PD-Ctrl PI* with *EmPD2000-EmPII1750* as well as with the respective results from that work. DRF at TOA and at the ground surface in *EmPD2000-EmPII1750* is estimated at  $-0.069 \text{ W m}^{-2}$  and  $-1.36 \text{ W m}^{-2}$ , compared to  $+0.03 \text{ W m}^{-2}$  and  $-1.18 \text{ W m}^{-2}$  in Seland et al. (2008). For *Ctrl PD-Ctrl PI* it is estimated at  $-0.072 \text{ W m}^{-2}$  and  $-1.89 \text{ W m}^{-2}$ , when the simulation period is the same as for *EmPD2000-EmPII1750*.

This means that the effect of just changing the emissions (in CAM4-Oslo) is a tiny shift of  $-0.003 \text{ W m}^{-2}$  in DRF at TOA and a  $-0.53 \text{ W m}^{-2}$  shift in DRF at the surface, and a

slight positive shift of  $+0.03 \text{ W m}^{-2}$  for IndRF, globally averaged. The surprisingly small shift in DRF at TOA is a result of approximately equal increase of absorption and scattering part of the AOD for PD-PI, see Table 6. But since this increase is considerable (about 38 % for ABS), the atmospheric forcing (DRF at TOA-DRF at the surface) has also increased considerably (41 %). The global reduction in IndRF is even smaller than expected from the decrease in  $r_{\text{eff}}$  at 870 hPa and LWP increments for PD-PI, since the largest reduction in absolute value for these two parameters is confined to areas with small cloud susceptibility (large CDNC and LWP) over eastern North America and northern Europe.

Zonally averaged DRF and IndRF for each of the sensitivity experiments, i.e. *EmPD2000-Ctrl PI* and *Ctrl PD-EmPI1750*, are shown separately in Fig. 12. For DRF at TOA the effect of swapping the emissions are largest at very high latitudes with high surface albedo, where using the old PD emissions (year 2000) leads to much smaller positive forcing values, and where the old PI emissions (year 1750) yield somewhat larger positive values for DRF. For IndRF (negative at all latitudes) on the other hand, the effect of swapping emissions is largest at low to mid-latitudes. The old PD emissions yield a much weaker forcing in the SH, and the old PI emissions lead to a much stronger forcing at NH mid-latitudes.

The joint effects of all other changes since Seland et al. (2008), most of which are discussed separately in the following subsections, is finally a shift of  $-0.10 \text{ W m}^{-2}$ , from a weak positive to a weak negative DRF at TOA, and a  $-0.18 \text{ W m}^{-2}$  shift in the surface DRF. For IndRF there is a much more substantial change from  $-1.88 \text{ W m}^{-2}$  in Hoose et al. (2009) to about  $-1.23 \text{ W m}^{-2}$  in this work. Estimated IndRF in the model version used in Seland et al. (2008) was even stronger,  $-2.34 \text{ W m}^{-2}$  (Kirkevåg et al., 2008), but the parameterization of aerosol–cloud interaction in that version was based on diagnostic CDNC and prescribed supersaturations, compared to prognostic CDNC with CCN activation based on realized supersaturations in Hoose et al. (2009) and in this work.

## 5.2 Changes in sea salt

Compared to the scheme for prognostic sea salt emission used in Struthers et al. (2011), i.e. in the test labeled *Struthers11* in Tables 6 and 7, the present parameterization for coarse mode sea salt emissions in CAM4-Oslo gives about 3 % lower total AOD (for PD conditions) globally averaged, and a 14 % decrease in the sea salt AOD. This is due to a reduction in sea salt residence time (5 %) and aerosol mass concentrations, which are quite sensitive to the number of coarse mode particles. Integrated over the whole atmospheric column the decrease amounts to 29 % globally, see Table 6. Although the sea salt burdens are actually somewhat higher over the high-latitude storm track areas, up to roughly a doubling in parts of the Southern Ocean, the burdens are

lower at most latitudes, with roughly a 40 % decrease over the larger ocean areas throughout the tropics. In summary, AOD over ocean is higher in parts of the high-latitude storm track areas (up to 35 % for sea salt AOD and 20 % for total AOD), while it is lower in the tropics (25–35 % smaller for sea salt AOD and up to 20 % for total AOD), compared to the *Struthers11* experiment.

Comparing with observations of near-surface concentrations averaged over the same stations as in Fig. 4 ( $4.57 \mu\text{g m}^{-3}$ ), the *Ctrl* simulation gives a much better average ( $5.93 \mu\text{g m}^{-3}$ ) than *Struthers11* ( $9.07 \mu\text{g m}^{-3}$ ) for the same time period (year 7 of the *Ctrl* simulation, see Sect. 3). *Ctrl* also yields a slightly improved correlation coefficient compared to *Struthers11*, 0.57 instead of 0.52.

The present sea salt treatment leads to improved latitudinal clear-sky AOD gradients over the oceans, compared with satellite- and ground-based remote retrieval, see Figs. 6 and 7, although we note that the large AOD over high to mid-latitude oceans in the MODIS product has a significant positive bias, up to 30 % averaged over a year (Zhang and Reid, 2006). As seen from Table 6, the influence of the modified sea salt parameterization on other aerosol components than sea salt is small. Therefore the modifications have a minor impact on the estimated globally averaged anthropogenic AOD, ABS and DRF, see Table 7. Although the change in natural sea salt in principle can affect the cloud susceptibility to anthropogenic aerosol changes, the impact of the new parameterization on natural and anthropogenic CDNC, and hence on  $r_{\text{eff}}$  and LWP, is also small enough to just give a  $0.01 \text{ W m}^{-2}$  weaker IndRF.

## 5.3 New treatment of natural primary organic matter (POM)

With the increased SOA over land and two new oceanic OM sources (see Sect. 2.1.2), the increase in present-day global OM burden in CAM4-Oslo (*Ctrl* compared to *natOM*) is about 25 %, slightly more than the 20 % increase found by Spracklen et al. (2008). The preindustrial OM burden is increased by as much as 53 %, see Table 6.

The effect of using the old treatment from Seland et al. (2008), without the additional natural OM components described in Sect. 2.1.2, is tested in the two experiments *natOM* (old treatment everywhere) and *natOMocn* (old treatment only over oceans). As already discussed in Sect. 4.2, this old treatment considerably underestimates near-surface OM mass concentrations for many atmospheric conditions. For the same stations as in Fig. 4, the European OM/1.4 values are 27 % lower in *natOM* ( $0.84 \mu\text{g m}^{-3}$ ) than in *Ctrl*, which is already 56 % lower than the measured OC values. The North American *natOM* values are 17 % larger (42 % in summer and 1 % in winter) than the observed OC, which are 66 % larger (107 % in summer, 1 % in winter) than the *Ctrl* values. Based on the assumed OM/OC ratio of 1.4 for all natural OM which does not come from biomass burning, the

old OM treatment thus actually seems to perform better with respect to surface mass concentrations for North America. However, as discussed in Sect. 4.2, a higher ratio is probably more realistic both for the European and the North American stations due to the influence of SOA. For *Ctrl* this implies improved validation statistics for North America (a smaller positive bias), while the statistics for Europe become worse (larger negative bias). With the old natural OM treatment, the European statistics are underestimated even more when the higher OM/OC ratios are accounted for.

As discussed in Sect. 4.2, the new treatment of natural OM does lead to improved modeled clear-sky AOD compared to observations at most latitudes, zonally averaged, see Fig. 6. The *natOM* experiment yields too small an AOD at most latitudes. As also seen from Figs. 7 and 8, clear-sky AOD and ABS (*Ctrl*) are both still clearly underestimated in most regions, except for e.g. North America where we find areas with both over and underestimations.

Differences in globally averaged DRF at TOA and at the ground surface are very small between *natOM* and *Ctrl*, see Table 7 and Fig. 12. Due to the large sensitivity of the indirect effect to the background aerosol, preindustrial CDNC and LWP, IndRF is about 37 % smaller with the additional OM emissions in *Ctrl*, with the largest reductions in the tropics and in the SH mid-latitudes. The effect of updating OM emissions over oceans only (*Ctrl* vs. the *natOMocn* test) is to reduce the IndRF by about 28 %. Thus the new treatment of natural *oceanic* OM emissions is more important than the emissions on *land*, as far as decrease in global anthropogenic aerosol forcing is concerned.

#### 5.4 Updated OM/OC ratios for biomass burning organics

Our *bbPOM* experiment assumes that the OM/OC ratio for biomass burning POM is 1.4, as in Seland et al. (2008). This is also the same ratio as we use for fossil fuel OM. Scatter plots and statistics for the surface concentrations of OM in *bbPOM* show similar results as the *natOM* test. The updated *Ctrl* treatment yield slightly alleviated validation results for Europe compared to *bbPOM*, a 56 % instead of a 61 % underestimate in average, while the North American results are slightly exacerbated, giving 66 % instead of 45 % higher OM/1.4 than the measured OC values. Taking into account somewhat higher OM/OC ratios for SOA modifies the results the same way as in Sect. 5.3.

This has a very small impact on IndRF globally, while the sign of the DRF at TOA is switched from a slightly positive value to an equally large but negative number,  $-0.072 \text{ W m}^{-2}$  in *Ctrl*, see Table 7 and Fig. 12. The reason for this change is a 16 % increase in anthropogenic AOD due to enhanced POM concentrations, while ABS only increases by 4 % (note that the BC emissions are unaltered). The new DRF result is closer to the AeroCom median model estimate

(Schulz et al., 2006) as well as the best estimate by IPCC AR4 (Forster et al., 2007).

Perhaps more importantly, as mentioned in Sect. 2.1.4, the updated OM/OC ratio also leads to significantly improved aerosol optical depths and absorption optical depths compared to observations and sun photometry (AERONET) retrievals in biomass burning dominated areas. Although the new OM/OC ratio for biomass burning is by far the only relevant update from Seland et al. (2008), the effect of this change can be seen in Fig. 7, where modeled clear-sky AOD in typical biomass areas in South America, Africa and South-east Asia is much closer to the composite of ground and satellite based retrieved AOD values. This improvement is most clearly seen in seasonal plots for specific AERONET stations (see <http://aerocom.met.no/data.html>).

#### 5.5 In-cloud scavenging of mineral dust

In the *dustscavin* experiment, the in-cloud scavenging efficiency of mineral dust is changed from 0.25 back to the Seland et al. (2008) value of 1, see Sect. 2.1.7. This reduces the dust concentrations considerably. The *Ctrl* simulation yields a 36 % larger global mineral dust column burden than *dustscavin*, see Table 6. As already discussed in Sect. 4.2, the *Ctrl* simulation gives much more realistic surface mass concentrations compared to observations.

The change from *dustscavin* to *Ctrl* has only a modest impact on the global aerosol radiative forcing at TOA, however. We get a  $+0.03 \text{ W m}^{-2}$  change for both DRF and IndRF, see Table 7 and Fig. 12.

#### 5.6 Gravitational settling of particles

In the *gravdep2d* experiment gravitational settling is calculated only in the bottom model level, as in Seland et al. (2008), see Sect. 2.1.7. The effect of calculating gravitational settling at all model levels is a more efficient aerosol removal, which is seen by comparing *Ctrl* and *gravdep2d* in Table 6. The new treatment impacts in particular aerosol components with considerable mass concentrations in the coarse mode. Sea salt column burdens over continental areas downstream from oceans are reduced by more than 50 % over extensive areas, and more than 80 % in parts of Siberia and Antarctica, averaged over a year. The respective reductions in mineral dust columns are up to about 75 %, while the maximum (PD) reductions for sulphate, POM and BC amount to about 15–18 % in the Antarctica.

Comparing *Ctrl* with *gravdep2d* for the same observation data sets as in Fig. 4, we find considerably improved results for sea salt, a 30 % overestimate instead of 57 %. For mineral dust the results are not quite as sensitive, at least not for the available data. *Ctrl* gives a 7 % overestimate, compared to a smaller underestimate of 3 % in *gravdep2d*.

The reduced aerosol burdens also give reduced AOD and ABS values. Anthropogenic (PD-PI) AOD decreases by



about 2 % and ABS by 4 %, globally, and the DRF becomes as much as  $0.05 \text{ W m}^{-2}$  stronger (more negative), see Table 7 and Fig. 12. Since accumulation mode and finer particles are largely unaffected, impacts on cloud droplet number concentrations are quite small, giving an IndRF which is only about  $0.01 \text{ W m}^{-2}$  weaker with the updated gravitational settling treatment.

### 5.7 Replenishment of oxidants in cloud droplets

In the *replH2O2* test we look at the effect of assuming a constant 1 h replenishment rate for  $\text{H}_2\text{O}_2$ , as in Seland et al. (2008). Comparing *Ctrl* with *replH2O2* for the same observation data sets as in Fig. 4, we find significantly improved results for sulphate in *Ctrl*. The average overestimate becomes 19 % instead of 33 %, while the correlation coefficient is 0.62 for both experiments.

The column burden of  $\text{SO}_2$  for PD is about 8 % higher in *Ctrl* than in *replH2O2*, and only 2 % higher for sulphate, globally averaged. Regionally the increase in the sulphate burden reaches a maximum of about 20 % just east of New Guinea, downwind of non-explosive volcanic activity, and ranges between 5 and 10 % in the Arctic, as well as in parts of South America, where absolute changes are very small. In major parts of central Europe it is 5–10 % lower, however, and also up to 5 % lower in limited areas around the most industrialized regions on all continents.

Although the global column burden for anthropogenic (PD-PI)  $\text{SO}_2$  is about 9 % higher in *Ctrl* than in *replH2O2*, it is only 1.5 % higher for sulphate, and there is very little impact on the globally averaged radiative forcing ( $\leq 0.01 \text{ W m}^{-2}$ ), see Table 7. Regionally the change in DRF at TOA reaches a maximum of about  $0.35 \text{ W m}^{-2}$  over north-eastern China, and up to about  $0.15 \text{ W m}^{-2}$  over Central Europe and eastern North America. For IndRF a maximum of  $0.5 \text{ W m}^{-2}$  is found just west of the Peruvian coast, while changes elsewhere are generally less than  $0.1 \text{ W m}^{-2}$ .

### 5.8 Cloud droplet spectral dispersion

In the *prescrβ* test the spectral shape factor  $\beta$  (see Sect. 2.2) is prescribed with one value over land (1.14) and another over oceans (1.08), as in Seland et al. (2008), Hoose et al. (2009) and in CAM4 (Neale et al., 2010). Since we run the model in an offline mode, this change affects effective droplet radii ( $r_{\text{eff}}$ ) and the first indirect effect, but neither the aerosol properties and the direct effect nor the cloud liquid water path (LWP) and the second indirect effect.

Comparing the *Ctrl* simulation with the older effective radius treatment used in *prescrβ*, the anthropogenic (PD-PI) change in  $r_{\text{eff}}$  at 870 hPa is 16 % smaller and IndRF is 10 % weaker, estimated at  $-1.20 \text{ W m}^{-2}$  instead of  $-1.34 \text{ W m}^{-2}$ , see Table 7 and Fig. 12. Regionally, IndRF is up to about  $1.0 \text{ W m}^{-2}$  weaker in *Ctrl* than in *prescrβ* in north-eastern China and off the coast of Peru, and more than 0.1–

$0.2 \text{ W m}^{-2}$  weaker in most industrialized land areas worldwide. Apart from the large changes in East Asia, the regional pattern is dominated by local maxima over coastal ocean areas downwind of polluted land areas, especially in the stratocumulus areas off the west coasts of Africa and America, where cloud susceptibility is generally high.

### 5.9 Coating insoluble particles with hydrophilic matter

The present treatment of coating of insoluble particles with hydrophilic matter, which only influences activation of CCN to form cloud droplets, is as described in Hoose et al. (2009). That is, the fraction of aerosols that activates to cloud droplets is based on the hygroscopic properties of the sulphate and POM coating whenever the thickness of the coating layer exceeds 2 nm. This (assumed) homogeneously mixed sulphate and POM coating affects the hygroscopicity of all particles which contain sulphate and/or POM, except for sea salt, giving them the hygroscopicity of the coating itself in the activation calculations.

In the *no coating* experiment we estimate the effect of assuming no coating, as in Seland et al. (2008), since the effect of the coating treatment was not tested explicitly in Hoose et al. (2009). In this sensitivity test the fraction of aerosols that activates to form cloud droplets is simply calculated based on the hygroscopicity of a homogeneously mixed particle, as is still assumed in the aerosol optics calculations.

Since this is assumed to not affect the aerosol life cycle or the optics, the direct effect is unchanged from *no coating* to *Ctrl*. However, we find a significant impact on cloud droplet properties and subsequent indirect effects, see Table 7. The smaller anthropogenic (PD-PI) contributions to  $r_{\text{eff}}$  (16 %) and LWP (13 %) in *Ctrl* (mostly due to an increased number of activated natural CCN) give 8 % weaker IndRF globally,  $-1.20 \text{ W m}^{-2}$  instead of  $-1.31 \text{ W m}^{-2}$ . Regionally the effect of the new coating treatment on IndRF varies between about  $-1$  to  $-2 \text{ W m}^{-2}$  (stronger IndRF) in Indonesia, central Africa and northern South America, to between 1 to  $1.5 \text{ W m}^{-2}$  (weaker IndRF) over eastern North America, parts of southern and central Africa (east and west of areas of maximum biomass burning activity), eastern Australia and the Tibetan mountain plateau. The effect is much smaller in Europe, where the changes nowhere exceed  $0.5 \text{ W m}^{-2}$  averaged over the year. Due to cancelling effects of both negative and positive contributions at different longitudes in the central tropics, the most prominent impact of coating assumptions on zonally averaged IndRF is found in the NH subtropics, see Fig. 12.

### 5.10 Tuning of cloud parameters

In the *cldtunorig* test the stratiform cloud-tuning parameters discussed in Sect. 2.3 are reset to their original CAM4 values, i.e. the minimum relative humidity threshold for formation of low clouds is 0.91, the critical mean droplet volume

radius for onset of auto-conversion is  $10\ \mu\text{m}$ , and the precipitation rate threshold for suppression of auto-conversion of cloud water to rain is  $0.5\ \text{mm d}^{-1}$ . This affects the modeled cloud fractions as well as precipitation patterns in space and time. Globally and annually averaged the changes are small, however. The cloud fractions for low, medium and high level clouds are 0.341, 0.187 and 0.318 in *Ctrl*, compared to 0.347, 0.191 and 0.318 in *cldtunorig*. Similarly, the stratiform and convective precipitation rates are 1.096 and  $1.725\ \text{mm d}^{-1}$  in *Ctrl*, compared to 1.108 and  $1.721\ \text{mm d}^{-1}$  in *cldtunorig*.

Comparing *Ctrl* with *cldtunorig* for the same observation data sets as in Fig. 4, we find somewhat poorer validation results for sulphate: the average bias is 19 % instead of 10 %, and the correlation coefficient is 0.62 instead of 0.64. The average bias is improved considerably for mineral dust, from 26 % to 7 %, but the correlation coefficient has dropped slightly from 0.49 to 0.46. The changes are smaller for the remaining aerosol components. Average bias for sea salt is slightly worse in *Ctrl*, for BC it is slightly improved, and for POM it is slightly improved in Europe and slightly worse in North America. This shows that the tuning of cloud macro- and microphysical parameters has not been done to improve the aerosol verification. Nevertheless, the results demonstrate that this tuning (in order to obtain radiative balance at TOA, see Sect. 2.2) can indeed affect the results significantly.

The DRF at TOA changes as little as  $0.01\ \text{W m}^{-2}$  from *cldtunorig* to *Ctrl*, while DRF at the ground surface changes with  $-0.08\ \text{W m}^{-2}$ , which is consistent with the increase in anthropogenic aerosol absorption in Table 7. A similar change, but with opposite sign, is found for the indirect effect: due to a 30 % larger global LWP in *Ctrl*, the cloud susceptibility is so much smaller that, even though anthropogenic (PD-PI) aerosol column burdens and their contribution to  $r_{\text{eff}}$  and LWP are a few percent larger than in *cldtunorig*, IndRF is decreased by about  $0.08\ \text{W m}^{-2}$  (6 %), see Table 7 and Fig. 12. The changes in LWP and  $r_{\text{eff}}$  relative to PI conditions, which are more relevant measures with respect to indirect effects than the absolute changes, are roughly the same in *Ctrl* and *cldtunorig*.

### 5.11 Convective mixing of aerosols and aerosol precursors

As described in Sect. 2.1.5, the special adjustment for aerosol processes in convective clouds in CAM-Oslo (Seland et al., 2008) was not ported to CAM4-Oslo. In the *convmix* test, however, the radical assumption of full mixing of transported constituents between convective downdraft and up-draft plumes is made, just as in Seland et al. (2008).

While *Ctrl* generally yield considerably larger mass concentrations than *convmix* in the upper troposphere for all aerosol components, the surface concentrations are smaller close to the ITCZ and over major parts of the continents for sulphate, BC, POM and mineral dust. Sea salt surface concentrations are generally smaller everywhere over the oceans.

For the same observation data sets as in Fig. 4 we find small differences in the verification results between *convmix* and *Ctrl*, however. Correlation coefficients between measured and calculated surface concentrations are very similar in the two simulations. For sulphate the average bias is somewhat improved in *Ctrl*, 19 % instead of 24 %. There is also a slight reduction in the mean bias for sea salt (from 31 % to 30 %) and mineral dust (from 7.3 % to 6.6 %), while it is unchanged for BC ( $-14\%$ ). For POM/1.4 the mean bias is improved from 72 % to 66 % for the North American stations in the *Ctrl* simulation, while it is slightly worse for the European stations,  $-57\%$  instead of  $-56\%$ .

Vertically integrated mass concentrations annually and globally averaged are larger for all components in *Ctrl* than *convmix*. For PD conditions, the increase in column burden is 25 % for sulphate, 24 % for BC, 27 % for OM, 10 % for sea salt, and 7 % for mineral dust. The increase in anthropogenic (PD-PI) AOD and ABS is about 25 % and 28 %, giving a 31 % increase in atmospheric forcing, defined as DRF at TOA minus DRF at the ground surface. Since the increase in AOD and ABS are almost the same, the resulting change in DRF at TOA is only  $0.02\ \text{W m}^{-2}$ , while the change in DRF at the surface is about  $-0.4\ \text{W m}^{-2}$ . Since the larger changes in aerosol concentrations are confined to the upper troposphere, where liquid clouds are less frequent, the estimated change in cloud droplet properties and subsequent indirect effects are relatively modest. IndRF is about  $0.05\ \text{W m}^{-2}$  (4 %) stronger in *Ctrl* than in the *convmix* test.

We find that the zonally averaged extinction coefficient at 550 nm is about 0–10 % lower in *Ctrl* than *convmix* in the lower troposphere between  $60^\circ\text{S}$  and  $60^\circ\text{N}$ , and up to about 900 hPa, or 800 hPa in the tropics. Above those heights it is higher in *Ctrl*, up to about 75 % higher near the tropopause in the tropics. In light of these results, we expect that *convmix* would have compared better with the CALIOP extinction profiles than *Ctrl* in Fig. 10. However, the chosen treatment of convective mixing of transported constituents is insufficient to explain the large biases that were discussed in Sect. 4.2, especially in the upper troposphere.

### 5.12 Primary emissions of accumulation mode BC

The BC(ac) mode in Table 1 and Fig. 1 represents fractally shaped accumulation mode particles of low mass density (Ström et al., 1992), assumed to have been formed by self-coagulation into agglomerates of BC(n) monomer particles (see Kirkevåg et al., 2002; Kirkevåg et al., 2005; Seland et al., 2008). The relative amount of fossil fuel BC from rapid combustion which in the model is directly emitted as BC(ac) is in *Ctrl* assumed to be 10 %, as in Seland et al. (2008). To test the sensitivity to this uncertain assumption, in the *noBCac* test we let all primary BC be emitted as nucleation mode particles, BC(n), i.e. with no contribution to the BC(ac) mode.

For the same observational data set as in Fig. 4 we get better validation results for BC with *Ctrl* than in the *noBCac* test: the average bias is  $-12\%$  instead of  $-21\%$ , and the correlation coefficient is 0.41 instead of 0.40. The BC column burden is about 25% larger in *Ctrl*, however, see Table 6. Regionally the relative changes are smallest in the source regions, while in large parts of the Arctic and over the tropical Pacific Ocean the BC burdens are more than 50% larger in *Ctrl*, i.e. when 10% of BC is assumed to be emitted directly in the accumulation mode.

The effect of this on cloud droplet properties and the indirect effect is negligible, see Table 7, but the anthropogenic (PD-PI) ABS and the corresponding atmospheric forcing is 12% larger in *Ctrl*, giving a  $0.09 \text{ W m}^{-2}$  larger (more positive) DRF at TOA and a  $0.11 \text{ W m}^{-2}$  stronger (more negative) DRF at the ground surface. The estimated DRF at TOA in the *noBCac* test,  $-0.16 \text{ W m}^{-2}$ , is closer to what other AeroCom models yield, probably due to more similar assumptions with respect to BC and the fact that many of these models use PD emissions valid for year 2000 instead of year 2006, see Sect. 5.1.

## 6 Summary and conclusions

As mentioned in the introduction, the purpose of this study is threefold: (1) to document the changes in the aerosol module of CAM4-Oslo/NorESM1-M compared to the latest predecessor versions (Seland et al., 2008; Kirkevåg et al., 2008; Hoose et al., 2009; Struthers et al., 2011); (2) to evaluate the new aerosol and aerosol-related cloud properties with emphasis on natural aerosols; and (3) to estimate the sensitivity of the aerosols and their direct and indirect radiative forcing to new model assumptions and parameterizations.

Although the properties and effects of increased natural aerosols are emphasized, other changes have also been shown to be important, such as the omitted mixing between updrafts and downdrafts in deep convective clouds, and the shift in basic years for present-day and preindustrial emissions.

We find a 7% bias in the modeled near-surface mass concentrations of mineral dust, which is considerably improved compared to the  $-55\%$  bias in Seland et al. (2008). In a sensitivity experiment where we use the same in-cloud scavenging coefficient as in that work, we obtain a  $-13\%$  bias and one third as many calculated values within a factor two of the observed, compared to the control experiment. Even though sea salt concentrations are estimated to have a 30% positive bias at the near-surface observation sites, they are also considerably improved compared to the relevant previous model version in Struthers et al. (2011). The slightly different sea salt emission parameterization used in that work turns out to give a three times larger positive bias in CAM4-Oslo.

Modeled near-surface concentrations of sulphate are found to have a positive bias of 20% at near-surface observation

sites, which is slightly more than in Seland et al. (2008). For BC the bias is  $-18\%$ , as in Seland et al. (2008). Comparing OM with measurements of OC is complicated by the fact that the model does not explicitly track OC or the OM/OC ratio after the point of emission. Taking into account the fact that the OM/OC ratio can vary from 2.6 for biomass burning to about 1.4 for fossil fuel, the modeled OM is still considerably underestimated at near-surface observation sites in Europe, despite the increase in natural and biomass burning OM levels compared to Seland et al. (2008). For the North American sites, however, the model now produces a positive bias.

Comparisons with a very few vertical profiles of sulphate indicate that the model, as in Seland et al. (2008), give reasonable results at low altitudes, while the mass mixing ratios are overestimated in the upper troposphere. Although the ad hoc assumption of full mixing of aerosols between convective cloud updrafts and downdrafts in Seland et al. (2008) has been omitted in CAM4-Oslo, the sulphate profiles are quite similar to that work. We also find positive biases in the aerosol extinction coefficients in the upper troposphere compared to the CALIOP layer product (Koffi et al., 2012a). On the other hand, since undetected values are set to zero and the CALIOP detection limit for extinction is 2–3 times larger than a high end estimate of background aerosol extinctions as well as the global mean extinction for CAM4-Oslo, the CALIOP values are probably underestimated at these altitudes. Even though we suspect that the upper tropospheric model aerosol extinctions are overestimated for present-day conditions, the sparse observations makes it difficult to draw any confident conclusion.

The new aerosol treatment, especially that of biomass burning and natural OM, sea salt emissions, gravitational settling, and in-cloud scavenging of mineral dust, has also lead to improved aerosol optical depth when compared with satellite- and ground-based sun photometry (AERONET) retrievals. The statistics for AOD worldwide is generally improved in CAM4-Oslo compared to Seland et al. (2008). Annually averaged AOD is still widely underestimated, although it is probably overestimated in remote regions at high latitudes where observations are sparse. More specifically, CAM4-Oslo simulates larger aerosol burdens, AOD, and ABS at high latitudes than most other models (Myhre et al., 2012), which are biased on the low side. Our results thus contribute to a wider range of uncertainty with respect to aerosols in global climate models.

The main findings concerning the sensitivity of radiative forcing to the changes in parameterizations in CAM4-Oslo can be summarized as follows. The improved treatment of natural OM aerosols and the introduction of a cloud droplet spectral dispersion formulation are the most important contributions to the decrease in globally averaged IndRF since the model version of Hoose et al. (2009). This is obtained without imposing an unrealistically high artificial lower threshold for cloud droplet number concentrations (Hoose et al., 2009). In CAM4-Oslo the IndRF is about

49 % smaller than in the version with the original diagnostic CDNC scheme (Kirkevåg et al., 2008), and about 36 % lower when compared to the corresponding value for prognostic CDNC (Hoose et al., 2009). Although this is not to be regarded as an objective quality criterion, the new value,  $-1.2 \text{ W m}^{-2}$ , is closer to the IPCC AR4 estimates constrained by the observed climate response (IPCC AR4, e.g. Fig. 2.20, Sect. 2.9).

Compared to Seland et al. (2008), the global DRF at TOA has changed from a small positive value to  $-0.08 \text{ W m}^{-2}$ , which incidentally is also closer both to the AeroCom median model estimates (Schulz et al., 2006; Myhre et al., 2012) and the best estimate by IPCC AR4 (Forster et al., 2007). This is explained mainly by the new treatments of biomass burning aerosols and gravitational settling. Estimated DRF at the ground surface has changed by 60 %, from  $-1.18$  to  $-1.89 \text{ W m}^{-2}$ . This can be attributed to the new emission data sets and the omitted mixing between convective updrafts and downdrafts in CAM4-Oslo.

In the CMIP5 intercomparison project, the year 1850 has been defined as preindustrial. This indicates that the bulk part of any anthropogenic influence on the global climate has occurred later. Earlier, 1750 was defined as preindustrial. We have demonstrated that this shift significantly changes the background levels of aerosols against which the anthropogenic influence is defined, and thus the magnitude of the estimated anthropogenic aerosol forcing.

Several research areas are pursued to improve the representation of aerosols in future versions of NorESM, i.e. online integration with oxidant chemistry including particulate nitrate and anthropogenic SOA, explicit treatment of aerosol mass in cloud water, explicit nucleation of new particles, activation of ice nuclei and the influence of the ice phase in clouds on the indirect effects of aerosols (Hoose et al., 2010). More explicit speciation of OM components, which influence the modelled OM/OC ratio, is a considerable challenge for the field. Furthermore, subgrid scale vertical transport and aerosol processing in the highly parameterized convective clouds will continue to be a topic for research.

**Acknowledgements.** We are deeply grateful to NCAR for providing early access to model code for CCSM/CESM and to NCAR staff for invaluable advice. NorESM has benefited from contributions by many scientists at member institutions of The Norwegian Climate Centre: BCCR, met.no, MetOs-UiO, NERSC, Cicero, NILU and NP; from NCAR and PNNL in USA, and MISU and The Bolin Centre in Sweden. We are grateful to the AeroCom community for valuable discussions and for making AeroCom model intercomparison and observation data available on the AeroCom web page (<http://aerocom.met.no>). Thanks also to Dirk Olivieri, Svetlana Tsyro, Leonor Tarrason, Hilde Fagerli, David Simpson and Brigitte Koffi for valuable discussions, and to Birthe Steensen for work with the CALIOP figures. The CALIOP data were prepared by Brigitte Koffi. This work has been supported by the Research Council of Norway through the NorClim, EarthClim (207711/E10)

and NOTUR/NorStore projects, by the Norwegian Space Centre through PM-VRAE, and through the EU projects PEGASOS and ACCESS. A. Ekman, E. D. Nilsson and H. Struthers would like to acknowledge the support from the Swedish Research Council, project GRACE, and the Bert Bolin Climate Center. S. Ghan was funded by the US Department of Energy (DOE), Office of Science, Scientific Discovery through Advanced Computing (SciDAC) Program and by the Office of Science Earth System Modeling Program. The Pacific Northwest National Laboratory is operated for DOE by Battelle Memorial Institute under contract DE-AC06-76RLO 1830.

Edited by: H. Tost

## References

- Abdul-Razzak, H. and Ghan, S. J.: A parameterization of aerosol activation, Part 2: Multiple aerosol types, *J. Geophys. Res.*, 105, 6837–6844, 2000.
- Ackerman, S., Toon, O. B., Stevens, D. E., Heymsfield, A. J., Ramanathan, V., and Welton, E. J.: Reduction of tropical cloudiness by soot, *Science*, 288, 1042–1047, 2000.
- Adams, P. J., Seinfeld, J. H., Koch, D., Mickley, L., and Jacob, D.: General circulation model assessment of direct radiative forcing by the sulfate-nitrate-ammonium water inorganic aerosol system, *J. Geophys. Res.* 106, 1097–1111, doi:10.1029/2000JD900512, 2001.
- Albrecht, B. A.: Aerosols, cloud microphysics and fractional cloudiness, *Science*, 245, 1227–1230, 1989.
- Assmann, K. M., Bentsen, M., Segsneider, J., and Heinze, C.: An isopycnic ocean carbon cycle model, *Geosci. Model Dev.*, 3, 143–167, doi:10.5194/gmd-3-143-2010, 2010.
- Barth, M. C., Rasch, P. J., Kiehl, J. T., Benkowitz, C. M., and Schwartz, S. E.: Sulphur chemistry in the National Center for Atmospheric Research Community Climate Model: Description, evaluation, features, and sensitivity to aqueous chemistry, *J. Geophys. Res.* 105, 1387–1415, 2000.
- Barth, M., Mcfadden, J. P., Sun, J., Wiedinmyer, C., Chuang, P., Collins, D., Griffin, R., Hannigan, M., Karl, T., Kim, S.-W., Lasher-Trapp, S., Levis, S., Litvak, M., Mahowald, N., Moore, K., Nandi, S., Nemitz, E., Nenes, A., Potosnak, M., Raymond, T. M., Smith, J., Still, C., and Stroud, C.: Coupling between Land Ecosystems and the Atmospheric Hydrologic Cycle through Biogenic Aerosol Pathways, *B. Am. Meteorol. Soc.*, 86, 1738–1742, doi:10.1175/BAMS-86-12-1738, 2005.
- Bergström, R., Denier van der Gon, H. A. C., Prévôt, A. S. H., Yttri, K. E., and Simpson, D.: Modelling of organic aerosols over Europe (2002–2007) using a volatility basis set (VBS) framework: application of different assumptions regarding the formation of secondary organic aerosol, *Atmos. Chem. Phys.*, 12, 8499–8527, doi:10.5194/acp-12-8499-2012, 2012.
- Bentsen, M., Bethke, I., Debernard, J. B., Iversen, T., Kirkevåg, A., Seland, Ø., Drange, H., Roelandt, C., Seierstad, I. A., Hoose, C., and Kristjánsson, J. E.: The Norwegian Earth System Model, NorESM1-M – Part 1: Description and basic evaluation, *Geosci. Model Dev. Discuss.*, 5, 2843–2931, doi:10.5194/gmdd-5-2843-2012, 2012.
- Berntsen, T. and Isaksen, I. S. A.: A global 3-D chemical transport model for the troposphere, 1, Model description and

- CO and Ozone results, *J. Geophys. Res.*, 102, 21239–21280, doi:10.1029/97JD01140, 1997.
- Bigg, K., Leck, C., and Tranvik, L.: Particulates of the surface microlayer of open water in the central Arctic Ocean in summer, *Mar. Chem.*, 91, 131–141, 2004.
- Brenguier, J.-L., Burnet, F., and Geoffroy, O.: Cloud optical thickness and liquid water path – does the  $k$  coefficient vary with droplet concentration?, *Atmos. Chem. Phys.*, 11, 9771–9786, doi:10.5194/acp-11-9771-2011, 2011.
- Buhaug, Ø., Corbett, J. J., Endresen, Ø., Eyring, V., Faber, J., Hanayama, S., Lee, D. S., Lee, D., Lindstad, H., Markowska, A. Z., Mjelde, A., Nelissen, D., Nilsen, J., Pålsson, C., Winebrake, J. J., Wu, W.-Q., and Yoshida, K.: Second IMO GHG study 2009; International Maritime Organization (IMO) London, UK, March, 2009.
- Cavalli, F., Facchini, M. C., Decesari, S., Mircea, M., Emblico, L., Fuzzi, S., Ceburnis, D., Yoon, Y. J., O’Dowd, C. D., Putaud, J.-P., and Dell’Acqua, A.: Advances in characterization of size-resolved organic matter in marine aerosol over the North Atlantic, *J. Geophys. Res.*, 109, D24215, doi:10.1029/2004JD005137, 2004.
- Charlson, R. J., Schwartz, S. E., Hales, J. M., Cess, R. D., Coakley Jr., J. A., Hansen, J. E., and Hofmann, D. J.: Climate forcing by anthropogenic aerosols, *Science*, 255, 423–430, 1992.
- Collins, W. D., Rasch, P. J., Boville, B. A., Hack, J. J., McCaa, J. R., Williamson, D. L., and Briegleb, B. P.: The Formulation and Atmospheric Simulation of the Community Atmospheric Model Version 3 (CAM3), *J. Climate*, 19, 2144–2161, 2006.
- Denman, K. L., Brasseur, G., Chidthaisong, A., Ciais, P., Cox, P. M., Dickinson, R. E., Hauglustaine, D., Heinze, C., Holland, E., Jacob, D., Lohmann, U., Ramachandran, S., da Silva Dias, P. L., Wofsy, S. C., and Zhang, X.: Couplings between changes in the climate system and biogeochemistry, in: *Climate Change 2007: The Physical Science Basis, Contribution of Working Group I to the Fourth Assessment Report of the Intergovernmental Panel on Climate Change*, edited by: Solomon, S., Qin, D., Manning, M., Chen, Z., Marquis, M., Averyt, K. B., Tignor, M., and Miller, H. L., Cambridge University Press, Cambridge, United Kingdom and New York, NY, USA, 499–587, 2007.
- Dentener, F., Kinne, S., Bond, T., Boucher, O., Cofala, J., Generoso, S., Ginoux, P., Gong, S., Hoelzemann, J. J., Ito, A., Marelli, L., Penner, J. E., Putaud, J.-P., Textor, C., Schulz, M., van der Werf, G. R., and Wilson, J.: Emissions of primary aerosol and precursor gases in the years 2000 and 1750 prescribed data-sets for AeroCom, *Atmos. Chem. Phys.*, 6, 4321–4344, doi:10.5194/acp-6-4321-2006, 2006.
- Després, V. R., Huffman, J. A., Burrows, S. M., Hoose, C., Safatov, A. S., Buryak, G., Fröhlich-Nowoisky, J., Elbert, W., Andreae, M. O., Pöschl, U., and Jaenicke, R.: Primary Biological Aerosol Particles in the Atmosphere: A Review, *Tellus B*, 64, 15598, doi:10.3402/tellusb.v64i0.15598, 2012.
- Eyring, V., Isaksen, I. S. A., Bernsten, T., Collins, W. J., Corbett, J. J., Endresen, O., Grainger, R. G., Moldanova, J., Schlager, H., and Stevenson, D. S.: Transport impacts on atmosphere and climate: Shipping, *Atmos. Environ.*, 44, 4735–4771, doi:10.1016/j.atmosenv.2009.04.059, 2009.
- Facchini, M. C., Rinaldi, M., Decesari, S., Carbone, C., Finessi, E., Mircea, M., Fuzzi, S., Ceburnis, D., Flanagan, R., Nilsson, E. D., de Leeuw, G., Martino, M., Woeltjen, J., and O’Dowd, C. D.: Primary submicron marine aerosol dominated by insoluble organic colloids and aggregates, *Geophys. Res. Lett.*, 35, L17814, doi:10.1029/2008GL034210, 2008.
- Fagerli, H. and Aas, W.: Trends of nitrogen in air and precipitation: Model results and observations at EMEP sites in Europe, 1980–2003, *Environ. Pollut.*, 154, 448–461, 2008.
- Fahlgren, C., Hagström, Å., Nilsson, E. D., and Zweifel, U.-L.: Annual Variations in the Diversity, Viability, and Origin of Airborne Bacteria, *Appl. Environ. Microbiol.*, 76, 3015–3025, doi:10.1128/AEM.02092-09, 2010.
- Formenti, P., Elbert, W., Maenhaut, W., Haywood, J., Osborne, S., and Andreae, M.-O.: Inorganic and carbonaceous aerosols during the Southern African Regional Science Initiative (SAFARI 2000) experiment: Chemical characteristics, physical properties, and emission data for smoke from African biomass burning, *J. Geophys. Res.*, 108, 8488, doi:10.1029/2002JD002408, 2003.
- Forster, P., Ramaswamy, V., Artaxo, P., Bernsten, T., Betts, R., Fahey, D. W., Haywood, J., Lean, J., Lowe, D. C., Myhre, G., Nanga, J., Prinn, R., Raga, G., Schulz, M., and Van Dorland, R.: Changes in Atmospheric Constituents and in Radiative Forcing, in: *Climate Change 2007: The Physical Science Basis, Contribution of Working Group I to the Fourth Assessment Report of the Intergovernmental Panel on Climate Change*, edited by: Solomon, S., Qin, D., Manning, M., Chen, Z., Marquis, M., Averyt, K. B., Tignor, M., and Miller, H. L., Cambridge University Press, Cambridge, United Kingdom and New York, NY, USA, 2007.
- Gent, P. R., Danabasoglu, G., Donner, L. J., Holland, M. M., Hunke, E. C., Jayne, S. R., Lawrence, D. M., Neale, R. B., Rasch, P. J., Vertenstein, M., Worley, P. H., Yang, Z.-L., and Zhang, M.: The Community Climate System Model Version 4. *J. Climate*, 24, 4973–4991, doi:10.1175/2011JCLI4083.1, 2011.
- Gottelman, A., Liu, X., Ghan, S. J., Morrison, H., and Conley, A. J.: Global simulations of ice nucleation and ice supersaturation with an improved cloud scheme in the Community Atmosphere Model, *J. Geophys. Res.*, 115, D18216, doi:10.1029/2009JD013797, 2010.
- Ghan, S. J., Liu, X., Easter, R. C., Zaveri, R., Rasch, P. J., Yoon, J.-H., and Eaton, B.: Toward a minimal representation of aerosols in climate models: Comparative decomposition of aerosol direct, semi-direct and indirect radiative forcing, *J. Climate*, 25, 6461–6476, doi:10.1175/JCLI-D-11-00650.1, 2012.
- Hansen, J. E., Sato, M., and Ruedy, R.: Radiative forcing and climate response. *J. Geophys. Res.*, 102, 6831–6864, 1997.
- Hegerl, G. C., Zwiers, F. W., Braconnot, P., Gillett, N. P., Luo, Y., Marengo Orsini, J. A., Nicholls, N., Penner, J. E., and Stott, P. A.: Understanding and Attributing Climate Change, in: *Climate Change 2007: The Physical Science Basis, Contribution of Working Group I to the Fourth Assessment Report of the Intergovernmental Panel on Climate Change*, edited by: Solomon, S., Qin, D., Manning, M., Chen, Z., Marquis, M., Averyt, K. B., Tignor, M., and Miller, H. L., Cambridge University Press, Cambridge, United Kingdom and New York, NY, USA, 2007.
- Hoose, C., Kristjánsson, J. E., Iversen, T., Kirkevåg, A., Seland, Ø., and Gottelman, A.: Constraining cloud droplet number concentration in GCMs suppresses the aerosol indirect effect, *Geophys. Res. Lett.*, 36, L12807, doi:10.1029/2009GL038568, 2009.
- Hoose, C., Kristjánsson, J. E., Chen, J.-P., and Hazra, A.: A classical theory-based parameterization of heterogeneous ice

- nucleation by mineral dust, soot, and biological particles in a global climate model, *J. Atmos. Sci.*, 67, 2483–2503, doi:10.1175/2010JAS3425.1, 2010.
- Hoyle, C. R., Bernsten, T., Myhre, G., and Isaksen, I. S. A.: Secondary organic aerosol in the global aerosol – chemical transport model Oslo CTM2, *Atmos. Chem. Phys.*, 7, 5675–5694, doi:10.5194/acp-7-5675-2007, 2007.
- Huneus, N., Schulz, M., Balkanski, Y., Griesfeller, J., Prospero, J., Kinne, S., Bauer, S., Boucher, O., Chin, M., Dentener, F., Diehl, T., Easter, R., Fillmore, D., Ghan, S., Ginoux, P., Grini, A., Horowitz, L., Koch, D., Krol, M. C., Landing, W., Liu, X., Mahowald, N., Miller, R., Morcrette, J.-J., Myhre, G., Penner, J., Perlwitz, J., Stier, P., Takemura, T., and Zender, C. S.: Global dust model intercomparison in AeroCom phase I, *Atmos. Chem. Phys.*, 11, 7781–7816, doi:10.5194/acp-11-7781-2011, 2011.
- Iversen, T. and Seland, Ø.: A scheme for process-tagged SO<sub>4</sub> and BC aerosols in NCAR-CCM3, Validation and sensitivity to cloud processes, *J. Geophys. Res.*, 107, 4751, doi:10.1029/2001JD000885, 2002.
- Iversen, T. and Seland, Ø.: Correction to “A scheme for process-tagged SO<sub>4</sub> and BC aerosols in NCAR-CCM3, Validation and sensitivity to cloud processes”, *J. Geophys. Res.*, 108, 4502, doi:10.1029/2003JD003840, 2003.
- Iversen, T. and Seland, Ø.: The role of cumulus parameterisation in global and regional sulphur transport, in: *Air Pollution Modeling and Its Application XVI*, edited by: Borrego, C. and Incecik, S., Kluwer Academic Publications, New York, 225–233, 2004.
- Iversen, T., Kirkevåg, A., Seland, Ø., Debernard, J., Kristjánsson, J. E., and Hoose, C.: Assessing Impacts of Aerosol Processes on Equilibrium Climate Sensitivity, in: *Air Pollution Modeling and Its Application XX*, edited by: Steyn, D. G. and Rao, S. T., Springer, ISBN, 978-90-481-3810-4, 493–497, 2010.
- Iversen, T., Bentsen, M., Bethke, I., Debernard, J. B., Kirkevåg, A., Seland, Ø., Drange, H., Kristjánsson, J. E., Medhaug, I., Sand, M., and Seierstad, I. A.: The Norwegian Earth System Model, NorESM1-M – Part 2: Climate Response and Scenario Projections, *Geosci. Model Dev. Discuss.*, accepted, 2012.
- Jaenicke, R.: Abundance of cellular material and proteins in the atmosphere, *Science*, 308, 73, doi:10.1126/science.1106335, 2005.
- Kent, G. S., Trepte, C. R., Skeens, K. M., and Winker, D. M.: LITE and SAGE II measurements of aerosols in the southern hemisphere upper troposphere, *J. Geophys. Res.*, 103, 19111–19127, doi:10.1029/98JD00364, 1998.
- Kirkevåg, A. and Iversen, T.: Global direct radiative forcing by process-parameterized aerosol optical properties, *J. Geophys. Res.*, 107, 4433, doi:10.1029/2001JD000886, 2002.
- Kirkevåg, A., Iversen, T., Seland, Ø., and Kristjánsson, J. E.: Revised schemes for optical parameters and cloud condensation nuclei in CCM-Oslo. Institute Report Series, Department of Geosciences, University of Oslo, 29 pp., ISBN 82-91885-31-1, ISSN 1501-6854-128, 2005.
- Kirkevåg, A., Iversen, T., Seland, Ø., Debernard, J. B., Storelvmo, T., and Kristjánsson, J. E.: Aerosol-cloud-climate interactions in the climate model CAM-Oslo, *Tellus A*, 60, 492–512, 2008.
- Koffi, B., Schulz, M., Bréon, F.-M., Griesfeller, J., Winkler, D., Balkanski, Y., Bauer, S., Bernsten, T., Chin, M., Collins, W. D., Dentener, F., Diehl, T., Easter, R., Ghan, S., Ginoux, P., Gong, S., Horowitz, L. W., Iversen, T., Kirkevåg, A., Koch, D., Krool, M., Myhre, G., Stier, P., and Takemura, T.: Application of the CALIOP layer product to evaluate the vertical distribution of aerosols estimated by global models: AeroCom phase I results, *J. Geophys. Res.*, 117, D10201, doi:10.1029/2011JD016858, 2012a.
- Koffi, B., Schulz, M., Steensen, B. M., Bréon, F.-M., Griesfeller, J., Winkler, D., Balkanski, Y., Bauer, S., Bellouin, N., Bernsten, T., Bian, H., Chin, M., Diehl, T., Easter, R., Ghan, S., Iversen, T., Kirkevåg, A., Liu, X., Lohmann, U., Myhre, G., Rasch, P., Seland, Ø., Skeie, R. B., Steenrod, S., Stier, P., Takemura, T., Tsigaridis, K., Vuolo, M. R., and Zhang, K.: An evaluation of the aerosol vertical distribution in IPCC AR5 global transport models through comparison against CALIOP layer products, *J. Geophys. Res.*, in preparation, 2012b.
- Kristjánsson, J. E.: Studies of the aerosol indirect effect from sulphate and black carbon aerosols, *J. Geophys. Res.*, 107, 4246, doi:10.1029/2001JD000887, 2002.
- Kulmala, M., Petäjä, T., Mönkkönen, P., Koponen, I. K., Dal Maso, M., Aalto, P. P., Lehtinen, K. E. J., and Kerminen, V.-M.: On the growth of nucleation mode particles: source rates of condensable vapor in polluted and clean environments, *Atmos. Chem. Phys.*, 5, 409–416, doi:10.5194/acp-5-409-2005, 2005.
- Kulmala, M., Asmi, A., Lappalainen, H. K., Baltensperger, U., Brenguier, J.-L., Facchini, M. C., Hansson, H.-C., Hov, Ø., O’Dowd, C. D., Pöschl, U., Wiedensohler, A., Boers, R., Boucher, O., de Leeuw, G., Denier van der Gon, H. A. C., Feichter, J., Krejci, R., Laj, P., Lihavainen, H., Lohmann, U., McFiggans, G., Mentel, T., Pilinis, C., Riipinen, I., Schulz, M., Stohl, A., Swietlicki, E., Vignati, E., Alves, C., Amann, M., Ammann, M., Arabas, S., Artaxo, P., Baars, H., Beddows, D. C. S., Bergström, R., Beukes, J. P., Bilde, M., Burkhardt, J. F., Canonaco, F., Clegg, S. L., Coe, H., Crumeyrolle, S., D’Anna, B., Decesari, S., Gilardoni, S., Fischer, M., Fjaeraa, A. M., Fountoukis, C., George, C., Gomes, L., Halloran, P., Hamburger, T., Harrison, R. M., Herrmann, H., Hoffmann, T., Hoose, C., Hu, M., Hyvärinen, A., Hörrak, U., Iinuma, Y., Iversen, T., Josipovic, M., Kanakidou, M., Kiendler-Scharr, A., Kirkevåg, A., Kiss, G., Klimont, Z., Kolmonen, P., Komppula, M., Kristjánsson, J.-E., Laakso, L., Laaksonen, A., Labonnote, L., Lanz, V. A., Lehtinen, K. E. J., Rizzo, L. V., Makkonen, R., Manninen, H. E., McMeeking, G., Merikanto, J., Minikin, A., Mirme, S., Morgan, W. T., Nemitz, E., O’Donnell, D., Panwar, T. S., Pawlowska, H., Petzold, A., Pienaar, J. J., Pio, C., Plass-Duelmer, C., Prévôt, A. S. H., Pryor, S., Reddington, C. L., Roberts, G., Rosenfeld, D., Schwarz, J., Seland, Ø., Sellegri, K., Shen, X. J., Shiraiwa, M., Siebert, H., Sierau, B., Simpson, D., Sun, J. Y., Topping, D., Tunved, P., Vaattovaara, P., Vakkari, V., Veefkind, J. P., Visschedijk, A., Vuollekoski, H., Vuolo, R., Wehner, B., Wildt, J., Woodward, S., Worsnop, D. R., van Zadelhoff, G.-J., Zardini, A. A., Zhang, K., van Zyl, P. G., Kerminen, V.-M., S Carslaw, K., and Pandis, S. N.: General overview: European Integrated project on Aerosol Cloud Climate and Air Quality interactions (EUCAARI) – integrating aerosol research from nano to global scales, *Atmos. Chem. Phys.*, 11, 13061–13143, doi:10.5194/acp-11-13061-2011, 2011.
- Lamarque, J.-F., Bond, T. C., Eyring, V., Granier, C., Heil, A., Klimont, Z., Lee, D., Lioussé, C., Mieville, A., Owen, B., Schultz, M. G., Shindell, D., Smith, S. J., Steffest, E., Van Aardenne, J., Cooper, O. R., Kainuma, M., Mahowald, N., McConnell, J. R., Naik, V., Riahi, K., and van Vuuren, D. P.: His-

- torical (1850–2000) gridded anthropogenic and biomass burning emissions of reactive gases and aerosols: methodology and application, *Atmos. Chem. Phys.*, 10, 7017–7039, doi:10.5194/acp-10-7017-2010, 2010.
- Leck, C. and Bigg, E. K.: Biogenic particles in the surface microlayer and overlying atmosphere in the central Arctic Ocean during summer, *Tellus B*, 57, 305–316, 2005.
- Lee, D. S., Fahey, D. W., Forster, P. M., Newton, P. J., Wit, R. C. N., Lim, L. L., Owen, B., and Sausen, R.: Aviation and global climate change in the 21st century, *Atmos. Environ.*, 43, 1751–1766, doi:10.1016/j.atmosenv.2009.04.024, 2009.
- Liu, X., Easter, R. C., Ghan, S. J., Zaveri, R., Rasch, P., Shi, X., Lamarque, J.-F., Gettelman, A., Morrison, H., Vitt, F., Conley, A., Park, S., Neale, R., Hannay, C., Ekman, A. M. L., Hess, P., Mahowald, N., Collins, W., Iacono, M. J., Bretherton, C. S., Flanner, M. G., and Mitchell, D.: Toward a minimal representation of aerosols in climate models: description and evaluation in the Community Atmosphere Model CAM5, *Geosci. Model Dev.*, 5, 709–739, doi:10.5194/gmd-5-709-2012, 2012.
- Lohmann, U. and Leck, C.: Importance of submicron surface-active organic aerosols for pristine Arctic clouds, *Tellus B*, 57, 261–268, 2005.
- Lohmann, U., Feichter, J., Penner, J. E., and Leaitch, W. R.: Indirect effect of sulfate and carbonaceous aerosols: a mechanistic treatment, *J. Geophys. Res.*, 105, 12193–12206, 2000.
- Martin, G. M., Johnson, D. W., and Spice, A.: The measurement and parameterization of effective radius of droplets in warm stratocumulus clouds, *J. Atmos. Sci.*, 51, 1823–1842, 1994.
- Matthias-Maser, S. and Jaenicke, R.: The Size Distribution of Primary Biological Aerosol Particles with Radii > 0.2 µm in an Urban/Rural Influenced Region, *J. Atmos. Res.*, 39, 279–286, 1995.
- Meskhidze, N., Xu, J., Gantt, B., Zhang, Y., Nenes, A., Ghan, S. J., Liu, X., Easter, R., and Zaveri, R.: Global distribution and climate forcing of marine organic aerosol: 1. Model improvements and evaluation, *Atmos. Chem. Phys.*, 11, 11689–11705, doi:10.5194/acp-11-11689-2011, 2011.
- Mieville, A., Granier, C., Lioussé, C., Guillaume, B., Mouillot, F., Lamarque, J. F., Grégoire, J. M., and Pétron, G.: Emissions of gases and particles from biomass burning during the 20th century using satellite data and an historical reconstruction, *Atmos. Environ.*, 44, 1469–1477, 2010.
- Monahan, E. C., Spiel, D. E., and Davidson, K. L.: A model of marine aerosol generation via whitecaps and wave disruption, in: *Oceanic Whitecaps and their role in Air-Sea Exchange Processes*, edited by: Monahan, E. C. and MacNiocaill, G., D. Reidel Publishing, Dordrecht, The Netherlands, 167–174, 1986.
- Morrison, H. and Gettelman, A.: A new two-moment bulk stratiform cloud microphysics scheme in the Community Atmosphere Model, version 3 (CAM3), Part I: Description and numerical tests, *J. Climate*, 21, 3642–3659, 2008.
- Myhre, G., Berglen, T. F., Johnsrud, M., Hoyle, C. R., Berntsen, T. K., Christopher, S. A., Fahey, D. W., Isaksen, I. S. A., Jones, T. A., Kahn, R. A., Loeb, N., Quinn, P., Remer, L., Schwarz, J. P., and Yttri, K. E.: Modelled radiative forcing of the direct aerosol effect with multi-observation evaluation, *Atmos. Chem. Phys.*, 9, 1365–1392, doi:10.5194/acp-9-1365-2009, 2009.
- Myhre, G., Samset, B. H., Schulz, M., Balkanski, Y., Bauer, S., Berntsen, T. K., Bian, H., Bellouin, N., Chin, M., Diehl, T., Easter, R. C., Feichter, J., Ghan, S. J., Hauglustaine, D., Iversen, T., Kinne, S., Kirkevåg, A., Lamarque, J.-F., Lin, G., Liu, X., Luo, G., Ma, X., Penner, J. E., Rasch, P. J., Seland, Ø., Skeie, R. B., Stier, P., Takemura, T., Tsigaridis, K., Wang, Z., Xu, L., Yu, H., Yu, F., Yoon, J.-H., Zhang, K., Zhang, H., and Zhou, C.: Radiative forcing of the direct aerosol effect from AeroCom Phase II simulations, *Atmos. Chem. Phys. Discuss.*, 12, 22355–22413, doi:10.5194/acpd-12-22355-2012, 2012.
- Mårtensson, E. M., Nilsson, E. D., de Leeuw, G., Cohen, L. H., and Hansson, H.-C.: Laboratory simulations and parameterization of the primary marine aerosol production, *J. Geophys. Res.*, 108, 4297, doi:10.1029/2002JD002263, 2003.
- Neale, R. B., Richter, J. H., Conley, A. J., Park, S., Lauritzen, P. H., Gettelman, A., Williamson, D. L., Rasch, P. J., Vavrus, S. J., Taylor, M. A., Collins, W. D., Zhang, M., Lin, S.-J.: Description of the NCAR Community Atmosphere Model (CAM 4.0), NCAR Technical Note, April 2010.
- Nilsson, E. D., Rannick, Ü., Swietlicki, E., Leck, C., Aalto, A. A., Zhou, J., and Norman, M.: Turbulent aerosol fluxes over the Arctic Ocean 2. Wind-driven sources from the sea, *J. Geophys. Res.*, 106, 32139–32154, 2001.
- O’Dowd, C. D., Facchini M. C., Cavalli, F., Ceburnis, D., Mircea, M., Decesari, S., Fuzzi, S., Yoon, Y. J., and Putaud, J.-P.: Biogenically driven organic contribution to marine aerosol, *Nature*, 431, 676–680, doi:10.1038/nature02959, 2004.
- Otterå, O. H., Bentsen, M., Drange, H., and Suo, L.: External forcing as a metronome for Atlantic multidecadal variability, *Nat. Geosci.*, 3, 688–694, doi:10.1038/ngeo955, 2010.
- Penner, J. E., Andreae, M., Annegarn, H., Barrie, L., Feichter, J., Hegg, D., Jayaraman, A., Leaitch, R., Murphy, D., Nganga, J., and Pitari, G.: Aerosols, their direct and indirect effects, in: *Climate change 2001: The scientific basis. Contribution of working group I to the Third Assessment Report of the Intergovernmental Panel on Climate Change*, Cambridge University Press, 289–348, 2001.
- Penner, J. E., Quaas, J., Storelvmo, T., Takemura, T., Boucher, O., Guo, H., Kirkevåg, A., Kristjánsson, J. E., and Seland, Ø.: Model intercomparison of indirect aerosol effects, *Atmos. Chem. Phys.*, 6, 3391–3405, doi:10.5194/acp-6-3391-2006, 2006.
- Putaud, J. P., Raes, F., van Dingenen, R., Brüggemann, E., Facchini, M. C., Decesari, S., Fuzzi, S., Gehrig, R., Hüglin, C., Laj, P., Lorbeer, G., Maenhaut, W. M., Mihalopoulos, N., Müller, K., Querol, X., Rodriguez, S., Schneider, J., Spindler, G., ten Brink, H., Tørseth, K., and Wiedensohler, A.: A European aerosol phenomenology-2 chemical characteristics of particulate matter at kerbside, urban, rural and background sites in Europe, *Atmos. Environ.*, 38, 2579–2595, 2004.
- Randall, D. A., Wood, R. A., Bony, S., Colman, R., Fichet, T., Fyfe, J., Kattsov, V., Pitman, A., Shukla, J., Srinivasan, J., Stouffer, R. J., Sumi, A., and Taylor, K. E.: *Climate Models and Their Evaluation*, in: *Climate Change 2007: The Physical Science Basis. Contribution of Working Group I to the Fourth Assessment Report of the Intergovernmental Panel on Climate Change* edited by: Solomon, S., Qin, D., Manning, M., Chen, Z., Marquis, M., Averyt, K. B., Tignor, M., and Miller H. L., Cambridge University Press, Cambridge, United Kingdom and New York, NY, USA, 2007.
- Rasch, P. J. and Kristjánsson, J. E.: A comparison of the CCM3 model climate using diagnosed and predicted condensate parameterizations, *J. Climate*, 11, 1587–1614, 1998.



- Ridley, D. A., Heald, C. L., and Ford, B.: North African dust export and deposition: A satellite and model perspective, *J. Geophys. Res.*, 117, D02202, doi:10.1029/2011JD016794, 2012.
- Rotstain, L. D. and Liu, Y.: Cloud droplet spectral dispersion and the indirect effect: Comparison of two treatments in a GCM, *Geophys. Res. Lett.*, 36, L10801, doi:10.1029/2009GL038216, 2009.
- Samset, B. H., Myhre, G., Schulz, M., Balkanski, Y., Bauer, S., Bernsten, T. K., Bian, H., Bellouin, N., Diehl, T., Easter, R. C., Ghan, S. J., Iversen, T., Kinne, S., Kirkevåg, A., Lamarque, J.-F., Lin, G., Liu, X., Penner, J., Seland, Ø., Skeie, R.B., Stier, P., Takemura, T., Tsigaridis, K., and Zhang, K.: Black carbon vertical profiles strongly affect its radiative forcing uncertainty, *Atmos. Chem. Phys. Discuss.*, 12, 28929–28953, doi:10.5194/acpd-12-28929-2012, 2012.
- Sand, M., Bernsten, T. K., Kay, J. E., Lamarque, J. F., Seland, Ø., and Kirkevåg, A.: The Arctic response to remote and local forcing of black carbon, *Atmos. Chem. Phys.*, 13, 211–224, doi:10.5194/acp-13-211-2013, 2013.
- Schulz, M., Textor, C., Kinne, S., Balkanski, Y., Bauer, S., Bernsten, T., Berglen, T., Boucher, O., Dentener, F., Guibert, S., Isaksen, I. S. A., Iversen, T., Koch, D., Kirkevåg, A., Liu, X., Montanaro, V., Myhre, G., Penner, J. E., Pitari, G., Reddy, S., Seland, Ø., Stier, P., and Takemura, T.: Radiative forcing by aerosols as derived from the AeroCom present-day and pre-industrial simulations, *Atmos. Chem. Phys.*, 6, 5225–5246, doi:10.5194/acp-6-5225-2006, 2006.
- Schulz, M., Chin, M., and Kinne, S.: The Aerosol Model Comparison Project, AeroCom, Phase II: Clearing Up Diversity, IGAC Newsletter, No 41., 2009.
- Schultz, M. G., Heil, A., Hoelzemann, J. J., Spessa, A., Thonicke, K., Goldammer, J., Held, A. C., Pereira, J. M., and van het Bolscher, M.: Global Wildland Fire Emissions from 1960 to 2000, *Global Biogeochem. Cyc.*, 22, GB2002, doi:10.1029/2007GB003031, 2008.
- Schuster, G. L., Vaughan, M., MacDonnell, D., Su, W., Winker, D., Dubovik, O., Lapyonok, T., and Trepte, C.: Comparison of CALIPSO aerosol optical depth retrievals to AERONET measurements, and a climatology for the lidar ratio of dust, *Atmos. Chem. Phys.*, 12, 7431–7452, doi:10.5194/acp-12-7431-2012, 2012.
- Seinfeld, J. H. and Pandis, S. N.: *Atmospheric Chemistry and Physics: From Air Pollution to Climate Change*, John Wiley, New York, 1326 pp., 1998.
- Seland, Ø., Iversen, T., Kirkevåg, A., and Storelvmo, T.: Aerosol–climate interactions in the CAM–Oslo atmospheric GCM and investigations of associated shortcomings, *Tellus A*, 60, 459–491, 2008.
- Smith, S. J., van Aardenne, J., Klimont, Z., Andres, R. J., Volke, A., and Delgado Arias, S.: Anthropogenic sulfur dioxide emissions: 1850–2005, *Atmos. Chem. Phys.*, 11, 1101–1116, doi:10.5194/acp-11-1101-2011, 2011.
- Spracklen, D. V., Arnold, S. R., Sciare, J., Carslaw, K. S., and Pio, C.: Globally significant oceanic source of organic carbon aerosol, *Geophys. Res. Lett.*, 35, L12811, doi:10.1029/2008GL033359, 2008.
- Stevens, B. and Feingold, G.: Untangling aerosol effects on clouds and precipitation in a buffered system, *Nature*, 461, 607–613, 2009.
- Stier, P., Feichter, J., Kinne, S., Kloster, S., Vignati, E., Wilson, J., Ganzeveld, L., Tegen, I., Werner, M., Balkanski, Y., Schulz, M., Boucher, O., Minikin, A., and Petzold, A.: The aerosol–climate model ECHAM5–HAM, *Atmos. Chem. Phys.*, 5, 1125–1156, doi:10.5194/acp-5-1125-2005, 2005.
- Storelvmo, T., Kristjánsson, J. E., Ghan, S., Kirkevåg, A., Seland, Ø., and Iversen, T.: Predicting cloud droplet number in CAM–Oslo, *J. Geophys. Res.*, 111, D24208, doi:10.1029/2005JD006300, 2006.
- Storelvmo, T., Kristjánsson, J. E., Lohmann, U., Iversen, T., Kirkevåg, A., and Seland, Ø.: Modelling of the Wegener–Bergeron–Findeisen process – implications for aerosol indirect effects, *Environ. Res. Lett.*, 3, 045001, doi:10.1088/1748-9326/3/4/045001, 2008.
- Storelvmo, T., Hoose, C., and Eriksson, P.: Global modeling of mixed-phase clouds: The albedo and lifetime effects of aerosols, *J. Geophys. Res.*, 116, D05207, doi:10.1029/2010JD014724, 2011.
- Struthers, H., Ekman, A. M. L., Glantz, P., Iversen, T., Kirkevåg, A., Mårtensson, E. M., Seland, Ø., and Nilsson, E. D.: The effect of sea ice loss on sea salt aerosol concentrations and the radiative balance in the Arctic, *Atmos. Chem. Phys.*, 11, 3459–3477, doi:10.5194/acp-11-3459-2011, 2011.
- Ström, J. S., Okada, K., and Heintzenberg, J.: On the state of mixing of particles due to Brownian coagulation, *J. Aerosol Sci.*, 23, 467–480, 1992.
- Textor, C., Schulz, M., Guibert, S., Kinne, S., Balkanski, Y., Bauer, S., Bernsten, T., Berglen, T., Boucher, O., Chin, M., Dentener, F., Diehl, T., Easter, R., Feichter, H., Fillmore, D., Ghan, S., Ginoux, P., Gong, S., Grini, A., Hendricks, J., Horowitz, L., Huang, P., Isaksen, I., Iversen, I., Kloster, S., Koch, D., Kirkevåg, A., Kristjánsson, J. E., Krol, M., Lauer, A., Lamarque, J. F., Liu, X., Montanaro, V., Myhre, G., Penner, J., Pitari, G., Reddy, S., Seland, Ø., Stier, P., Takemura, T., and Tie, X.: Analysis and quantification of the diversities of aerosol life cycles within AeroCom, *Atmos. Chem. Phys.*, 6, 1777–1813, doi:10.5194/acp-6-1777-2006, 2006.
- Tjiputra, J. F., Roelandt, C., Bentsen, M., Lawrence, D. M., Lorentzen, T., Schwinger, J., Seland, Ø., and Heinze, C.: Evaluation of the carbon cycle components in the Norwegian Earth System Model (NorESM), *Geosci. Model Dev. Discuss.*, 5, 3035–3087, doi:10.5194/gmdd-5-3035-2012, 2012.
- Tsigaridis, K. and Kanakidou, M.: Global modelling of secondary organic aerosol in the troposphere: a sensitivity analysis, *Atmos. Chem. Phys.*, 3, 1849–1869, doi:10.5194/acp-3-1849-2003, 2003.
- Twomey, S.: The Influence of Pollution on the Shortwave Albedo of Clouds, *J. Atmos. Sci.*, 34, 1149–1152, 1977.
- Twomey, S.: Aerosols, Clouds and Radiation, *Atmos. Environ.*, 11, 2435–2442, 1991.
- van der Werf, G. R., Randerson, J. T., Giglio, L., Collatz, G. J., Kasibhatla, P. S., and Arellano Jr., A. F.: Interannual variability in global biomass burning emissions from 1997 to 2004, *Atmos. Chem. Phys.*, 6, 3423–3441, doi:10.5194/acp-6-3423-2006, 2006.
- Vertenstein, M., Craig, T., Middleton, A., Feddema, D., and Fischer, C.: CCSM4.0 User’s Guide, available at: <http://www.cesm.ucar.edu/models/ccsm4.0/ccsm-doc/book1.html>, 2010.

- Winker, D. M., Tackett, J. L., Getzewich, B. J., Liu, Z., Vaughan, M. A., and Rogers, R. R.: The global 3-D distribution of tropospheric aerosols as characterized by CALIOP, *Atmos. Chem. Phys. Discuss.*, 12, 24847–24893, doi:10.5194/acpd-12-24847-2012, 2012.
- Yttri, J. E., Aas, W., Tørseth, K., Fiebig, M., Fjaraa, A. M., Tsyro, S., Simpson, D., Bergström, R., Marečková, K., Wankmüller, R., Klimont, Z., Borken-Kleefeld, J., Cavalli, F., Putaud, J.-P., Schultz, M., Querol, X., Alastuey, A., Amato, F., Cusack, M., Reche, C., Karanasiou, A., Viana, M., Moreno, T., Pey, J., Pérez, N., Laj, P., and Wiedensohler, A.: EMEP Status Report 4/11: Transboundary Particulate Matter in Europe: Status Report 2011, Joint CCC & MSC-W & CEIP & CIAM Report, available at: <http://www.nilu.no/projects/ccc/reports.html>, 2011.
- Zhang, J. and Reid, J. S.: MODIS aerosol product analysis for data assimilation: Assessment of over-ocean level 2 aerosol optical thickness retrievals. *J. Geophys. Res.*, 111, D22207, doi:10.1029/2005JD006898, 2006.